Identification and Validation of Circular RNAs in Mouse Tissues and in a Transverse Aortic Constriction Induced Heart Hypertrophy Model

Inauguraldissertation
zur Erlangung des Grades eines Doktors der Medizin
des Fachbereichs Medizin
der Justus-Liebig-Universität Gießen

Vorgelegt von Schubert, Florian
aus Heppenheim

Gießen 2023

Aus dem Fachbereich Medizin der Justus-Liebig-Universität Gießen,
Abteilung für Innere Medizin

Gutachter: Prof. Dr. Dr. Thomas Braun
Gutachter: Prof. Dr. Saverio Bellusci

Tag der Disputation: 04.03.2024

TABLE OF CONTENT

I INTRODUCTION

I.1 Discovery of circular RNAs

Circular RNAs were first reported by Sanger and colleagues in 1976, when they characterized the structure of infectious viroids. The authors provided evidence, that these single stranded RNA molecules obtain a closed, circular structure (Sanger et al., 1976). In the following years, circular RNAs were sporadically discovered and described in various organisms such as yeast (Arnberg et al., 1980) and mammals (Capel et al., 1993; Cocquerelle et al., 1992; Nigro et al., 1991; Zaphiropoulos, 1996). More recently, high throughput RNA sequencing and new bioinformatic algorithms revealed thousands of circular RNA species. Many thereof are expressed in an organ-specific manner (Chen et al., 2016; Xu et al., 2017; X. Zeng et al., 2017; Zou et al., 2017), involved in various pathologies, such as cardiovascular diseases (W. W. Du, W. Yang, et al., 2017), malignancies (Ahmed et al., 2016), auto-immune diseases (Haixia Li et al., 2018) as well as neurological disorders (Lukiw, 2013). Initially, circular RNAs were classified as a particular class of non-coding RNAs (ncRNAs), a large group of RNAs not translated into proteins and involved in regulation of cell physiology and cellular functions (Panni et al., 2020). However, this classification might not be completely accurate, as recent studies suggest a subset of circRNAs encode for small peptides and are translated *in vivo* (Pamudurti et al., 2017).

I.2 Classification of circular RNAs

Depending on the genomic origin of the corresponding sequence, circular RNAs are categorized into 3 groups: circRNAs, EIcircRNAs and ciRNAs.

CircRNAs contain exclusively exonic sequences, are predominantly localized in the cytoplasmatic compartment and obtain the highest abundance among the different varieties of circRNAs. In contrast, intron-containing circular RNAs (ciRNAs) consist only of intronic sequences and are localized in the nuclear compartment (Wu et al., 2014; Zhang et al., 2013). The last group of circular RNAs encompass both, exonic and intronic sequences, so called exon-intron-containing circular RNAs (EIcircRNAs) (Jeck et al., 2013; Li et al., 2015), which are predominantly localized in the nuclear compartment and enhance parental gene transcription (Li et al., 2015).

All three circular RNA subtypes derive from loci within their host gene and are therefore defined as intragenic circular RNAs. In contrast, intergenic circular RNAs arise from loci located between two genes (Qu et al., 2017).

I.3 Biogenesis of circular RNAs

CircRNAs, as well as their linear counterparts, are generated by an RNA maturation mechanism termed splicing. During this process, non-coding introns are removed from the newly transcribed precursor mRNA (pre-mRNA), resulting in messenger RNA (mRNA). This complex process requires characteristic splicing recognition sequences within introns and is mediated by a protein-RNA complex called spliceosome as well as multiple additional proteins for assembling the spliceosomal complex. The characteristic splice sites include a dinucleotide 5' splice donor, as well as a dinucleotide 3' splice acceptor site. Both sites are located at the margin of the spliced intron, next to an adjacent exon (Figure 1 a).

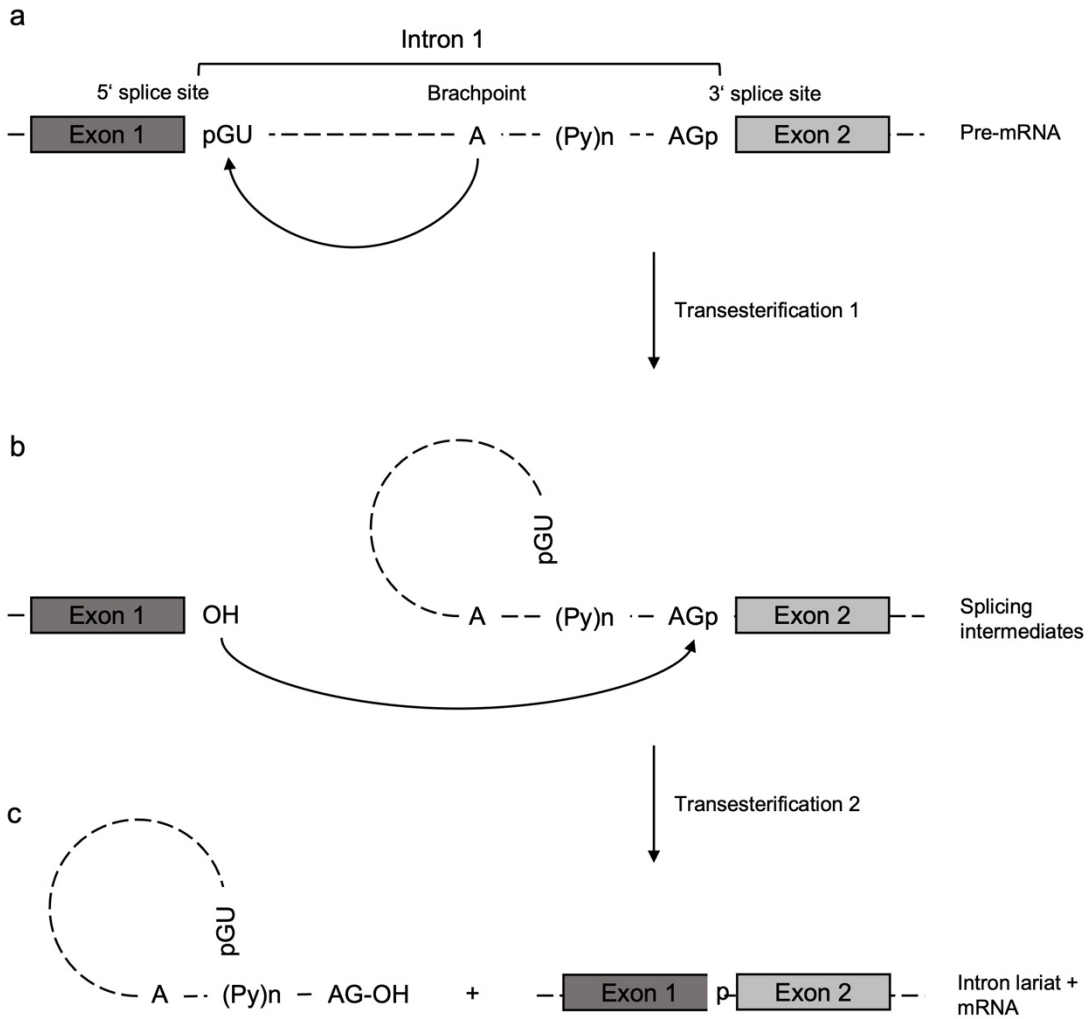

Figure 1 Splicing mechanism

a) Pre-mRNA transcript containing characteristic splice sites: The 5' splice donor site (containing a GU dinucleotide) and 3' acceptor site (containing an AG dinucleotide) are located next to exon 1 and 2 within the border region of the intron. The upstream region of the 3' splice site harbors the typical branch-point characterized by conserved adenosine residue (A). Between the branch-point and the 3' splice acceptor site, the polypyrimidine tract ((Py)n) is located. b) The splicing process is characterized by two consecutive transesterification reactions. During the first transesterification, an exon 2 lariat-intermediate and a cleaved 5' splice site is formed. c) A second transesterification results in the ligation of exon 1 and 2 and concomitant 3' splice site cleavage, releasing an intron-lariat and mRNA. Figure modified from Chandler and colleagues (Chandler, 2011)

Within the intronic region, a so-called branch-point, containing conserved adenosine residues, is typically located 20-50 nucleotides upstream the acceptor site. Additionally, a 15-20 bp long, pyrimidine-rich sequence, termed polypyrimidine tract, located at the 3' end of the intron, mediates the assembly of the spliceosome. (Burset et al., 2000; Lodish H., 2004). The vast majority of splicing events derive from canonical splice sites, encompassing the splice acceptor site, encoded by an AG dinucleotide and the splice donor site, characterized by a GU sequence. In canonical splicing, the splicing process is catalyzed by the major spliceosome complex, containing multiple small nuclear ribonucleoproteins (U1, U2, U4, U5 and U6 snRNPs). In contrast, a minority of splicing events originate from splicing sites with non-conserved dinucleotide sequences, also referred to as non-canonical sites (Burset et al., 2000). Herby, rare introns are removed by the minor spliceosome complex comprising U11, U12, U4atac and U6atac minor spliceosomal RNA (Patel & Steitz, 2003).

During the splicing process, two transesterifications are catalyzed by different spliceosomal complexes. The first transesterification occurs as a result of a nucleophilic attack of the 2' OH group from the adenosine at the branching point onto the 5' phosphate at the donor site (Figure 1 a). As a result, exon 1 is released with a newly formed 3' OH group and an intron-containing lariat-intermediate of exon 2 (Figure 1 b). A second transesterification occurs consecutively between the 3' OH group of exon 1 and the 5' phosphate group of the acceptor site. As a consequence, two exons are joined together, thereby forming the mRNA and releasing the intron-lariat (Figure 1 c).

In canonical splicing, the relative order of the resulting mRNA matches the order of the exons in the genome. Exon shuffling, also called non-colinear splicing, a splicing process resulting in an altered exon order (out of its genomic context), is not observed. (Jeck et al., 2013). However, the diversity of mRNAs derives from different combinations of retention and inclusion of exons in the mature transcript. This process, called alternative splicing, allows the generation of multiple mRNAs deriving from a single pre-mRNA transcript. Alternative splicing is regulated by a complex system of trans-acting (deriving from other genes) repressors and activators binding to cis-acting sequences, so called RNA binding motifs. In 95% of all multiexon pre-mRNAs, this process is observed and thus leading to an increase of proteome diversity in higher organisms (Pan et al., 2008). Interestingly, circular RNAs are subjected to alternative splicing as well: Multiple isoforms of circRNAs can be generated from a single host gene (X. O. Zhang et al., 2016). In fact, currently over 400 host genes are known to originate more than one circRNA (Y. Li et al., 2017) and over 32000 circRNAs in human cells have been discovered so far (Xu et al., 2017; X. Zeng et al., 2017).

In contrast to linear mRNAs, circular RNAs are generated through a unique splicing mechanism called back-splicing: The 3’ end of an exon is spliced to the 5’ end upstream of the same, or another 5’ located exon (Jeck et al., 2013). Subsequently, back-splicing disrupts the exon order, resulting in shuffled exons. This exon shuffling is not an exclusive characteristic of circular RNAs (Jeck & Sharpless, 2014), although it is used bioinformatically alongside the back-splice-junction, to detect circular RNAs. Currently, there are two models describing the biogenesis of circRNAs through back-splicing: 1. The lariat precursor and 2. the direct back-splice model (also intron-pairing-derived circularization) (Jeck et al., 2013).

In the lariat precursor model (Figure 2), at minimum 2 distinct splicing events are required to generate a circRNA. The first transesterification occurs between the donor site and a downstream branching point of 2 introns with various number of intronic and exonic sequences in between (Figure 2 a). As a result, a free 3’ OH group is generated at the donor site. In the following step, this 3’ OH group attacks the acceptor site of a downstream intron (Figure 2 b), thereby merging the two flanking exons and releasing an exon-intron-containing lariat with a 2’-5’ phosphodiester bond (Figure 2 c). This process, also referred to as exon skipping, is exhibited in the alternative splicing of various genes (Kelly et al., 2015).

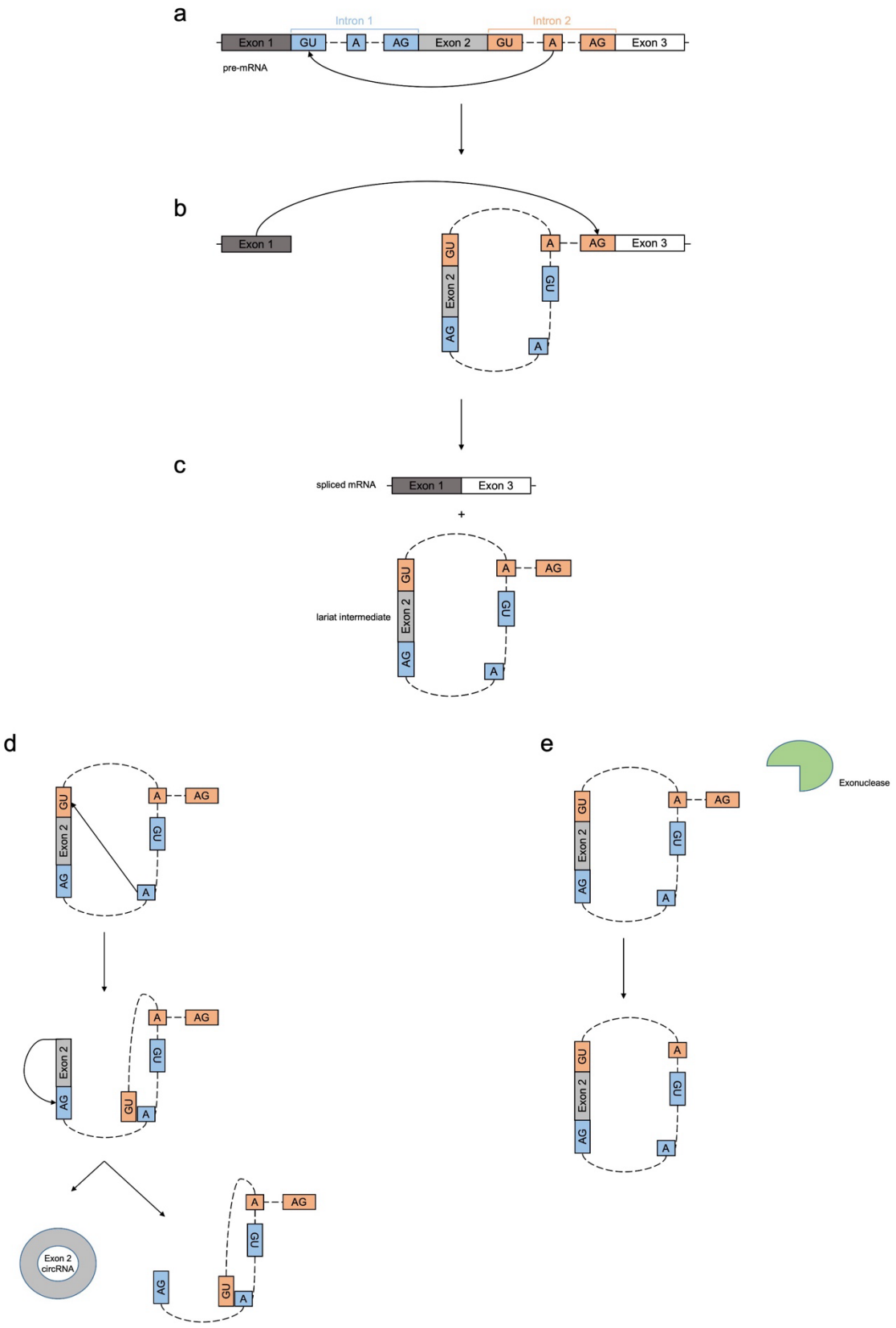
a
Intron 1
Intron 2
Exon 1
GU
A
AG
Exon 2
GU
A
AG
Exon 3
pre-mRNA
b
Exon 1
GU
Exon 2
AG
A
GU
A
AG
Exon 3
c
spliced mRNA
Exon 1
Exon 3
+
lariat intermediate
GU
Exon 2
AG
A
GU
A
AG
d
GU
Exon 2
AG
A
GU
A
AG
Exon 2
AG
GU
A
Exon 2
circRNA
AG
A
GU
A
AG
e
Exonuclease
GU
Exon 2
AG
A
GU
A
AG
GU
Exon 2
AG
A
GU
A

Figure 2 Lariat precursor model for circRNA and EIcircRNA formation
a) Nucleophilic attack of the branching point (intron 2, A) on the upstream donor site (intron 1, GU). b) Attack of the 3'-OH group of exon 1 on the splicing acceptor site (intron 2, AG). As a result c), a spliced mRNA with a skipped exon 2 and a lariat intermediate arises. d) During circRNA formation a second splicing reaction occurs, resulting in a circularized exon 2 and a double lariat structure. e) In EIcircRNA formation, a ribonuclease degrades the 3' tail of the lariat intermediate, producing an exon and intron containing EIcircRNA. Figure modified from Altesha et al. (Altesha et al., 2019)

The second splicing event is performed within the released exon-intron-containing lariat: A first transesterification occurs between an upstream branching point and a downstream splicing donor site and subsequently, a second transesterification is catalyzed from the donor site to an upstream acceptor site (Figure 2 d).
The close proximity between the splicing sites within the exon-intron intermediate catalyzes this second splicing event (Barrett et al., 2015). Depending on the content of the exon-intron-containing lariat, either a single circularized exon or another exon-intron-containing lariat with residual exons is generated concomitantly to an intron-containing lariat by-product. In multiple exon circRNAs, intronic sequences are subsequently removed by splicing. EIcircRNAs are generated by degradation of the 3' tail of the exon-intron intermediate (Figure 2 e).
The lariat precursor model is based on findings indicating, that exon skipping events are correlated with circRNA production for numerous genes (Jeck et al., 2013; Surono et al., 1999; Zaphiropoulos, 1996). However, this causality is controversial: Zhang and colleagues postulated inverted sequences flanking circularizable exons as the main determinants for circularization and regarded increased exon skipping events as mere by-products (Zhang et al., 2014). In contrast, a recent study by Barett and colleagues provided first evidence of the involvement of lariat formation in the production of circular RNAs (Barrett et al., 2015). They argue, that the lariat structure catalyzes back-splicing by positioning back-splice sites in close proximity and thereby preventing competing splice sites from catalysis.
Additionally, a positive correlation between the length of the circularized exons and circRNA formation is described (Barrett et al., 2015). Furthermore, Starke et al. indicated

the role of the canonical spliceosomal machinery and both canonical splice sites in circRNA biogenesis (Starke et al., 2015).

The second circRNA biogenesis model is defined as the direct back-splice model (Figure 3): Here, complementary sequences in the flanking introns of a circularizable exon cause the formation of secondary pre-mRNA structures. These structures lead to close proximity of non-sequential splicing donor and acceptor pairs (Figure 3 a). In contrast to the first model, only a single splicing event is required without the production of a lariat precursor. The transesterification is catalyzed at the branching point and the donor site of the downstream flanking intron (Figure 3 a), followed by an attack of the free 3'OH end of the circularized exon at an upstream acceptor site (Figure 3 b). As a result (Figure 3 c), a non-functional, terminated fork product and a circularized, exonic RNA (circRNA), are generated (Jeck et al., 2013). This model is based on the abundant circRNA derived from the mouse sex-determining gene locus (SRY) (Capel et al., 1993), in which the circularized exon is flanked by long, inverted complementary sequences, necessary for circularization (Dubin et al., 1995). Interestingly, long introns tend to undergo less efficient splicing and might therefor favorize less efficient splicing mechanisms like back-splicing (Ashwal-Fluss et al., 2014; Jeck et al., 2013). In accordance, further studies demonstrated increased circRNA formation of exons flanked by complementary sequences (Liang & Wilusz, 2014; Pasman et al., 1996; Zhang et al., 2014) and genome-wide computational sequence analysis suggests this mechanism is widespread and associated with repetitive short DNA sequences such as Alu elements (Jeck et al., 2013; Zhang et al., 2014). Alu elements are retrotransposons, a class of repetitive DNA sequences, copied by repeated integration of their transcripts into the genome, thereby amounting to approximately 10% of the whole human genome.

However, repetitive sequences are far less common in lower eukaryotes compared to higher (e.g., mammals) and circRNAs deriving from genes without complementary sequences exist.

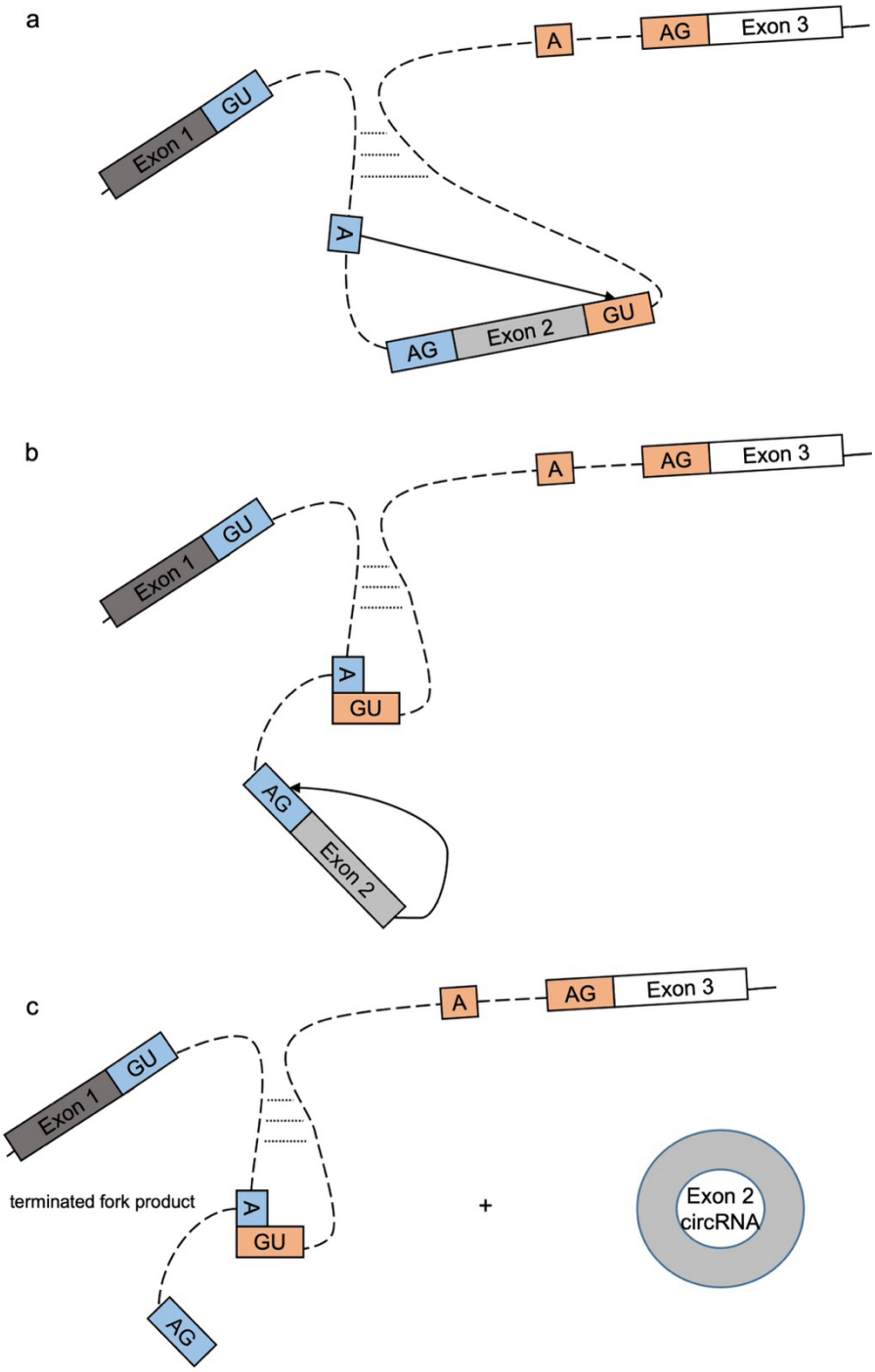

Figure 3 Direct back-splice model of circRNA formation

a) Complementary sequences in the flanking introns of exon 2 lead to the formation of a pre-mRNA secondary structure (dotted lines), ameliorating a nucleophilic attack of the branching point (A, intron 1) on the splicing donor site downstream (GU, intron 2). b) Attack of the free 3'-OH group of exon 2 on the acceptor site of intron 1 (AG). c) As a result, a terminated fork product and a circularized exon 2 are generated. Figure modified from Altesha et al. (Altesha et al., 2019)

These findings suggest inverted sequences may ameliorate circRNA formations, but are not essential (Barrett & Salzman, 2016; Barrett et al., 2015). Interestingly, besides the mechanism, the timepoint of circRNA formation remains an ongoing topic of research. Ashwal-Fluss and colleagues gathered evidence of circRNA formation in a co-transcriptional manner by identifying reads covering back-splice junctions in chromatin-bound RNAseq data. Furthermore, a competition between canonical pre-mRNA splicing and back-splicing was demonstrated (Ashwal-Fluss et al., 2014). However, Zhang et al. used a metabolic tagging of nascent RNAs suggesting circRNA splicing mainly occurs post-transcriptionally (Y. Zhang et al., 2016).

In contrast to circRNAs and EIcircRNAs, ciRNAs can be generated form intronic-lariats deriving from canonical splicing (Figure 1 c). Regularly, these lariats are debranched at their 2'-5' phosphodiester bond and subsequently degraded by exonucleases (Fica et al., 2013). However, intronic-lariats are partly protected from degradation, if they contain a 7 nucleotide GU-rich motif at the 5' splicing site and an 11 nucleotide C-rich motif at the branching point. As a consequence, only the region from the 3' end of the lariat up to the branching point is degraded, resulting in a circularized intron (Shen et al., 2015).

Recently, the regulation of circular RNA formation has become the focus of research. In addition to inverted sequence repeats acting as cis-motifs, trans-acting factors were shown to influence circular RNA expression, in particular RNA binding proteins (RBPs) such as RNA binding motif protein 20 (RBM20), muscleblind protein (MBL) and quaking 1 (QK1). Reports indicated, that RBPs increase circRNA expression or induce circularization in regularly linear spliced transcripts by binding to specific intronic motifs (Kelly et al., 2015; Khan et al., 2016).

Furthermore, a functional correlation between circRNA abundance and the RNA editing enzyme adenosine deaminase acting on RNA 1 (ADAR1) has been reported: ADAR1 mediates substitutions from adenosine (A) to inosine (I) in RNA transcripts, which were enriched in complementary regions of introns flanking circularized exons. Due to the altered sequences, secondary structures are destabilized via base-pairing, resulting in a reduction of circular RNA expression. Consecutively, ADAR1 expression correlates negatively to circRNA levels (Ivanov et al., 2015; Rybak-Wolf et al., 2015).

I.4 Properties of circular RNAs

Until now, the majority of detected circular RNA molecules belong to the class of exonic circRNAs. They are abundantly expressed throughout various different organisms (Jeck et al., 2013) and display variation in a cell type, development stage and tissue-specific manner (Jakobi et al., 2016; Y. Li et al., 2017; Memczak et al., 2013; Xu et al., 2017). Recent studies reported altered circRNA profiles during cardiac development (Y. Li et al., 2017) as well as during the maturation of the neonatal to the adult heart (Werfel et al., 2016). Interestingly, homologous circRNAs exist across numerous species, suggesting an evolutionary conservation of circRNA expression (Jeck et al., 2013).

Circular RNAs are not co-expressed with their linear counterparts in most cases (Y. Li et al., 2017; Siede et al., 2017) although the regulatory factors and mechanisms for this are not fully understood yet. As a consequence, circular RNA expression can even exceed its linear isoform for certain host genes (Siede et al., 2017).

Subsequent to circRNA biogenesis, the majority of circular RNAs is exported from the nucleus to the cytoplasm, mediated by the ATP-dependent RNA helicases DDX39A and DDX39B, according to the size of the circRNA molecule (Huang et al., 2018). Furthermore, an additional study revealed, that circRNAs are actively exported in terms of a potential clearance mechanism (Lasda & Parker, 2016). By now, reports detecting an enrichment of circular RNAs in extracellular vesicles are still increasing, however, the functional role of extracellular export in context of intracellular circRNA levels remains unknown (Lasda & Parker, 2016). Interestingly, circRNA ciRS-7 e.g., maintains its circular structure within the vesicle and functions after release in other cells, suggesting a form of intercellular communication mechanism (Preußer et al., 2018). The export mechanism as a potential option for circRNA level regulation is particular interesting, since circRNAs are exceptionally stable molecules. Due to their closed loop structure, circRNAs cannot be degraded by RNA exonucleases and therefor exhibit a higher stability and longer half-life than their linear counterparts (Jeck et al., 2013; Suzuki & Tsukahara, 2014).

Furthermore, recent studies correlated various diseases with altered circRNAs expression patterns (Gupta et al., 2018; Siede et al., 2017; Werfel et al., 2016). In combination with detectability in blood plasma, circRNAs were demonstrated to resemble sensitive biomarkers for diagnosis and prognosis of diseases (e.g. Hsa_circ_0000190 for gastric cancer) (Salgado-Somoza et al., 2017).

I.5 Detection and validation of circular RNAs

Generally, next-generation RNA sequencing, as well as circRNA microarrays are routinely used to detect and quantify circular RNAs at a large scale. Both approaches are based on the characteristic back-splice junction to distinguish circular RNA candidates from their linear counterparts. For sequencing, mainly ribosomal RNA (rRNA) depleted RNA probes of next-generation sequencing (NGS) data sets are used. NGS is a sequencing method broadly used in genomic and transcriptomic research nowadays: In contrast to previous sequencing techniques e.g. Sanger sequencing, millions of small DNA fragments are sequenced simultaneously (Behjati & Tarpey, 2013). Subsequently, RNA sequencing reads are aligned to a reference genome to identify specific reads (inferred sequences corresponding to a DNA or RNA fragment) spanning the back-splice junction (Jeck & Sharpless, 2014). Within the last years, numerous bioinformatic algorithms were developed to detect circRNAs from RNA sequencing data with a broad diversity in terms of precision and sensitivity (e.g. PTESFinder, KNIFE, NCLscan, circRNA_Finder, CIRCexplorer, DCC, find_circ, UROBORUS, CIRI, Mapsplice and so on) (Hansen et al., 2016; Xiangxiang Zeng et al., 2017). So far, many additions to this approach have been published, among which CircleSeq is the most frequently used. It involves an enrichment analysis of circRNA candidates by comparing RNA sequencing results from RNAse R treated and RNAse R untreated samples (Jeck et al., 2013). Since RNAse R acts as an exoribonuclease preferentially degrading linear RNA, circular RNAs are enriched in treated samples (Vincent & Deutscher, 2006). However, removal of linear RNA by RNAse R digestion, followed by polyadenylation and poly(A)-RNA depletion (so called RPAD-treatment), was shown to further enrich circRNAs and therefore ameliorate analysis of circRNA sequencing (Panda et al., 2017). Besides detection, relative quantification of circRNA expression can be deduced by RNA sequencing. Therefore, normalized counts of back-splice junction spanning reads are compared at different time points or conditions (Ivanov et al., 2015). Furthermore, recent studies implemented statistical analysis methods to detect host gene independent expression alliterations (Cheng et al., 2016). In contrary, microarray analysis detects and quantifies circRNAs by targeting back-splice junctions via specific sequence probes at high sensitivity and specificity (Jeck et al., 2013). These probes are designed exclusively for circRNAs that have already been annotated, therefore novel candidates cannot be studied this way.

In order to validate or quantify RNA-seq derived circRNA, Northern blots, as well as qPCR using outward orientated primer directed against the back-splice junction, are commonly performed. However, the back-splice junction is not an utterly unique characteristic of circRNAs, since corresponding sequencing reads can also arise from genomic alterations, e.g., tandem duplications, where duplicated exons are located within the same gene. Other causes for back-splice formation include template switching of reverse transcriptase during cDNA preparation. Hereby, the enzyme dissociates from the template and subsequently starts transcription of another copy of an upstream exon.
Additionally, trans-splicing provides another way to generate back-splice junction reads mediated by independent transcript merging during splicing (Jeck & Sharpless, 2014).
As mentioned above, RNAse R is a 3' - 5' exoribonuclease with the ability to degrade linear RNA molecules. Due to the circularity, circRNAs lack a discrete 3' end and are therefore resistant to RNAse R digestion. As a result, RNAse R treatment is a useful tool to enrich for circRNAs (Jeck & Sharpless, 2014).
In summary, multiple validation techniques are required to correctly identify the circular structure of circRNA candidates.

I.6 Function of circular RNAs

Up until now, multiple modes of action of circRNAs have been described in literature, in particular acting as competing endogenous RNAs (ceRNAs) or miRNA-sponges. Furthermore, circRNAs are involved in regulation of splicing and transcription, act as protein scaffolds and modify parental gene expression and target-RNA decoys. However, the function of the majority of detected circRNAs is yet unknown.

I.6.1 MiRNA-sponges

MicroRNAs (miRNAs) represent a class of small, non-coding RNAs of approximately 22 nucleotides, which regulate gene expression of their target mRNA by partial base-pairing to the untranslated regions (UTR). As much as 60% of the whole transcriptome is estimated to be affected by miRNA regulation (Friedman et al., 2009). MiRNAs detect mRNA targets via hybridization to complementary miRNA responsive elements (MREs) within a miRNA-protein complex called miRNA-induced RNA silencing complex (miRISC). Generally, miRNA-MRE interactions are performed by a 5' seed sequence within the miRNA, however additional 3' pairing can ameliorate specificity of mRNA

targeting (Broughton et al., 2016). Besides miRNA, the miRISC complex contains argonaute proteins, encoding an endonuclease activity. Depending on the complementarity of MRE-miRNA interaction, miRNAs can affect target mRNAs either by AGO-dependent mRNA slicing or miRISC-mediated target mRNA decay. In case of full complementarity, a mRNA is degraded by the AGO endonucleases (Jo et al., 2015). However, most miRNA-MRE interactions show at minimum central mismatches, hence preventing AGO-dependent endonuclease activity (Jonas & Izaurralde, 2015). In these cases, RNA interference is mediated subsequently via formation of a silencing miRISC, containing various effector proteins such as poly(A)-deadenylases, as well as decapping proteins and exoribonucleases that mediate target mRNA decay (Behm-Ansmant et al., 2006).

Until now, numerous circular RNAs were discovered encoding an enrichment of miRNA-binding sites, thereby acting as a miRNA sponges to neutralize their function (Figure 4 a). Captured miRNAs fail to bind to corresponding target mRNAs and therefore lose the ability to regulate target mRNA function. CDR1as e.g., a circRNA derived from the *Cerebellar Degeneration Related Protein 1* (*CDR1*) gene, is one of the most studied circRNAs and was shown to contain over 70 binding sites for miRNA-7 (Hansen et al., 2013; Memczak et al., 2013). CDR1as represses miRNA-7s' function and thus influence its gene expression regulation (Geng et al., 2016). Contrary, miRNA-directed circRNA cleavage was observed as well for miR-671 and CDR1as (Hansen et al., 2011). Nowadays, various computational pipelines predicting circRNA-miRNA interactions are available such as CircInteractome (Dudekula et al., 2016), Circ2Traits (Ghosal et al., 2013), CircNet (Liu et al., 2016) and StarBase V2.0 (Li et al., 2014). To date, several circRNAs have been identified with multiple miRNA binding sites. However, no enrichment of these binding sites could be detected for the majority of circRNAs discovered so far. Accordingly, miRNA sponging appears to be a function of only a fraction of the class of circRNAs (Khan et al., 2016). In particular, for ciRNAs, only minor enrichment at miRNA-binding sites has been found so far (Wu et al., 2014; Zhang et al., 2013).

I.6.2 Protein/RBP sponges

In addition, circRNAs were also shown to interact with RNA-binding proteins (RBPs) in various ways, e.g. by competitive binding, regulation of RBP functions, as well as "sponging" RBPs, work as a platform for RBP assembly and RBP concentration (William

W Du et al., 2017). RBPs represent a large group of proteins with the ability to bind RNA. They exhibit fundamental roles in various cellular mechanisms mainly by post-transcriptional gene regulation, e.g. in terms of splicing, polyadenylation, translation, as well as localization and stabilization of mRNAs (Gerstberger et al., 2014).

However, RBP sponging is the best investigated interaction with circRNAs by far (Figure 4 b).

Recent studies addressing circRNA functions identified numerous circRNAs encoding multiple binding motifs of RBPs. Among them, circMbl represents a circular RNA originating from the *musleblind* (*Mbl*) gene, containing binding sites for MBL protein. MBL is an RBP, regulating alternative splicing of *Mbl* pre-mRNA transcripts as well as circMbl. MBL binds strongly to circMbl-binding sites, thereby affecting levels of circMbl biogenesis (Ashwal-Fluss et al., 2014). Besides *Mbl*, the *poly(A) binding protein nuclear 1* (*Pabpn1*) gene also generates a circRNA, which is enriched in binding sites for RBP Hu-antigen R (HUR). CircPabpn1 sponges HUR, leading to suppression of HUR binding to its target *Pabpn1* mRNA. As a result, HUR fails to enhance *Pabpn1* translation (Abdelmohsen et al., 2017). In summary, these singular circRNAs regulate transcription and splicing by binding RBPs. However, some reports state, that RBP-binding sites are underrepresented in circular RNAs compared to the linear counterparts (You et al., 2015).

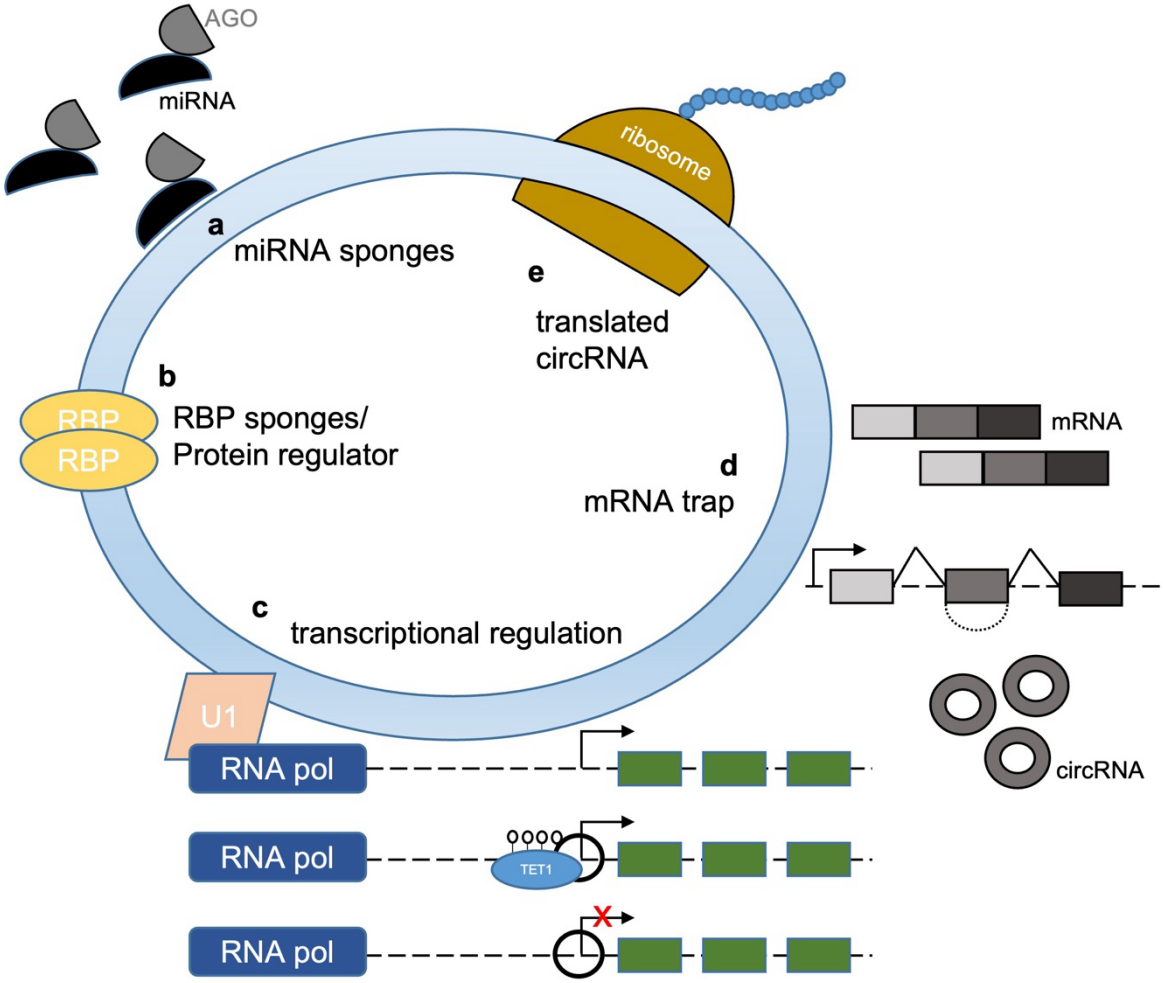

Figure 4 Function of circular RNAs

Circular RNAs feature various functions: a) CircRNAs as miRNA sponges: CircRNAs enriched in miRNA-binding sites inhibit AGO (argonaute) dependent miRNA function in regulatory networks by sponging. b) circRNAs as RBP sponges / protein regulators: CircRNAs can scaffold proteins, herby influencing their interactions and functions. c) Regulation of parental gene transcription in cis- and trans-manner: Transcription is enhanced via interaction with U1 snRNP (U1) and promotor demethylation enzyme demethylation via ten-eleven translocation methylcytosine dioxygenase 1 (TET1) demethylase. Gene silencing is induced by inhibition of a promotor region d) Circular RNAs act as mRNA traps: CircRNA formation (dotted lines) competes with mRNA formation (straight lines). e) Translation into protein: CircRNAs with open reading frames (ORF) are translated by ribosomes. Figure modified from Tan et al. (Tan & Lim, 2020)

I.6.3 Scaffolds for assembly of proteins

Recent studies have shown that some circRNAs have the ability to scaffold proteins, thereby facilitating their contact and assembly. For example, circFoxo3, which originates from the *Forkhead Box O* 3 (*Foxo3*) gene, has a high affinity to various transcription factors (TFs) factors such as Inhibitor of DNA-binding 1 (Id-1), E2F transcription factor (E2F1), Hypoxia Inducible Subunit Alpha (HIF-α) and Focal Adhesion Kinase (FAK) and an enhanced expression inhibits the translocation of these TFs to the nuclear or mitochondrial compartment (W. W. Du, L. Fang, et al., 2017). Furthermore, circAmotl1, a circular RNA deriving from *Angiomotin-like Protein 1* (*Amotl1*), involved in the Wnt/beta-catenin signaling-pathway, was reported to act as a protein scaffold in cardiomyocytes, suggesting that circAmotl1 forms tertiary complexes with the serine/threonine kinase Protein kinase B (PKB) and Pyruvat Dehydrogenase Liponamide Kinase Isoenzym 1 (PDK1). Subsequently, PKB is phosphorylated and translocated to the nuclear compartment, where it exhibits a cardioprotective role (Y. Zeng et al., 2017).

I.6.4 Splicing and transcription enhancement

In contrast to the generally cytoplasmic localization of circRNAs, ciRNAs and EIciRNAs are predominantly localized in the nuclear compartment, enabling interaction with the transcriptional machinery. Indeed, EIcicRNAs were shown to enhance transcription of their parental gene in a cis-manner. This function is most likely mediated by an interaction with U1 small nuclear ribonucleoprotein (U1 snRNP), polymerase II (Pol II) and the parental gene promotor in a positive feedback loop (Figure 4 c). Higher EIcircRNA levels enhance host gene transcription, resulting in enhanced EIcircRNA production (Li et al., 2015). In addition, ciRNAs also act as cis regulators by enhancing elongation polymerase II activity. As an example, ci-ankr52 accumulate to its own transcription sites, where it associates with polymerase II to enhance its transcription activity (Zhang et al., 2013).

I.6.5 Translation of circRNAs

Generally, circRNAs are categorized as non-coding RNAs since they lack a 5’ cap structure obligatory for translation (Kozak, 1979). However, synthetic circRNAs encoding internal ribosome entry sites (IRES) were shown to be translated *in vitro,* as well as cap-independently in cell-culture (Abe et al., 2015; Chen & Sarnow, 1995; X. Li et al., 2017) and recent studies indicate a subset of endogenous circRNAs exhibiting

translation potential (Schneider & Bindereif, 2017; Tatomer & Wilusz, 2017) (Figure 4 e). As an example, human circ-ZNF609, derived from the *Zinc Finger Protein 609* (*ZNF 609)* gene, is translated in a splicing-dependent and cap-independent manner. Circ-ZNF609 contains an open reading frame at the same site used for linear mRNA translation, which terminates at a stop codon located 3 nucleotides downstream of the back-splice junction (Legnini et al., 2017). In accordance, mass spectrometry analysis identified peptides, spanning endogenous back-splicing junctions of 19 human circRNAs (Yang et al., 2017). Furthermore, Pamuduti et al. detected circRNAs in Drosophila associated with ribosomes in deeply sequenced ribosome profiling data sets. Hereby, the predicted translation was spanning the start codon of their linear counterpart up to the back-splice junction (Pamudurti et al., 2017). Additionally, not only the first translated circRNA circFBXW7, but also a synergetic function of the resulting protein together with the product of the host gene, was revealed. circFBXW7 is translated to the protein FBXW7-185aa, which was shown to regulate the stability of the proto-oncogene *c-Myc* together with the host protein FBXW7, resulting in repressed tumorgenesis (Yang et al., 2018).

I.7 Heart hypertrophy and circular RNAs

Hypertrophy of the heart generally refers to an enlargement of cardiomyocytes as a consequence of adaptations to increased pre- or afterload. Initially, function of the heart is maintained by enhanced contractility via addition of sarcomere units and an increase in wall thickness, following Laplace's law (James et al., 2000; Selvetella et al., 2004). As a consequence, gene expression is altered, resulting in changes in cardiomyocyte metabolism, survival and contractility. Generally, two primary types of hypertrophy with discrepancies in pathogenesis and prognosis are described. Physiological heart hypertrophy is characterized by a maintained cardiac function, whereas in pathological hypertrophy ejection fraction is not preserved, leading to heart failure, arrhythmias and ultimately death. Generally, heart failure is considered one of the leading causes of morbidity and mortality worldwide, thus accounting for its exceptional importance in medicine (Roger, 2013). Physiological hypertrophy is defined by a fully reversible increase in cardiac mass (10-20%) without signs of cardiac fibrosis or apoptosis. Hereby, neither progression to heart failure, nor alterations in expression of fetal genes encoding for proteins such as natriuretic peptide A and B (ANP and BNP), myosin 7 (MYH7) or skeletal muscle α-actin, is observed. In contrast, pathological hypertrophy is

characterized by an initial concentric growth of the ventricle, as an adaption to increased workload, which results in a dilatation of the chambers accompanied by the thinning of ventricular walls, contractive dysfunction and heart failure (Schiattarella & Hill, 2015). Additionally, typical features including proliferation of activated myofibroblasts, collagen deposition, as well as apoptosis, are characteristic for pathological hypertrophy. The development of either physiological or pathological hypertrophy depends rather on upstream stimuli and signaling pathways than on the duration of cardiac stress (Tham et al., 2015). Pregnancy, as well as exercise are typical stimuli for physiological hypertrophy. Hereby, increased pressure (e.g. in strength training) results in a concentric hypertrophy (Vega et al., 2017), whereas volume overload (e.g. in endurance training) leads to eccentric hypertrophy. In contrast, pathologic hypertrophy is typically induced by systemic hypertension, valvular dysfunctions (most commonly aortic stenosis, mitral or aortic regurgitation), myocardial ischemia, storage diseases and hereditary cardiomyopathies (e.g. hypertrophic cardiomyopathy). These stimuli lead to a variety of cellular pathways: In physiological hypertrophy, adaptive mechanisms regarding cell growth, proliferation, angiogenesis and survival are triggered. Hereby, thyroid hormone (T_3) exhibits a crucial function by regulating heart contractility and electric coupling as well as postnatal hypertrophy (Pantos et al., 2011; Trivieri et al., 2006). Additionally, Insulin and insulin-like growth factor 1 (IGF1) are involved in pathways targeting peptide synthesis, cellular enlargement and survival (Maillet et al., 2013; Saltiel & Kahn, 2001). Furthermore, angiogenesis and cell survival are mediated via vascular endothelial growth factor (VEGF) and platelet-derived growth factor (PDGF) (Carmeliet et al., 1999; Chintalgattu et al., 2010; Izumiya et al., 2006). Moreover, nitric oxide (NO) ameliorates cardiomyocyte contractility via an increase in cyclic guanosine monophosphate (cGMP) levels and subsequent activation of protein kinase G (PKG). Here, NO levels are regulated by β-adrenergic receptors in endothelial cell, which are stimulated by exercise (Calvert et al., 2011). Regarding the cellular energy metabolism, peroxisome proliferator-activated receptor-ɣ co-activator 1 α (PGC1α) dependent AMP-activated protein kinase K (AMPK) signaling way exhibit an enhancement (X. Li et al., 2019).

In contrast, pathologic hypertrophy is characterized by additional processes leading to maladaptive compensation. These processes encompass apoptosis, fibrosis, dysregulation of Ca^{2+} homeostasis, alteration of the metabolism, reactivation of fetal gene expressions, lack of quality control for proteins and mitochondria, as well as changes in sarcomere structure and impaired angiogenesis. These signaling pathways are mainly induced

through an increase in neuroendocrine hormones and mechanical stress by the underlying diseases. Angiotensin II and endothelin 1, respectively, are peptide hormones, causing an increase in inositol triphosphate (IP_3) by binding to their corresponding receptors. IP_3 subsequently leads to maladaptive gene expression via calcium-dependent calcineurin – nuclear factor of activated T cells (NFAT) signaling way (Molkentin et al., 1998), as well as inhibition of cell growth through Ca^{2+}/calmodulin-dependent protein kinase II (CaMKII) (Ling et al., 2009). In addition, antihypertrophic factors ANP and BNP are upregulated in response to pathologic stimuli leading to increased cGMP levels, thereby activating PKG (Rainer & Kass, 2016) and thus prohibiting cell growth (Holtwick et al., 2003).

Moreover, β-adrenergic receptors activity is chronically increased in hypertrophy-inducing diseases due to elevated catecholamine levels (Lymperopoulos et al., 2013). As a result, cyclic adenosine monophosphate (cAMP) levels rise and subsequently intracellular Ca^{2+} is increased via protein kinase A (PKA) activation. Besides, cAMP induces exchange proteins directly activated by cAMP (EPACs), involved in contractility, hypertrophy as well as arrhythmias (Métrich et al., 2008; Pereira et al., 2013). Additionally, chronic β-adrenergic activation manifests as hypertrophy and receptor desensitization through GPCR kinase (GRK)- mediated β-arrestin signaling (Sato et al., 2015). Another essential player in pathologic hypertrophy development is mechanistic target of rapamycin (mTOR) signaling, a protein kinase essential for coordination of growth factor signaling and control of protein synthesis (Laplante & Sabatini, 2012). In hypertrophy, mTOR activity is enhanced, causing repressed autophagy and reduced protein quality control (Shioi et al., 2003).

Besides cardiomyocytes, immune cells, as well as non-myocytes and adipocytes are influenced by hypertrophic stimuli. In this scenario, production of cytokines, fibroblast growth factors (FGF) and C1q/TNF-related protein 9 (CTRP9) is increased, thereby inducing hypertrophy pathogenesis (Frieler & Mortensen, 2015). Transforming growth factor β (TGFβ) was reported to be upregulated in response to hypertrophy stimuli, causing hypertrophy and fibrosis via SMAD family member 2 & 3 (SMAD2/3)-dependent signaling (Kuwahara et al., 2002). Lastly, mechanosensors obtain a crucial role in hypertrophy development. The cation channels transient receptor potential channels (TRPCs) are involved in pathogenesis via calcineurin-dependent signaling. Hereby, calcineurin – nuclear factor of activated T-cells (NFAT) signaling promotes cardiac remodeling. Another Ca^{2+} mechanosensor is stromal interaction molecule 1 (STIM1),

which is upregulated in mice that have previously undergone transverse aortic constriction (TAC) surgery - a surgical model in which hypertrophy and later heart failure are induced by aortic stenosis. Hypertrophy and arrhythmias are mediated via activation of the transcription factor NFAT and CaMKII signaling pathways (Correll et al., 2015).

In contrast to the well-established signaling pathways, the potential role of circRNAs in the pathogenesis of heart hypertrophy, as well as their clinical applications, are under investigated. Multiple studies demonstrated expression of numerous circRNAs in healthy murine, rat and human heart tissue, as well as under disease conditions and during cardiac development (Jakobi et al., 2016; Tan et al., 2017; Werfel et al., 2016; Y. Li et al., 2017). CircRNA transcriptome studies in heart hypertrophy and heart failure models in mice revealed significant smaller alliterations on circRNA expression compared to different timepoints in cardiac development (Tan et al., 2017; Werfel et al., 2016). Interestingly, Tan and colleagues provide RNAseq-based data, demonstrating lack of differential expression of circRNAs in TAC vs. sham mice hearts 3 weeks post-surgery (Tan et al. 2017). Werfel and colleagues however describe a tendency towards an increased circRNA expression in failing hearts using a similar methodical approach (Werfel et al., 2016). Contrary, other data indicate significant changes in circRNA expression in TAC- (X. Li et al., 2022) and isoproterenol-induced heart failure mouse models (M. H. Yang et al., 2020).

Up until now, the majority of investigated circRNA functions in the pathogenesis of cardiac hypertrophy is based on circRNA-miRNA interactions. MiRNAs are involved in various cardiac processes, such as contraction of the heart muscle, as well as cardiac morphogenesis. Additionally, miRNAs influence the onset of heart hypertrophy (Care et al., 2007; Wang et al., 2012).

In this context, Wang and colleagues detected a reduction of heart-related circRNA (HRCR or mm9-circ-012559) and an increase of miR-233 levels for thoracic aortic constriction- and isoproterenol-induced cardiac hypertrophy models compared to controls. HRCR encodes 6 miR-233 binding sites and acts as a sponge to sequester unbound miR-233, thereby attenuating cardiac hypertrophy. Overexpression of HRCR results in an increase of the apoptosis repressor with CARD domain (ACR) by inhibiting its miR-233 mediated repression (Wang et al., 2016).

Another study indicates, that circSlc8a1, one of the most abundant circRNAs in heart tissue, (Lim et al., 2019) can act as a sponge for miR-133a, a miRNA exerting a protective

regulatory role in cardiac hypertrophy (Care et al., 2007; Lim et al., 2019). Overexpression of circSlc8a1 results in an increased onset of heart failure and cardiac dilation, whereas repression protects cardiomyocytes from pressure overload induced hypertrophy. Interestingly, circSlc8a1 expression is unaltered during cardiac stress, suggesting a modulated interaction depending on miR-133a levels (Lim et al., 2019).

Moreover, the circRNA from *Myosin IXA* gene (*Myo9a*), circRNA_000203, is involved the development of cardiac hypertrophy. It was demonstrated, that circRNA_000203 mediates an inhibition of miR-26b-5p and miR-140-3p, leading to increased expression of the pro-hypertrophic transcription factor *GATA Binding Protein 4* (*Gata4*) in an Ang-II-induced hypertrophy model in mice (Li et al., 2020; Nishida et al., 2002). In accordance, its human homolog hsa-circ-0036167 was also upregulated in samples from hypertrophic myocardium from heart failure patients (Li et al., 2020).

Yang and colleagues detected approximately 400 differentially expressed circRNAs derived from circRNA sequencing with an isoproterenol-induced mouse hypertrophy model. Amongst them, circRNA wwp1 influences hypertrophy via downstream targets ANF and miR-23a (M. H. Yang et al., 2020)

The common mode of action of the circRNAs presented here is a sponging of miRNAs that have effects on cardiac hypertrophy. Lavenniah and colleagues took advantage of this principle by generating custom-build circRNA sponges, so-called circmiRs, to target miRNAs driving cardiac hypertrophy. Cardiomyocytes transfected with these circmiRs sponging miR-132 and miR-212, demonstrated a maintained cardiac function in pressure overload-induced heart hypertrophy (Lavenniah et al., 2020). These artificial circRNAs might be used in the future to target specific miRNAs therapeutically.

Apart from these reports of individual circRNAs with involvement in the pathogenesis of cardiac hypertrophy, the importance of the class of circRNAs in this disease remains unclear.

I.8 Aim of this study

In this study, I aimed to validate our in-house pipeline for circRNA detection from existing RNA sequencing data sets in various tissues. Therefore, I made use of RT-PCR and qPCR targeting the circular junctions of potential circRNA candidates, combined with sequencing and RNAse R enrichment analysis. Furthermore, I focused on altered circRNA expression profiles gained by a circRNA specific microarray in a TAC-induced heart hypertrophy disease model to deduce novel circRNA candidates for further

functional studies. Since various circRNAs provide their function as miRNA sponges, I aimed to identify potential miRNA targets by a circRNA-miRNA interaction prediction tool. To my best knowledge, this is one of the first studies using this approach to investigate differential expression of circRNAs in a murine TAC model. The newly gained knowledge from this study could prove useful for further approaches addressing the role of circular RNAs in the pathogenesis of ventricular hypertrophy, as well as in the identification of novel biomarkers.

II MATERIALS & METHODS

All following steps, that required direct contact with the animals, including the killing, were carried out by Dr. André Schneider and Marion Wiesnet. Animals were killed according to § 4 Abs. 3 S. 1 TierSchG and § 2 TierSchVersV, animal studies were approved by the Regierungspräsidium Darmstadt (V54 – 19 c 20/15 – B2/1136).

II.1 Transverse aortic constriction (TAC) heart hypertrophy model

The TAC model is a widely used surgical technique introduced by Rockman et al. (Howard A Rockman et al., 1991) for studies of heart hypertrophy and heart failure (Bosch et al., 2020). In summary, an aortic constriction is performed, leading to a pressure overload, hereby inducing heart hypertrophy and failure. Furthermore, this procedure generates limited fibrosis, inflammation, and cardiac dilatation (Xia et al., 2009).

In this study, 4 C57BL/6 male mice (mean age 53 days) underwent TAC surgery and 4 C57BL/6 male mice (mean age 52 days) served as a control and were sham operated (internal term USP13W). Subsequently, TAC surgery mice developed cardiac hypertrophy within 27.67±0.33 days compared to sham mice, that were sacrificed after 21.67±0.67 days (Table 1).

The sacrifice was performed individually, followed by isolation of cardiomyocytes and RNA extraction (II.1.3 and II.3.1). For validating the induced pathologic changes, established cardiac stress marker mRNA levels for beta myosin heavy chain (β-MHC) and atrial natriuretic peptide (ANP) (Izumo et al., 1987; Wang et al., 2003) were analyzed (II.8.2).

Table 1 Mice for TAC and sham surgery

ID	OP	Age at surgery (d)	Age at sacrifice (d)
Sham1 ♂	sham	53	74
Sham2 ♂	sham	53	74
Sham3 ♂	sham	50	73

Sham4 ♂	sham	50	73
TAC1 ♂	TAC	53	80
TAC2 ♂	TAC	53	80
TAC3 ♂	TAC	53	81
TAC4 ♂	TAC	53	81

II.1.1 TAC surgery procedure

Mice were anesthetized in an induction chamber with 5% isoflurane. Followed by the short time anesthesia, an endotracheal intubation with a 22 gauge catheter was performed. Intubation is needed to maintain anesthesia during the operational procedure. The tube was connected to a minivent (HSE), which ventilated with 220 breaths/min at a tidal volume of 0,25ml. Ventilation gas consisted of 1,5% isoflurane in 100% oxygen. Mice were placed on a heating table in dorsal position during surgery to prevent hypothermia. After proper skin disinfection, a left lateral thoracotomy was performed: The first 3 ribs were cut through next to the sternal bone. Thymus and fatty tissue were separated from the aortic arc in a next step. Following identification of the transverse aorta, a piece of 26 gauge blunt needle was placed parallel to the aorta. 6/0 silk suture was used to constrict the aorta up to the diameter of the needle. After knotting, the needle was removed, resulting in an aortic stenosis with a remaining flow through surface as big as the diameter of the needle. Subsequently, the thorax was surgically closed in layers with 5/0 vicryl sutures and the artificial ventilation was stopped under surveillance.

Pre- and post-surgery analgesia was assured by subcutaneous buprenorphine injection (0,1mg/kg), 1x pre-surgery and 3 days post-surgery, 2x daily. Bupivacaine intra surgery injection (1mg/kg body weight). Administration of metamizole in drinking water for 1 day pre-surgery and 5 days post-surgery (200mg/kg body weight).

II.1.2 Sham surgery procedure

As a control, the same operational procedure as described in II.1.1 was performed, except for the aortic constriction.

II.1.3 Isolation of cardiomyocytes from TAC/sham mice

Mice were narcotized by injection with 10µl/g of the mix described in Table 2 Injection master mix. In a first step, the aorta was cannulated on a perfusion system and cardiac arrest was introduced. Perfusion with 15ml Calcium-free buffer (Table 16) was started afterwards. In addition, myocytes were dissociated by perfusing with an 15ml Enzyme buffer (Table 17). Proper perfusion was visually controlled by swelling and slight paleness of the heart. After dissociation, the heart was cut from the cannula, vessels and aorta. Ventricles were minced into small pieces with forceps in 5ml Stop buffer 1 (Table 18). For homogenization, the suspension was gently pipetted several times with a sterile pipette and transferred into a 50ml centrifuge tube. Cells were left to settle down and subsequently, the supernatant was transferred into a 15ml centrifuge tube and spun down for 1min at 300-500rpm. The supernatant was also discarded and both cell pellets were resuspended in Stop buffer 2 (Table 19) up to 10ml. The suspension was filtered into a new 50ml centrifuge tube using a 100µm cell strainer. Then, every 4 minutes Ca^{2+} content was adjusted up to 1mM in 5 steps. As final step, cells were spun down again for 1 minute at 300-500rpm and supernatant was discarded. For RNA isolation, isolation reagent (either TriReagent® or TriFast™ solution) was added.

II.2 Organ isolation

II.2.1 Anesthesia and analgesia of mice

Mice were narcotized by injection with 10µl/g of the mix described in Table 2 Injection master mix.

Table 2 Injection master mix

Ketamine 10% (Medistar)	500µl
Xylazin 20mg (Xylariem ®)	250µL
NaCl (0,9%) (B Braun)	3,25ml

II.2.2 Heart isolation

After anesthesia, the abdominal cavity was opened by a medial laparotomy. The thoracic cavity was opened by cutting through the ribs and the diaphragm. To ensure complete removal of the circulating blood, the right atrium was punctured and ice-cold PBS (Table

14) was injected trough a needle puncturing the apex of the heart continually until the liver turned pale. Afterwards, the heart was removed by cutting through the pulmonary trunk. Remaining vessels and connective tissue were removed in a petri dish filled with cold PBS (Table 14). Atria were separated from ventricle, transferred to 2ml tubes and frozen in liquid nitrogen. Samples were stored at -80°C.

II.2.3 Soleus muscle isolation

Legs were isolated from the torso and thereafter skin was removed. The achilles tendon was dissected and the muscles were lifted cranially. Afterwards, the upper soleus tendon was cut. As a last step soleus muscle was removed and frozen in liquid nitrogen. Samples were stored at -80°C.

II.2.4 Extensor digitorum longus muscle (EDL) isolation

The leg was prepared as described in II.2.3. Lower tendons were cut and the tibialis anterior muscle (TA) was lifted. EDL was prepared from underneath the TA. Afterwards, EDL was dissected at its origin and removed. Samples were frozen in liquid nitrogen and stored at -80°C.

II.2.5 Kidney isolation

The peritoneal cavity was opened and the intestine was removed to unveil the retroperitoneal space. The kidney was removed by cutting through its vessels and removing the fatty tissue. Samples were frozen in liquid nitrogen and stored at -80°C.

II.2.6 Lung isolation

The thoracic cavity was opened by cutting through the ribs and the diaphragm. The chest was retracted and the two lungs were displayed. On both sides of the pulmonary trunk, the vessels were cut and the lung was removed. Additionally, remaining vessels and tissues were removed in a petri dish with ice cold PBS (Table 14). Samples were frozen in liquid nitrogen and at -80°C.

II.3 RNA extraction and isolation

II.3.1 RNA extraction from isolated cardiomyocytes (cm's)/ non-cardiomyocytes (non-cm's)

As described in II.1.3, RNA isolation reagent was added into the tubes directly after isolation. For TriFast™ isolation 1 ml TriFast™ Reagent (#30-2010 - Peqlab) was used, for Direct-zol™ 600 µl Tri Reagent® (supplied with Direct-zol™ Mini Prep Plus Kit #R2071 - Zymo Research). The samples were homogenized by pipetting up and down carefully. After homogenization, samples were spun down for 30 sec at 12.000 g and the supernatant was transferred into new 2 ml tubes.

II.3.1.1 RNA extraction from isolated CMs/ non-CMs using peqGOLD® Tri Fast™

The sample was incubated for 5 minutes at RT to ensure dissociation of the nucleotide complexes. Afterwards, 200 µl Chloroform (#63402 - Roth) were added and the sample was mixed. Once the sample was incubated again for 5 minutes, it was centrifuged at 12000 rcf (4 °C) to perform a phase separation. The upper aqueous phase was transferred to a fresh tube (the residual inter- and organic phase were discarded). Isopropanol was added to precipitate the RNA (10 minutes on ice). After centrifugation (12000 rcf, 4°C, 10 min), the RNA pellet was washed 2 times with 75% EtOH. As a last step, the RNA pellet was eluted in RNAse free water, depending on the size of the pellet. RNA samples were stored at -80°C.

II.3.1.2 RNA extraction from isolated cm's/ non-cm's with Direct-zol™ Mini Prep Plus

The sample was incubated at RT for 5 min to ensure dissociation of the nucleotide complexes. Afterwards, 600 µl 95% EtOH were added and mixed. The mixture was transferred to a Zymo-Spin™ IIICG Column (supplied with Direct-zol™ Mini Prep Plus Kit #R2071 - Zymo Research) in a collection tube and centrifuged (16000 rcf, RT, 30 sec). The flow-through was discarded and the column was transferred to a new collection tube. DNAse I treatment was performed as follow: 400 µl RNA Wash Buffer (supplied with Direct-zol™ Mini Prep Plus Kit #R2071 - Zymo Research) were added to the column and centrifuged as mentioned before. In a next step, a mixture of 5 µl DNAse I (6U/µl) and 75 µl DNA Digestion Buffer (supplied both with Direct-zol™ Mini Prep Plus Kit #R2071 - Zymo Research) were added to the column and incubated at room temperature for 15 min. Afterwards, 400 µl Direct-zol™ RNA PreWash Buffer (supplied

with Direct-zol™ Mini Prep Plus Kit #R2071 - Zymo Research) were added and centrifuged as before. The flow-through was discarded and the step was repeated. As a next step, 700 µl RNA Wash Buffer (supplied with Direct-zol™ Mini Prep Plus Kit #R2071 - Zymo Research) were added to the column and centrifuged for 1 min at 16000 rcf. The column was transferred into a RNAse free tube, whereas the previous collection tube was discarded. To elute the RNA, 100 µl DNAse/RNAse-free Water (supplied with Direct-zol™ Mini Prep Plus Kit #R2071 - Zymo Research) was added to the column and centrifuged (16000 rcf, RT, 30 sec). RNA samples were stored at -80°C.

II.3.2 RNA extraction from organs

Depending on the organ size, organs were dissected into smaller pieces to fit into 2 ml tubes and not exceed 25 mg tissue per tube. RNA isolation reagent (1 ml TriFast™ Reagent per 100 mg or 600 µl Tri Reagent® per 25 mg) was added immediately and samples were stored at -80°C to be processed at once. For RNA isolation, 1 metal bead (grinding balls ss 5 mm, #22.455.0003 – Retsch) was added to the tube for homogenization. The sample was shacked for 5 min at the highest level in a tissue homogenizer (Retsch MM301). Afterwards the suspension was spun down at 12.000 g for 10 minutes. The supernatant was transferred into a new, RNAse free, 2 ml tube. The sample was incubated at RT for 5 min to ensure dissociation of the nucleotide complexes. The next steps were performed as described in II.3.1.1 and II.3.1.2.

II.4 cDNA synthesis

In order to analyze linear transcripts, Superscript II Reverse Transcriptase (SSIIRT) cDNA preparation was performed (II.4.1). cDNA synthesis for circular studies was in vitro transcribed using iScript™ Select cDNA synthesis Kit (# 1708896 - Bio-Rad).

II.4.1 cDNA synthesis using Superscript II Reverse Transcriptase (SSIIRT)

Concentration of purified RNA was measured (Nanodrop 2000c spectrophotometer - Peqlab). Regularly, 1 µg or 0,5 µg RNA were used for cDNA synthesis. The ingredients from Table 3 were mixed and incubated at 65°C for 5 minutes. 7 µl synthesis mix from Table 4 were added and incubated at 42°C for 2 min. 1,0 µl Superscript II Reverse Transcriptase (#18064071 - Invitrogen) was added to the mix and incubated at 42 °C for 50 min followed by incubation at 70 °C for 15 min to inactivate the reaction. 1µl E.coli

RNAse H (2U/µl, #EN0201- Thermo Fischer Scientific) was added and incubated at 37°C for 20 min as a last step. cDNA was stored at -20°C.

Table 3 cDNA synthesis using SSIIRT - step 1

RNA	x µl	
oligo dT primer	1 µl	#C1101 – Promega
dNTP	1 µl	#R0186 - Fermentas
double distillated water	(10-x) µl	

Table 4 cDNA synthesis using SSIIRT - step 2

0,1M DTT	2 µl	#18064071 – Invitrogen
5x FS buffer	4 µl	#18064071 – Invitrogen
RNasin Plus	1 µl	#N2615 – Promega

II.4.2 cDNA synthesis using iScript™ Select cDNA Synthesis Kit

Concentration of purified RNA was measured (Nanodrop 2000c spectrophotometer - Peqlab). Regularly 1 µg or 0,5 µg RNA were used for cDNA synthesis. Random priming option was selected for circRNA studies. The components were mixed as described in Table 5 and incubated 10 min at 42°C for oligo(dT) primer, or 5 min at 25°C followed by 30 min at 42°C for random primers. Afterwards, to inactivate the reverse transcriptase, the mixture was incubated at 85°C for additional 5 min. cDNA was stored at -20°C.

Table 5 iScript™ Select cDNA Synthesis Kit master mix

5x iScript Select Reaction Mix	4µl	#1708896 - Bio-Rad
iScript Reverse Transcriptase	1µl	#1708896 - Bio-Rad
Oligo(dT)$_{20}$ or random primer	2µl	#1708896 - Bio-Rad
RNA template	xµl	#1708896 - Bio-Rad
Nuclease free water	13-xµl	#1708896 - Bio-Rad

II.5 Semi-quantitative Polymerase Chain Reaction (PCR)

All PCR experiments were performed with REDTaq® Ready Mix™ DNA Polymerase kit (#R2523 - Sigma Aldrich) following Table 6. For PCR analysis, cDNA was diluted 1:5, whereas primers were diluted 1:10 (primer sequences displayed in II.14.1). Table 7 PCR-program was used, if not specified otherwise. As a positive control, GAPDH or a linear counterpart of the investigated circRNA was selected, as a negative control, water was used. PCR was performed using a thermocycler (C1000™ Thermocycler - Bio Rad, Labcycler Basic - Sensoquest). Expected product sizes were controlled after gel electrophoresis.

Table 6 REDTaq® Ready Mix™ DNA Polymerase master mix

REDTaq® Ready Mix™	10 µl
H_2O	10 µl
forward primer	0,5 µl
reverse primer	0,5 µl
DNA	1 µl

Table 7 circRNA PCR program 1

	temperature	time	repeats
step 1	95	3:00	
step 2	94	0:30	35
step 3	59	0:30	35
step 4	72	0:30	35
step 5	72	7:00	

II.5.1 Primer design

Predicted circRNA candidate sequence from RNA sequencing analysis was downloaded using the Ensembl genome browser (www.ensembl.org/index.html, genome GRCm38). For primer design, the primer3 v.0.4.0 primer design tool (bioinfo.ut.ee/primer3-0.4.0/) was used. Primer with a size from 20-24bp, GC content > 50%, Tm values in the range from 58-64°C and an annealing temperature around 58-60°C were selected for semi-quantitative PCR. Amplification length was restricted between 150-250bp. Alignment to non-target sequences was controlled by NCBI Basic Local Alignment Search Tool (blast.ncbi.nlm.nih.gov/Blast.cgi).

II.5.1.1 PCR to detect linear junctions

To analyze linear counterparts of circRNAs, a convergent primer pair was used (Figure 5 b). One of the primers was designed to align to one of the circular junction forming exons. The other one is located in an upstream or downstream located exon not included in the circRNA sequence. As a result, specifically linear transcripts in the neighborhood of the circRNA locus are amplified. This setup was used as a control for circRNA expression.

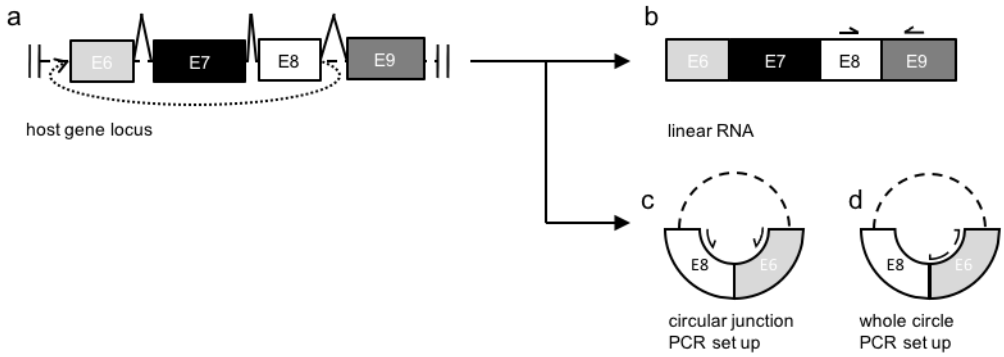

Figure 5 circRNA splicing mechanism and PCR setup

a) The host gene locus can generate 2 RNA isoforms: Linear and circular RNA. b) Mediated by canonical splicing of a pre-mRNA transcript (indicated by straight lines), a linear RNA with ascending exon numbers is processed. Quantification of its expression is achieved by designing primer pairs spanning a junction, not contained in the circRNA (E8 to E9). c) In contrast, circular splicing (dotted line in a)) results in a back-splice junction detectable by a junction spanning primer pair. d) Displays the setup for whole circRNA amplification: An outward facing primer pair within one of the back-splice junction-forming exons is needed. E= exon, arrows indicate primer location.

II.5.1.2 PCR for circular junctions

To detect circRNAs by PCR, primer were designed to span the characteristic back-splice junction. Therefore, a PCR with convergent facing primer on each exon, neighboring the back-splice junction site, was established for each circRNA candidate (Figure 5 c). As a result, linear isoforms of each circRNA candidates sharing the same exons are not amplified. Nonetheless, PCR products might not invariably detect circRNAs, as the back-splice junction is not a unique characteristic (Lasda & Parker, 2014).

II.5.1.3 PCR for whole circle amplifications

For whole circle sequence studies, another PCR design was established. As displayed in Figure 5 d, a divergent primer pair inside one of the circular junctions-forming exons was used. As a product, all circular isoforms containing the exon are amplified. This set up was used for estimations of actual length of the examined circRNA and for further analysis by sequencing.

II.5.2 Gel electrophoresis of PCR products

PCR products were loaded on a 1% or 2% agarose gel (Table 8) depending on estimated product size and separated in 1x TAE buffer (Table 12). Gels were placed in electrophoresis chambers (variable sizes: #700-0909 and #00-0814 - PeqLab) at 120-200 V (power supply: E455 – Consort). Gel documentation was performed on a UV gel documentation device (BioDocAnalyze – Biometra).

Table 8 Agarose gel mix

	1%	**2%**	
Agarose NEEO Ultra Qualität	1 g / 100 ml	2 g / 100 ml	#267.1 - Roth
TAE buffer	100 ml / 1 g	100 ml / 2 g	
Ethidium bromide	3 µl / 100ml	3 µl / 100ml	#A1151 - PanReacAppliChem

II.6 DNA extraction from gel electrophoresis

To extract DNA from gel electrophoresis, the Nucleo Spin® Gel and PCR clean-up kit (#740609.50 – Machery-Nagel) was used. 200 µl NTI Buffer (#740609.50 – Machery-

Nagel) per 100 mg gel were incubated for 5-10 min at 50 °C on a Thermo Mixer (Thermo Mixer F 1.5 – Eppendorf). The solution was transferred to the NucleoSpin® Gel and PCR clean up column (#740609.50 – Machery-Nagel) in a collection tube (#740609.50 – Machery-Nagel) and spined down for 30 sec at 11.000 x g, RT to bind the DNA. In the next step, the silica membrane was washed 2 times: 700 µl NT3 buffer (#740609.50 – Machery-Nagel) was added and spined down again for 30 sec at 11.000 x g, RT. The silica membrane was dried for 1 min at 11.000 x g and the column transferred to a new tube to elute the DNA. Depending on the band size, DNA was eluted using 15-30 µl NE buffer (#740609.50 – Machery-Nagel).

II.7 DNA sequencing of PCR products

Sanger sequencing was supplied by the Sanger sequencing service (Microsynth SeqLab) with the Economy Run option. Samples were prepared according to sample requirements (https://www.microsynth.seqlab.de/sample-requirements-de.html). In case of low DNA contents in extracts, samples were reamplified with the identical primer pair.

II.8 Quantitative PCR (qPCR)

For examination of relative expression of circRNAs and linear RNAs, qPCR was performed. Due to the lack of circRNA Taq Man® assays, SYBR® green qPCR was mainly used for circRNA quantification. Taq Man® assays on the other hand, were utilized to validate cardiac stress markers. qPCR was performed using a qPCR thermocycler (StepOnePlus Real-Time PCR System - Applied Biosystem). For each sample, runs were performed including 3 technical and at least 3 biological replicates. If not mentioned otherwise, target cycle threshold (Ct) - values were normalized to GAPDH.

II.8.1 SYBR ® green qPCR

SYBR green qPCR was performed with KAPA SYBR® FAST qPCR Kit (#KK4602 - KapaBiosystems). cDNA was diluted 1:20 using TE buffer (Table 15). PCR machine was set to “Quantitation – Comparative Ct” and “Fast run”. qPCR SYBR® green master-mix was pipetted following Table 9. qPCR program from StepOne software was adopted. Primers were designed similar to II.5.1, except for the limitation to product sizes between

50-150bp and annealing temperature. qPCR program was set to 20 sec at 95 °C and 46 cycles of 3 sec at 95 °C and 30 sec at 60 °C. For passive reference, none was selected. Melt curve analysis indicated distinct maxima, geometric PCR efficiency of 100% was ensured by the visual assessment method.

Table 9 qPCR SYBR® green master mix

PCR-grade water	2,7 µl
KAPPA SYBR® FAST qPCR Master Mix (2x)	7,5 µl
Forward primer (diluted 1:10)	0,4 µl
reverse primer (diluted 1:10)	0,4 µl
Template DNA	4 µl

II.8.2 Taq Man® Assays

The quantitation of RNA expression levels of cardiac stress markers (β-MHC and ANP) was performed by TaqMan® Gene Expression Assays. Targets (FAM Dye) were designed using a different dye compared to the endogenous loading control, e.g. GAPDH (VIC Dye). For ANP, Mm01255747_g1 assay (#4331182 - ThermoFisher Scientific) and for β-MHC Mm00600555_m1 assay (#4331182 - ThermoFisher Scientific) was used. The master mix was prepared as mentioned in Table 10. In StepOne Software v2.3 "Comparative Ct" and "Standard run" was selected. Passive reference was set to ROX. qPCR program was set to 20 sec at 95 °C and 40 cycles of 3 sec at 95 °C and 30 sec at 60 °C. cDNA was diluted 1:100 in TE buffer.

Table 10 Taq Man® qPCR master mix

Taq Man® Gene Expression Assay (FAM) - target	0,5 µl
Taq Man® Gene Expression Assay - control	0,5 µl

Taq Man® Gene Expression master mix (2x)	0,4 µl
cDNA template (1:100 dilution)	4 µl

II.8.3 Analyzation of data

Relative expression was calculated as follows:

1. Calculation of ΔCt-values:

$$\Delta Ct\ sample\ 1 = Ct\ sample\ 1 - Ct\ endogenous\ ctrl\ 1$$

$$\Delta Ct\ sample\ 2 = Ct\ sample\ 2 - Ct\ endogenous\ ctrl\ 2$$

2. Formation of ΔΔCt value: $\Delta\Delta\ Ct\ sample = \Delta Ct\ sample\ 1 - \Delta Ct\ sample\ 2$
3. Formation of relative quantity (RQ): $2^{-(\Delta\Delta Ct\ sample)}$

Relative expression levels were used to form column graphs and for statistical analysis. Therefore, Prism7 software (GraphPad Software, San Diego, CA) was utilized. To calculate correlation between two conditions unpaired Students' t-test was performed. Results are presented as mean± standard error of mean (SEM), significant difference was set to p-values <0,05 and n represents number of separate experiments.

II.9 Microarray for differential expressed circRNAs

To investigate differential circRNA expression in TAC/sham mice, a mouse circular RNA microarray V2.0 (#AS-S-CR-M-2.0 – Arraystar, Rockville, MD) was used. RNA from 3 mice of each condition (TAC and sham) were submitted for array service to Arraystar. The RNA was extracted from isolated cardiomyocytes as described in II.1.3 and II.3.1. To ensure comparable cardiac damage of the corresponding samples before Microarray analysis, a Taq-Man® assay for β-MHC and ANP was performed (Figure 15 b). 3 TAC mice (TAC2-4) and 3 sham mice (Sham1-2, 4) were submitted to the array service.

Manufacturer summarizes the array service as follows: The concentrations of the RNA samples were determined by OD260 using a NanoDrop ND-1000 instrument. The integrity of RNA was assessed by electrophoresis on a denaturing agarose gel.

The sample preparation and microarray hybridization were performed based on the Arraystar's standard protocols. Briefly, total RNAs were digested with Rnase R (Epicentre, Inc.) to remove linear RNAs and enrich circular RNAs. Then, the enriched circular RNAs were amplified and transcribed into fluorescent cRNA utilizing a random

priming method (Arraystar Super RNA Labeling Kit; Arraystar). The labeled cRNAs were hybridized onto the Arraystar Mouse circRNA Array V2 (8x15K, Arraystar). After having washed the slides, the arrays were scanned by the Agilent Scanner G2505C. Agilent Feature Extraction software (version 11.0.1.1) was used to analyze acquired array images. Quantile normalization and subsequent data processing were performed using the R software limma package. Differentially expressed circRNAs with statistical significance between two groups were identified through volcano plot filtering. Differentially expressed circRNAs between two samples were identified through Fold Change filtering. Hierarchical Clustering was performed to show the distinguishable circRNAs expression pattern among samples. circRNAs with foldchanges ≥1.5 and p-values ≤ 0.05 were regarded as differentially expressed. Arraystar miRNA target-prediction software utilizing the TargetScan (Enright et al., 2003) and miRanda (Pasquinelli, 2012) databases was used to investigate circRNA-miRNA relationships, with the top five predicted miRNAs for each differentially expressed circRNA extracted for further analysis.

In total, 14,236 previously detected different circRNA candidates (Guo et al., 2014; Memczak et al., 2013; You et al. 2015), originating from various mouse data, including brain, liver, lung, heart, testis tissue as well as leukemia, b-cell lymphoma and embryonic stem cell lines, were investigated using the circular RNA microarray V2.0 (Arraystar).

II.10 RNAse R assay

To validate whether circRNA candidates from sequencing data obtain circular characteristics, a RNAse R resistance assay was performed. Following the protocol from Ahmed and colleagues (Ahmed et al., 2016), 2 µg total DNAse digested RNA was incubated at 70°C for 30 sec and then cooled down to 40°C for 30 sec. 20 U RNAse R (#RNR07250 - Epicentre) and 1 U/µl murine ribonuclease inhibitor (#M0314S - New England Biolabs) was added. The mix was incubated for 1 hour at 40°C. All incubation steps were performed in a PCR thermocycler (Labcycler Basic (#011-103 - Sensoquest)). RNA was isolated from the ventricle of 3 wild-type male C57BL/6 mice (II.3.2). As control all samples were mock-treated with a similar amount of H_2O instead of RNAse R. cDNA was in vitro transcribed as described in II.4.1 cDNA synthesis using Superscript II Reverse Transcriptase (SSIIRT)

with 0,5 µg RNA input. qPCR was performed following the protocol from II.8.1. with a 1:5 cDNA dilution in TE buffer, targeting the back-splice junction for circRNAs and linear junctions as degradation controls. Relative enrichment scores were adapted form Werfel et al. (Werfel et al., 2016) and calculated as follows:

$$rel.enrichment = \frac{2^{-(avg.Ct(tRNAse) - avg.Ct(ctrRNAse))}}{2^{-(avg.Ct(tMock) - avg.Ct(ctrMock))}}$$

Abbreviations displayed: avg. ΔCt = average Ct-value, tRNAse = target RNAse treated, ctrRNAse = control RNase treated, tMock = target mock-treated, ctrMock = control mock treated. GAPDH was used for the normalization control, whereas HPRT and β-actin were used as linear controls for degradation. An enrichment score above 1 was considered increased stability to RNAse R digestion compared with GAPDH. Graphs were created in Prism 7 (GraphPad Software, San Diego, CA).

II.11 RNA sequencing and bioinformatical approach to detect circRNAs

In this study, 2 different RNA sequencing data were used for identification of circRNAs. The first data derived from rRNA and poly-A depleted soleus muscle RNA of methyltransferase knockout (n=2) and wildtype (n=2) mice. The second data was rRNA depleted, total heart RNA from C57BL/6 mice (postnatal, n=2) downloaded from the ENCODE portal (https://www.encodeproject.org) with following identifiers: ENCFF002FAA and ENCFF002FAC (Davis et al., 2018).

Raw sequencing data was processed with the command-line tool reaper to remove low quality bases from read ends and trimmed reads were mapped to the mouse genome version mm10 (GRCm38) using GSNAP (Wu et al., 2010), a splice-site aware mapping tool.

The maximal mismatch rate was set to seven percent and known splice-sites from Gencode (https://www.gencodegenes.org) were used as additional input. Sorted alignments were first classified into non-spliced and spliced alignments based on the presence of XT/XS alignment tags added by GSNAP. Spliced alignments were further classified into linear splices if they spanned (potentially multiple) consecutive donor/acceptor splice sites and circular splices, if the genomic location of the (last) donor splice site was downstream of a previously used and annotated acceptor splice site. For each circular RNA detected, we then summed up circular and linear alignments spanning the splice site involved in circulation into a circular and a linear score respectively. For

the ENCODE datasets, an additional downsampling step was implemented. The reduction of reads led to a decrease of detected circRNAs by about 20%.
The previously mentioned steps were performed by the bioinformatics service group of the Max-Planck-Institute (Bad Nauheim) under the direction of Prof. Dr. Mario Looso trough Dr. Jens Preussner.

II.12 Gene expression profiles

Gene expression profiles of host genes of circRNA candidates were extracted from the publicly available BioGPS platform (http://biogps.org/#goto=welcome) based on microarray expression analysis by Su et al. (Su et al., 2004).

II.13 Gene ontology analysis

For ontology analysis, Panther V16.0 (http://pantherdb.org) (Mi et al., 2021; Mi et al., 2019), set to mus musculus, was used. Panther GO-Slim Annotation data sets are based on the data from the Gene Ontology phylogenetic annotation effort (Gaudet et al., 2011). In the statistical overrepresentation test, a list of differentially expressed genes (up- or downregulated) from microarray analysis was divided into groups based on annotation classifications (GO-Slim: Biological process) and tested against a reference list (reference genome), prepared similarly. For each Panther category, an expected number of genes based on the reference (expected value) was predicted and compared to the actual number of genes in the test list. Overrepresentation was stated, if the actual number of genes in the test list exceeded the expected value and underrepresentation if it fell below. Fisher's Exact test with Benjamini-Hochberg false discovery rate (FDR) correction for multiple testing was performed to validate statistical significance and p-value cut of was set to <0.05. Host gene GO-classifications were based on annotation of GO-Slim annotation sets for molecular and biological function, cellular component and protein class.

II.14 Primer

All primers are displayed in a 5' to 3' orientation, brackets indicate expected product sizes:

II.14.1 PCR primer

Figure 8 PCR validation of selected circRNA candidates

circZfp827

Circular (289bp)	P1: GATCTGCTGCCTGGTGAATCTGTG
	P2: CCGAGAGCTGAAAAAGCAGCTCAG
full-length	P1: CCCAGCCGGAACATTGGCTACAGC
	P2: TGATATGGAGGCTGGGGAGTCCTG
Linear (319bp)	P1: GGTGAATCTGTGCTGCACGGAAG
	P2: CACTGCCCTCAGAAGTGACAGCAC
circNeb	
Circular (267bp)	P1: GTGTACAAGTCAGATCTCCAGTGG
	P2: CTCCGGTGTATCAGGCATTACATG
full-length	P1: CTCCGGTGTATCAGGCATTACATG
	P2: GCTGGCAAGGCAGAACAGAATC
Linear (285bp)	P1: GATGTCATCCACGCTCGGCAGGC
	P2: CTGGGTCTTGTCTTTGTCCCAGGC
circSec24b	
Circular (157bp)	P1: CTACAAGAAGGGTTATCCCAGCC
	P2: CTGCTTCCTCATCCTCCTCCTGC
full-length	P1: ACCATAGTCACCATACTGCATGC
	P2: CAAGCTAGCTCCACAGCGACTCCC
Linear (269bp)	P1: CCGGCCTCCTCAGCCCGCGGTC
	P2: GATTCACAAGCAGACTATCCGGC
circNfix	
Circular (283bp)	P1: GGAAAGTACTGATGGGGAGCGGC
	P2: GCGCAGCTTGGCCAACAGCCGGG
full-length	P1: GGAAAGTACTGATGGGGAGCGGC
	P2: GCGCAGCTTGGCCAACAGCCGGG
Linear (245bp)	P1: GTGGCGGCTGGACCTGGTCATGG
	P2: GCGCAGCTTGGCCAACAGCCGGG

Figure 11 Expression of predicted circRNAs in different mouse tissues

GAPDH	
Linear (173bp)	P1: ACCACAGTCCATGCCATCAC
	P2: CATGCCAGTGAGCTTCCCGT
circZfp827	
Circular (289bp)	P1: GATCTGCTGCCTGGTGAATCTGTG

	P2: CCGAGAGCTGAAAAAGCAGCTCAG
Linear (319bp)	P1: GGTGAATCTGTGCTGCACGGAAG
	P2: CACTGCCCTCAGAAGTGACAGCAC
circNeb	
Circular (267bp)	P1: GTGTACAAGTCAGATCTCCAGTGG
	P2: CTCCGGTGTATCAGGCATTACATG
Linear (248bp)	P1: CGATTATACACAGAGGCCTGGGAC
	P2: CCCAGCTGCTTACGGTAGCCAAC
circSec24b	
Circular (157bp)	P1: CTACAAGAAGGGTTATCCCAGCC
	P2: CTGCTTCCTCATCCTCCTCCTGC
Linear (270bp)	P1: GCTAGCTCCACAGCGACTCCCTTG
	P2: CTTGGCTGGCTGAGCTGCAGGGGG
circNfix	
Circular (395bp)	P1: GTGGCGGCTGGACCTGGTCATGG
	P2: GCGCAGCTTGGCCAACAGCCGGG
Linear (245bp)	P1: GTGGCGGCTGGACCTGGTCATGG
	P2: CGTTGGGCAGTGGTTTGATGTCCG

Figure 12 Expression of selected circRNAs in cardiomyocytes and non-cardiomyocytes

circZfp827	P1: GATCTGCTGCCTGGTGAATCTGTG
	P2: TGATATGGAGGCTGGGGAGTCCTG
circNeb	P1: CCAGTGTGACTGATTCTCTGGAGC
	P2: GATTCTGTTCTGCCTTGCCAGC
circSec24b	P1: GGGTTATCCCAGCCGCAGATGTTG
	P2: CCTCCTCATCATCGGAAGCTGAT
circNfix	P1: CAGCCACATCACATTGGAGTCAC
	P2: GTTGAACCAGGTGTAGGAGAAGG

II.14.2 SYBR ® green qPCR primer

Figure 10 Relative enrichment of circRNAs after RNAse R treatment

β-actin	P1: GGCTGTATTCCCCTCCATCG
	P2: CCAGTTGGTAACAATGCCATGT

HPRT	P1: TCAGTCAACGGGGGACATAAA
	P2: GGGGCTGTACTGCTTAACCAG
GAPDH	P1: ACCACAGTCCATGCCATCAC
	P2: CATGCCAGTGAGCTTCCCGT
circZfp827	P1: GATCTGCTGCCTGGTGAATCTGTG
	P2: TGATATGGAGGCTGGGGAGTCCTG
circNeb	P1: CCAGTGTGACTGATTCTCTGGAGC
	P2: GATTCTGTTCTGCCTTGCCAGC
circSec24b	P1: GGGTTATCCCAGCCGCAGATGTTG
	P2: CCTCCTCATCATCGGAAGCTGAT
circNfix	P1: CAGCCACATCACATTGGAGTCAC
	P2: GTTGAACCAGGTGTAGGAGAAGG

Figure 12 Expression of selected circRNAs in cardiomyocytes and non-cardiomyocytes

circZfp827	P1: GATCTGCTGCCTGGTGAATCTGTG
	P2: TGATATGGAGGCTGGGGAGTCCTG
circNeb	P1: CCAGTGTGACTGATTCTCTGGAGC
	P2: GATTCTGTTCTGCCTTGCCAGC
circSec24b	P1: GGGTTATCCCAGCCGCAGATGTTG
	P2: CCTCCTCATCATCGGAAGCTGAT
circNfix	P1: CAGCCACATCACATTGGAGTCAC
	P2: GTTGAACCAGGTGTAGGAGAAGG

Figure 14 Expression profiles of selected circRNA candidates from murine heart RNA sequencing data in atrial and ventricular RNA

<u>Fhl2</u>	
circular	P1: TGTGGGTTCTCCTCCTTTAGAA
	P2: AATGCAAGAAAACCATCATGC
linear	P1: ACAGTGCTGGCCCTCATC
	P2: GCAGTGGTGGCAGTCAAAG
<u>Mmp15</u>	
circular	P1: GTGAAAGCCAACCTGCGT
	P2: AGAGCGCATGGTGGACAT

linear	P1: CTGCTACTGGTGCTTCTGGA
	P2: AGAGCGCATGGTGGACAT
Zfp827	
circular	P1: ATCTGCTGCCTGGTGAATCT
	P2: GATATGGAGGCTGGGGAGTC
linear	P1: ATCTGCTGCCTGGTGAATCT
	P2: GTCCGAACACTTTCCCACAC
Smad4	
circular	P1: GCCCCTCTACTCTTCCTCGT
	P2: CAGCAAAGGCAGGTGAGTTA
linear	P1: GCCCCTCTACTCTTCCTCGT
	P2: GGGCCATCATTTCCTCATAA

II.15 Buffers and solutions

Table 11 50x TAE (Tris-acetate-EDTA)

Tris	1210g	#5429.2 – Roth
100% Acetic Acid	285,5 ml	
0,5 M EDTA	500 ml	
MilliQ-H_2O fill up to	5 l	

Table 12 1x TAE

50x TAE	200 ml
MilliQ-H_2O, fill up to	10 l

Table 13 10x PBS

NaCl	80 g (1,37 M)	#3957.2 – Roth
KCl	2 g (27mM)	#6781.3 – Roth
Na_2HPO_4	14,4 g (100mM)	

KH_2PO_4	2,4 g (18mM)	
dissolve in ddH_2O	800 ml	
adjust to pH 7,4 (30% HCL), fill up to	1 l	

Table 14 1x PBS

10x PBS	100 ml
H_2O dest.	900 ml

Table 15 TE (Tris-EDTA) buffer

1 M Tris pH 8,0	0,5 ml
0,5 M EDTA pH 8,0	0,1 ml
MilliQ-H_2O	49,4 ml

Table 16 Calcium-free buffer

NaCl	113mM	Sigma
KCl	4,7mM	Sigma
KH2PO4	0,6mM	Sigma
Na2HPO4	0,6mM	Sigma
MgSO4 x 7H2O	1,2mM	Sigma
NaHCO3	12mM	Sigma
KHCO3	10mM	Sigma
Hepes	10mM	Sigma
Taurin	30mM	Sigma

2,3-Butanedionemonoxime	10mM	Sigma
Glucose	5,5mM	Sigma

Table 17 Enzyme buffer

Calcium-free buffer		
Liberase DH	0,25mg/ml	Roche
Trypsin	0,14mg/ml	Sigma
CaCl2	12,5 µM	

Table 18 Stop buffer 1

Enzyme buffer	
FCS	10%
CaCl2	12,5 µM

Table 19 Stop buffer 2

Enzyme buffer	
FCS	5%
CaCl2	12,5 µM

III RESULTS

III.1 Identification of circRNA candidates

In a first step, in-house generated RNA sequencing data were used to develop and test a novel bioinformatic approach detecting circRNA candidates (as displayed in II.11). Therefore, sequencing data from rRNA and poly-A depleted murine soleus muscle samples (Figure 6 a), as well as data from rRNA depleted murine heart samples, were analyzed (Figure 6 b). In order to identify novel circRNAs in soleus muscle, bioinformatic analysis was performed using *methyltransferase like 21c* (*Mettl21c*) knockout (mt1-2) and wildtype (wt1-2) RNA sequencing data. METTL21C resembles a skeletal muscle-specific lysine methyltransferase modulating protein degradation in skeletal muscle (Wiederstein et al., 2018). Until now, differential expressed circRNAs in *Mettl21c* knockout soleus muscle have not been investigated. However, we do not assume any impact of METTL21C deficiency on circRNA formation, since METTL21C does not act on RNA.

On average, approx. 3.300 circular RNA candidates were identified per sample (Figure 6 a). The overlap of wt replicates comprise 155 candidates (7,7% and 5,4% of detected candidates in wt1 and 2), in contrary to mt replicates, which display an overlap of 130 candidates (5,1% and 9,7% of mt1 and mt2). Taking all data into account, only 47 circRNA candidates were commonly identified among all samples (0,6% of all detected candidates).

In parallel, the bioinformatic approach was applied to two publicly available adult, rRNA depleted, mouse heart RNAseq data sets (derived from ENCODE as mentioned in II.11) (ENCFF002FAA and ENCFF002FAC). Additionally, a downsampling analysis was integrated to detect candidates with higher accuracy, resulting in a reduction of approximately 20% of overall detected circRNA candidates. As a result, 147 and 203 robust circRNA candidates were detected in the ENCFF002FAA and ENCFF002FAC data set, respectively (Figure 6 b). The striking lower number of circRNA candidates compared to results from soleus muscle (on average 20- fold less detected circRNAs in heart samples) could be due to different experimental methods and bioinformatic analyses. For soleus muscle, an RNAseq library preparation protocol containing a poly-A depletion step was used to enhance circRNA detection.

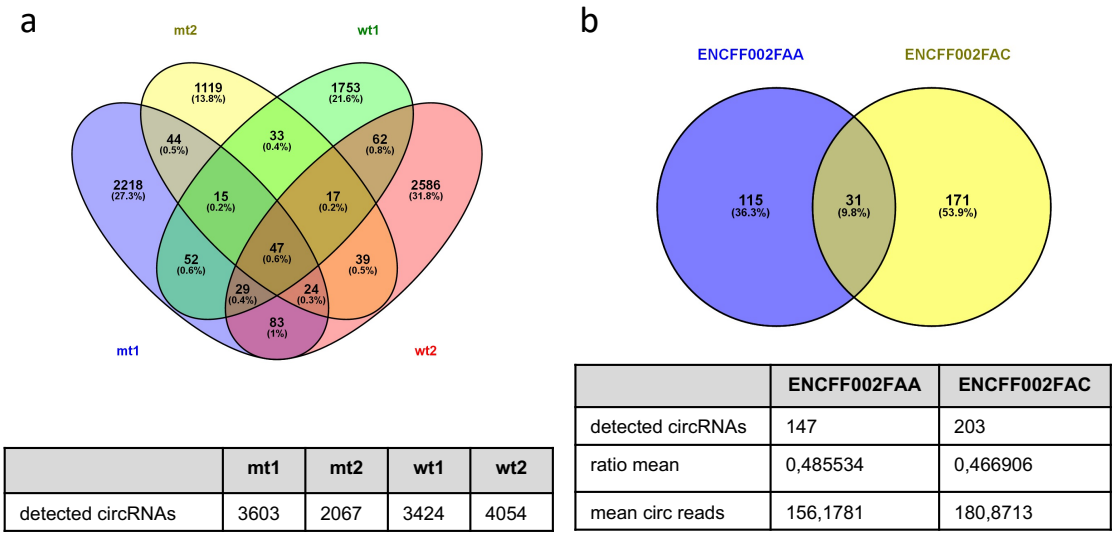

	mt1	mt2	wt1	wt2
detected circRNAs	3603	2067	3424	4054

	ENCFF002FAA	ENCFF002FAC
detected circRNAs	147	203
ratio mean	0,485534	0,466906
mean circ reads	156,1781	180,8713

Figure 6 Application of circRNA detection approach using pre-existing RNA sequencing data

Venn diagrams of circRNA predictions from the in-house detection approach. a) Overlap of detected circRNA candidates in *methyltransferase like 21c* (*Mettl21c*) knockout (mt1-2) and wildtype (wt1-2) mouse using soleus muscle ribo-minus and poly-A negative RNA sequencing data. b) Robust heart circRNA candidates detected in 2 biological replicates (ENCFF002FAA and ENCFF002FAC) using rRNA depleted, total RNA sequencing of the mouse heart after downsampling analysis. *Ratio mean* defines the mean circular reads normalized to the sum of circular and liner reads for all detected circRNA candidates. *Mean circ reads* indicates the average read count per candidate. Total sums of venn diagram and chart differ due to multiple detections. The term *detected circRNAs* indicates the number of identified candidates per sample.

In contrast, preexisting heart sequencing data from ENCODE made use of rRNA depleted RNA and the subsequent circRNA detection pipeline implemented a downsampling analysis to improve the quality of detected circRNA candidates, thereby reducing the number of candidates.

In total, 115 candidates (36.3% of all candidates) in ENCFF002FAA and 171 candidates (53.9% of all candidates) in the ENCFF002FAC data set were distinctly detected. The overlap between both heart samples comprises a total of 31 candidates (9.8% of all candidates). Detailed analysis of identified candidates in ENCFF002FAA revealed, that the majority derives from exonic sequences (84.3%), followed by intronic (8.9%) and

intergenic (6.8%). For quantification, read counts were studied. On average, 156 circular reads per candidate were detected in ENCFF002FAA. Subsequently, circular reads were normalized to the sum of circular and linear reads of individual loci. The mean of this analysis for all circRNA candidates approaches 0.5 (Figure 6 b mean ratio), indicating similar expression level of circRNAs and linear RNAs of the same host gene. Comparable results were obtained from the ENCFF002FAC dataset. Here, 87.1% of candidates derive from exons, 9.4% from introns and only 3.5% from intergenic loci. The average circular read count is approximately 180 whereas the ratio count averages 0,49.

III.2 Validation of predicted circRNA candidates

To test our in-house bioinformatics circRNA detection pipeline, 4 candidates were selected, which were repetitively identified in the overlap of all replicates from soleus muscle sequencing data (Figure 6 a). For simplification purposes, candidates were named according to their host gene. CircZfp827 represents the first candidate, which derives from the widely expressed *zinc finger protein 827* (*Zfp827*) gene, mediating transcriptional regulation, as well as exerting nucleic acid binding capacities (Gaudet et al., 2011). The second candidate, circNeb, originates from the *nebulin* (*Neb*) gene, which is highly expressed in skeletal muscle and acts as an integral part of the muscle sarcomere. NEB exerts important functions in the regulation of actin filament length, sarcomere organization and cardiac muscle thin filament assembly. Furthermore, *Neb* mutations result in a muscle disease called Nemaline Myopathy, characterized by a progressing muscle weakness (Labeit et al., 2011). The third selected circRNA candidate represents circSec24b, encoded by the *Sec24 related gene family, member B* (*Sec24b*) gene. SEC24B is ubiquitously expressed and mediates protein and zinc ion binding capacities. It is involved in morphogenesis of various organs such as the auditory and circulatory system (Gaudet et al., 2011). Lastly, circNfix, a circular RNA candidate originating from the host gene *nuclear factor I/X* (*Nfix*), was selected. *Nfix* encodes for a transcription factor, involved in various developmental processes in the brain such as astrocyte differentiation, cerebellar Purkinje cell layer development, cerebellar granule cell differentiation and cerebellum development (Gaudet et al., 2011).

Since next generation sequencing generates relatively short reads, these circular reads are mainly restricted to the characteristic back-splice junction. This junction consists of the two exons forming the circRNA via circular splicing. In relation to the reference genome, these exons label beginning and end of the circRNA. As a result, alignment of circular

reads to the reference genome GRCm38 (Genome Reference Consortium Mouse Reference 38, INSDC Assembly, Jan 2012) generates start and end of the corresponding circRNA (referred to as start and end). However, neither exon/intron composition, nor total length of the circRNA candidates can be predicted using standard NGS. The genomic position, that can be obtained from these data for the 4 selected circRNA candidates is shown in Figure 7 a.

CircZfp827 represents a circRNA encoded by the Zfp827 gene locus (Figure 7 b), characterized by back-splice junction reads spanning exon 8 and 6 of the linear isoform (Zfp827-201) (Figure 7 c). As a consequence, circZfp827 might encode variable intronic and exonic sequences flanked by circularized exons 8 and 6.

Length predictions for the selected candidates demonstrate that circZfp827, circNeb and circSec24b might contain multiple exons, whereas circNfix encodes only a single exon (Exon 2) (Figure 7 a). Generally, circRNAs can originate from different genomic regions, including exonic, intronic or intergenic sequences (as described in I.2). However, in our study, we selected only circRNAs, which encode back-splice junction sites derived from exons.

a

ID	type	chromosome	start	end	strand	hostgene	length (nt)	cicularized exons
circZfp827	exonic	8	79118175	79136664	+	ZfP827	18489	E8 - E6 (Zfp827-201)
circNeb	exonic	2	52243193	52246865	-	Neb	3672	E70 - E67 (Neb-002)
circSec24b	exonic	3	129996681	130020643	-	Sec24b	23962	E12 - E4 (Sec24b-001)
circNfix	exonic	8	84771784	84772316	-	Nfix	532	E2 - E2 (Nfix-001)

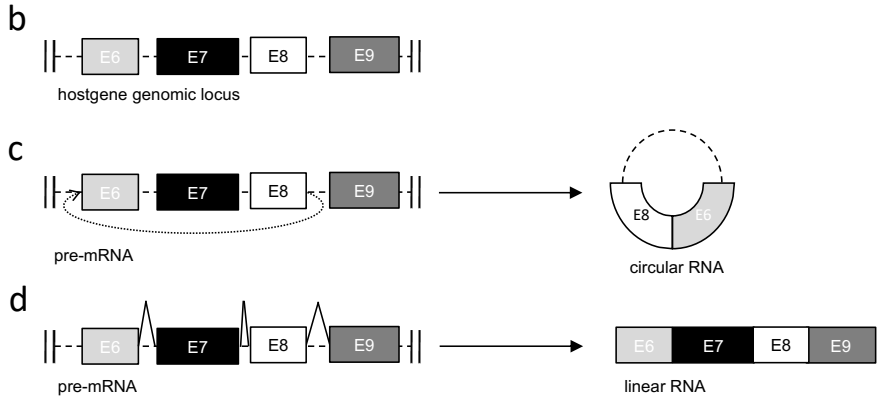

Figure 7 Validation of selected candidates from the soleus muscle

a) Overview of 4 selected circRNA candidates deduced from the overlap of soleus muscle RNAseq data. *Chromosome, start* and *end*, as well as *strand*, refers to the genomic position of predicted circRNAs in GRCm38. *Type* indicates whether the circRNA originates from exons, introns or intergenic regions. *Length* displays the estimated maximum size of the predicted circRNA including all exons and introns within the circularized exons. The term *circularized exons* defines both exons forming the circular junction in regard to a linear isoform (bracketed) b) Host gene locus of Zfp827-201 transcript spanning exon 6-9. c) Circular splicing (dotted arrow) forms a back-splice junction from exon 8 to exon 6, resulting in a circRNA with either retained or removed exon 7 (indicated by dotted lines). d) In contrast, linear splicing (straight lines) events results in a product with ascending exon numbers. Exon numbering based on annotated linear transcript in the region of circRNA (transcript name bracketed). E=exon.

To validate selected circRNA candidates, back-splicing specific RT-PCRs were established as described in II.5.1. For each selected candidate, a convergent primer pair (Figure 8 b) (in respect to the mature circRNA sequence - divergent in regard to genomic sequence) spanning the characteristic circular junction, was designed. To amplify the entire circRNA, a second primer pair with divergent primers (in respect to the mature circRNA template, as well as the genomic sequence) within one of the circularized exons, was designed (Figure 8 c). Following this approach, full-length sequences of our circRNA candidates, including the characteristic back-splice junction, can be determined by PCR amplification and direct Sanger sequencing, thereby indicating differential inclusion or exclusion of exons. As a gene-specific control, we made use of RT-PCR covering linear splice junctions adjacent to one of the circularized exons (Figure 8 d).

As depicted in Figure 7 a, RNA sequencing revealed, that circNfix derives from a single exon (exon 2 of the Nfix-001 transcript) of approximately 530 nt. Due to the relative short size of the potential PCR product, we designed one primer pair to detect the circular junction as well as the full-length circRNA simultaneously for this candidate. RT-PCR products are depicted after gel-electrophoresis in Figure 8 e.

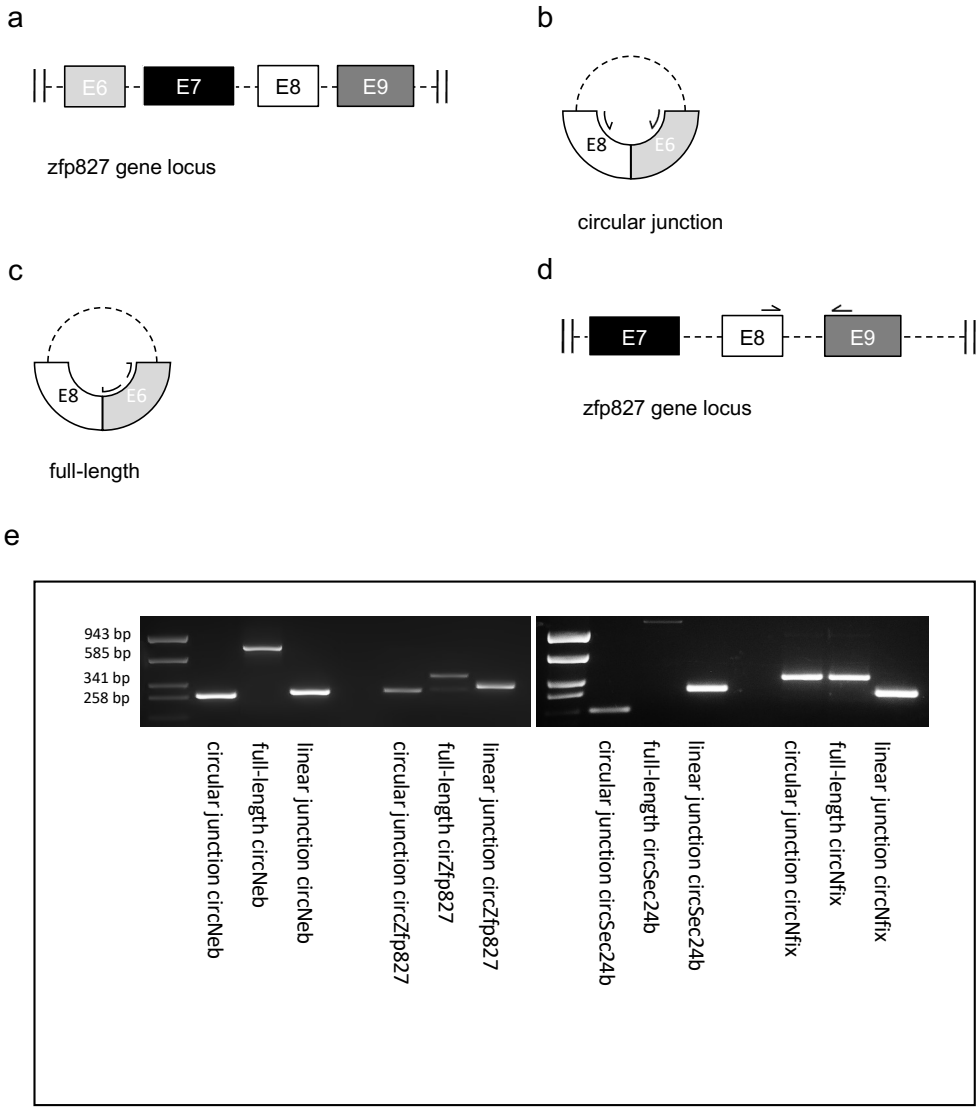

Figure 8 PCR validation of selected circRNA candidates

a) Exemplary illustration of the Zfp827 host gene locus (exon numbers for transcript zfp827-201) of circZfp827. Sanger sequencing of PCR fragments revealed a circular junction comprising exon 6 and 8. E=exon. b) Two inward-facing primer were used in RT-PCR to amplify specifically the circular junction (exon 8 to exon 6). E=exon. c) For amplification of the full length circRNA, outward-facing primer in a selected circularized exon were used. E=exon. d) As control, a linear junction in the vicinity of the circularized exons was targeted (exon 8 to 9). E=exon) PCR results for the 4 circRNA candidates circNeb, circZfp827, circSec24b and circNfix using soleus muscle RNA as template. RT-PCR conditions according to Table 7, primer list displayed in II.14.1. Water controls are not displayed and were negative. N=3.

In summary, all predicted circular junctions from our circRNA candidates were detected by RT-PCR in parallel to the corresponding control linear splice junctions.

Due to primer design, the size of full-length and circular junction amplificants differs for all candidates except circNfix. The calculated circular junction PCR sizes are 289bp for circZfp827, 267bp for circNeb and 157bp for circSec24b (II.14.1). The resulting amplicon product size generated by full-length PCR exceeds the size of the sum of both circularized exons for all candidates but circNfix, indicating inclusion of various introns or exons in the circular RNA candidates. However, full-length PCR products are considerably shorter than the predicted maximum calculated length encompassing all potential exons and introns from RNA seq analysis (Figure 7 a). For example, circZfp827 was predicted to have a maximum length of about 14.000 nt, whereas full-length PCR fragment size is around 400bp. In summary, these findings indicate, that introns and/or exons are excluded during the process of circRNA generation for these candidates.

Interestingly, circZfp827 full-length PCR identified a second, smaller PCR amplification product of 340bp size, indicating an additional circRNA isoform generated by an exclusion of exonic or intronic sequences.

For sequence analysis, full-length and circular junction products from Figure 8 e were processed as described in II.6 and II.7. The back-splice junction was confirmed by Sanger sequencing in all circular junction PCR amplificants, as well as in most full-length products. As suggested by the full-length PCR product size in Figure 8 e, Sanger sequencing detected, that circZfp827, as well as circNeb, encode multiple exons (Figure 9): Analogous to the corresponding linear transcripts, circular counterparts contain all exons flanked by both circularized exons. Hence, circZfp827 contains 3 exons, whereas circNeb consists of 4 exons. In contrast, circNfix includes exclusively circularized exon 2 (sequences displayed in XI.1.).

All 4 analyzed circRNAs lack intronic sequences and can therefore be categorized as exonic circRNAs. Due do experimental constrains, we were unable to determine the entire sequence of circSec24b, most likely due to premature termination of the direct PCR sequencing. As a result, we were only able to detect exon 4 to 7, lacking the back-splice junction.

ID	circularized exons	sequencing result	length
cicZfp827	E8 - E6 (Zfp827-201)	E6→E8-E7-E6	402bp
circNeb	E70 - E67 (Neb-002)	E67→E70-E69-E68-E67	729bp
circSec24b	E12 - E4 (Sec24b-001)	E4-E5-E6-E7	779-1232bp
circNfix	E20 - E20 (Nfix-001)	E20→E20	532bp

Figure 9 Full-length sequencing results

Results from Sanger sequencing of full-length RT-PCR amplificants from Figure 8. For circZfp827, circNeb, and circNfix, sequencing revealed, that only exons within the circular junction are retained in the circRNA sequence. For circSec24b, sequencing was incomplete and the circular junction not detected. The length stated is only an estimate based on the RNAseq results. Accordingly length can only be estimated.
Arrows indicate back-splice junctions, dashes linear junctions. E = exon. Exon numbering based on annotated linear transcript in the region of circRNA (transcript name bracketed).

Although the PCR amplification of the back-splice junction is a characteristic of circRNAs, this phenomenon might also occur in linear RNAs due to template switching during cDNA synthesis, trans-splicing, tandem duplications or read mapping artefacts (described in I.5). Therefore, an additional verification is necessary to proof the circular properties of the investigated candidates. A commonly used experimental approach to test circularity is the enrichment of circRNAs after RNAse R treatment. RNAse R is a 3' to 5' exoribonuclease, which preferentially degrades linear RNA from the 3' end. In contrast, circRNAs are protected against RNAse R degradation since they do not provide accessible 3´ends (Figure 10 a). Accordingly, circRNAs are enriched after RNAse R treatment in comparison to linear RNA.

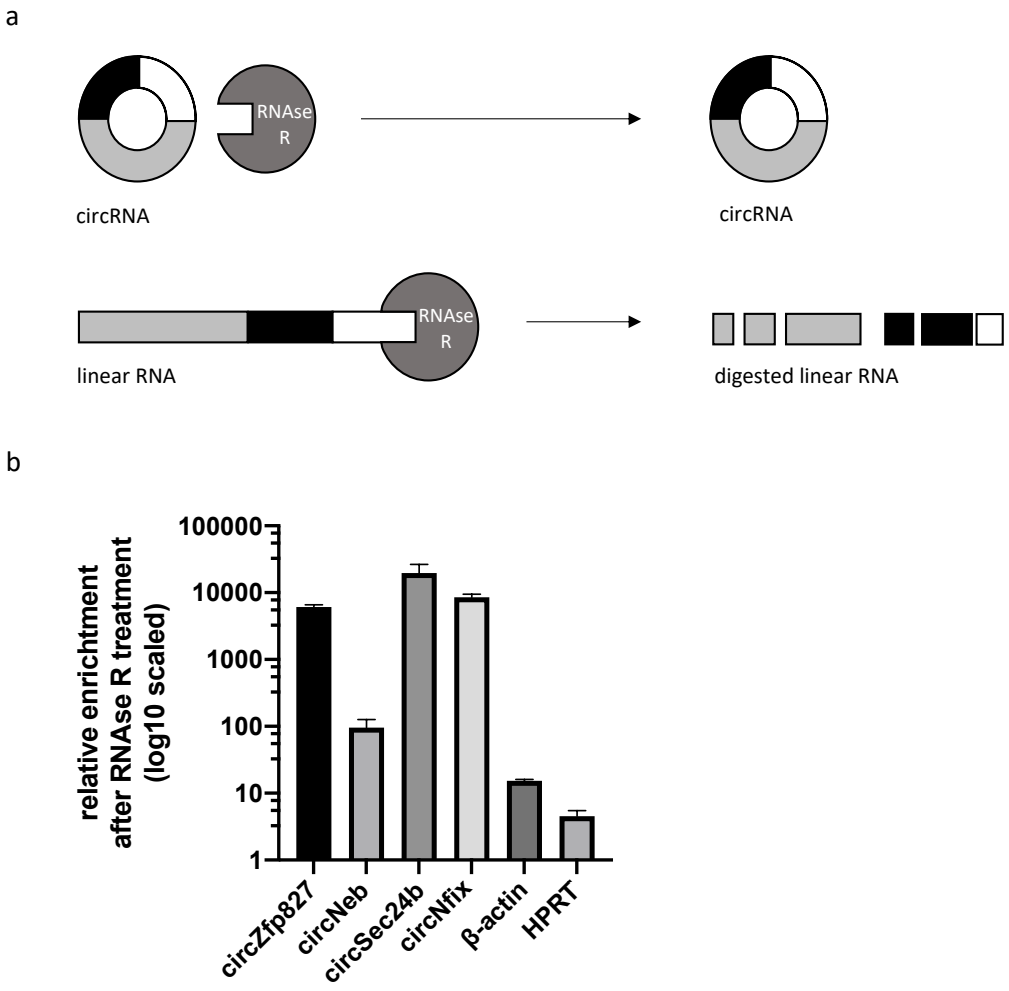

Figure 10 Relative enrichment of circRNAs after RNAse R treatment

a) Schematic view of RNAse R activity: RNAse R acts as a 3‘ to 5‘ exoribonuclease, degrading all linear RNAs from the unprotected 3‘ ends, whereas circRNAs are protected. b) Relative enrichment after RNAse R treatment for circular (circZfp827, circNeb, circSec24b and circNfix) and linear targets (β-actin, HPRT) compared to water control. Values above 1 indicate increased stability compared to linear control (GAPDH). Total ventricular RNA (N=3) was used for quantification via qPCR (protocol as mentioned in II.10, primer list in II.14.2). All graphs presented as mean ±SEM.

All 4 previously characterized circRNA candidates (circZfp827, circNeb, circSec24b and circNfix) were tested in comparison to linear HPRT and β-actin controls according to II.10. Relative enrichment scores were calculated based on GAPDH-normalized Ct-values from qRT-PCR targeting circular or linear junctions in RNAse R compared with untreated RNA. Enrichment scores higher than 1 indicate increased stability of the target compared to linear GAPDH.

Since the overall aim of this study was the identification of novel circRNAs in heart, we thereafter switched to RNA isolated from the heart ventricle. Specific circRNA back-splice junctions in ventricle were validated by RT-PCR previously (distinct expression was detectable for all targets except for circSec24b).

As a result, circRNA candidates circZfp827, circSec24b and circNfix demonstrate explicit high relative enrichment scores (values range from 6126±483.9 to 19604±6948), thereby indicating circular properties (Figure 10 b). In contrast, linear controls comprising HPRT and β-actin are affected by RNAse R treatment as demonstrated by the severe decline of relative enrichment scores (β-actin 15.28±0.72, HPRT 4.54±0.95). Notably, values do not fall below 1, herby indicating increased stability compared to GAPDH.

These results are most likely due to a different RNAse R-based degradation of the linear targets and GAPDH, as the latter was used for normalization in the process of enrichment score formation (see II.10). Interestingly, circRNA candidate circNeb displays lower enrichment compared to the other circRNA candidates (96.01±30.49), but significantly higher values than linear controls.

In conclusion, these results provide a strong proof regarding the circularity of circZfp827, circSec24b, circNfix and circNeb. Increased stability to RNAse R treatment was demonstrated for circNeb as well, even though it was significantly lower than for the other circRNAs.

III.3 circRNAs identified by RNA sequencing of soleus muscle are differentially expressed in various mouse tissues

To investigate whether circRNAs deduced from soleus muscle RNAseq data are expressed in other mouse tissues, a semi quantitative RT-PCR detecting the circular junction was performed using cDNA from heart, lung, soleus muscle (SM), extensor digitorum longus muscle (EDL), kidney and aorta (Figure 11).

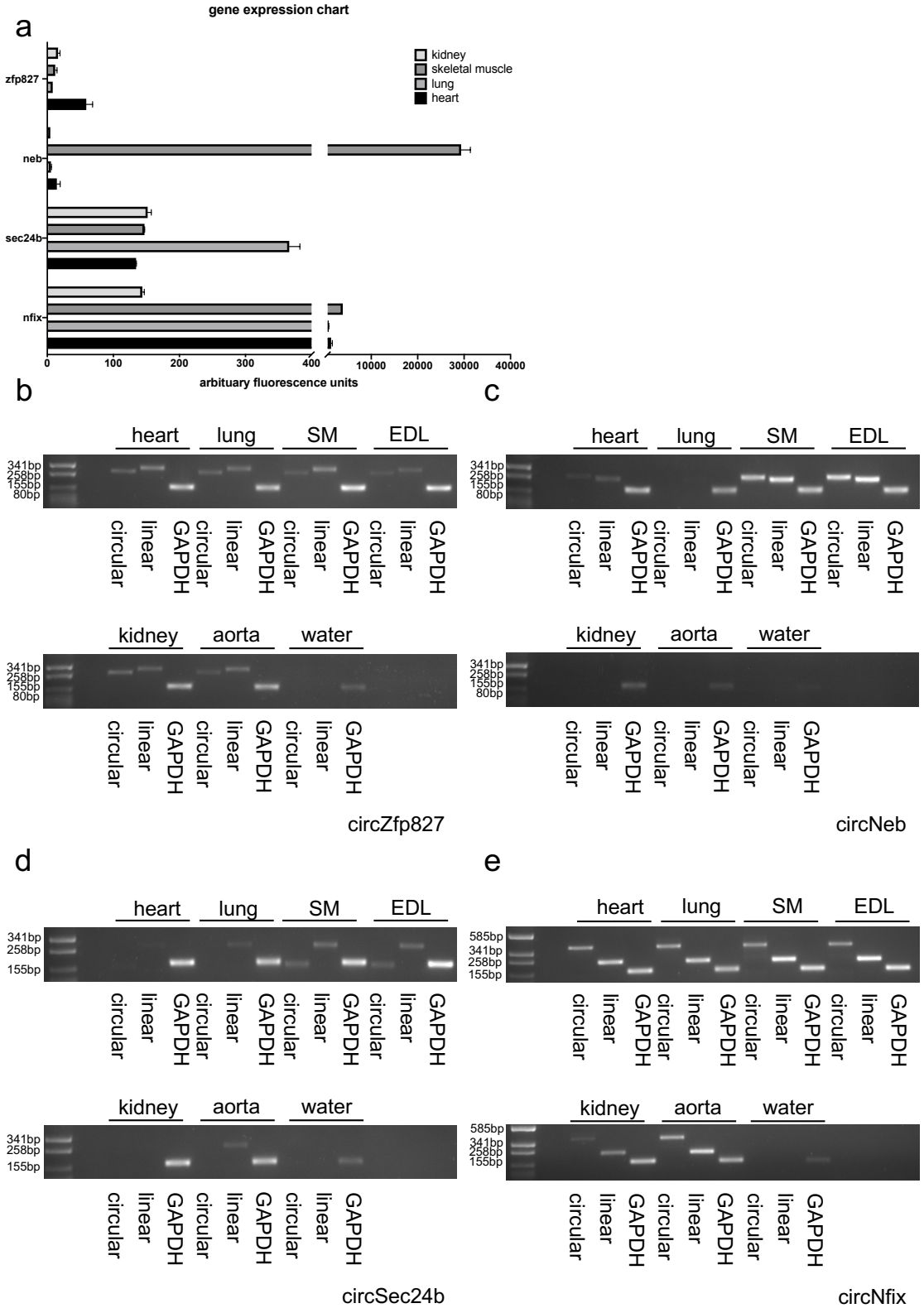

Figure 11 Expression of predicted circRNAs in different mouse tissues

a) Gene expression profiles of linear mRNA transcripts in various mouse tissues based on BioGPS b) - e) Semi quantitative RT-PCR detecting the circular and linear junctions

of circRNA and corresponding linear transcripts derived from host genes: b) CircZfp827 and *Zfp827*, c) circNeb and *Neb*, d) circSec24b and *Sec24b*, e) circNfix and *Nfix*. GAPDH was used as positive, water as negative control. N=3. PCR protocol as mentioned in Table 7, primer sequences are listed in II.14.1. SM = soleus muscle, EDL = extensor digitorum longus muscle.

As a result, circZfp827 and the linear mRNA are expressed in heart, lung, SM, EDL and aorta (Figure 11 b). In contrast, circNeb, is exclusively detected in heart, SM and EDL, along with the corresponding linear isoform (Figure 11 c). These findings are consistent with the previously reported expression profile of Neb in mouse, which is restricted to skeletal muscle (Figure 11 a). However, the circular junction of circSec24b is solely detectable in SM and EDL tissue. Here, the linear counterpart is expressed as well. In contrast, for heart, lung and aorta, exclusively the linear transcript was detected, whereas in kidney neither circular, nor linear transcripts do exist (Figure 11 d).
In addition, the circular, as well as the linear junction of circNfix, are detected in all investigated tissues (Figure 11 e).
In summary, circRNA junctions from all investigated circRNAs co-occur with the corresponding linear junctions of the host genes. However, circRNAs differ in their expression profiles: CircZfp827 and circNfix are detected in all investigated tissues, whereas RT-PCRs detecting the circular junction of circNeb and circSec24b revealed a specific expression exclusively in muscle tissue. Here, circNeb is detected in heart, SM and EDL. In contrast, circSec24b is only detected in skeletal muscle (SM, EDL).
(Figure 12) (illustrated in II.8).

To quantify the expression of circRNAs in heart more precisely, quantitative PCR covering the circular junction (illustrated in II.8) was performed using isolated cDNA from adult cardiomyocytes (cm) and non-cardiomyocytes (non-cm) (Figure 12). Cardiomyocyte-specific ANP is significantly reduced in the non-cardiomyocyte fraction (mean rel. expression in non-cm's 0.00±0.00 vs. mean rel. expression in cm's 1.03±0.19, p=0.02), indicating the separation of both fractions (Figure 12 a).

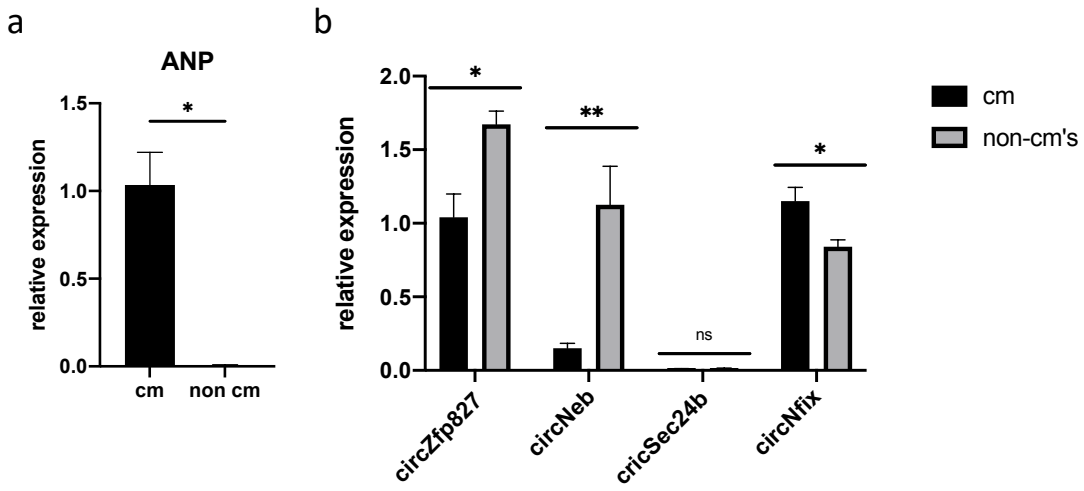

Figure 12 Expression of selected circRNAs in cardiomyocytes and non-cardiomyocytes

a) Taq Man® Assay targeting *Anp* mRNA expression in cardiomyocytes and non-cardiomyocytes (n=4, samples normalized to GAPDH, assay see II.8.2). b) SYBR® green qPCR for circular junctions of circZfp827, circNeb, circSec24b and circNfix in cardiomyocytes and non-cardiomyocytes (n=4, samples normalized to GAPDH, primer list see II.14.2). All graphs are presented as mean ±SEM with p values *<0.05, **<0.01 and ns = not significant.

Expression level of circular RNAs in CMs and non-CMs varies strongly for each target circRNA. CircZfp827 and circNeb are significantly more abundant in non-cardiomyocytes (mean rel. expression level for circZfp827 in non-CMs 1.67±0.09 vs. 1.04±0.16 in CM's, p=0.01 and mean rel. expression level for circNeb in non-CMs 1.13±0.26 vs. 0.15±0.03 in CM's, p=0.01) up to approximately 7-fold in case of circNeb. In contrast, circNfix displays a higher expression in cardiomyocytes (mean relative expression in CM's 1.15±0.09 vs. 0.84±0.05 in non-CM's, p=0.04). However, circSec24b displays low expression without statistical significance between these two fractions (mean rel. expression in CM's 0.01±0.00 vs. 0.01±0.00, p=0.47) (Figure 12 b). This finding is consistent with the results of RT-PCR on the circular junction of circSec24b in cardiac tissue (Figure 11 d).

III.4 Characterization of common circRNA candidates derived from murine heart sequencing data

As described in III.1, our bioinformatic circRNA detection approach reanalyzed a publicly available data set of two biological replicates (ENCFF002FAA and ENCFF002FAC) of rRNA depleted mouse heart RNA (Figure 6 b). In total, 31 circRNAs (9,8% of all detected candidates) were identified in both replicates and subsequently selected for further validation (Figure 13 a). For simplification, the nomenclature of circRNA candidates was adapted to the corresponding host gene. In accordance with the distribution of circRNA types in both individual samples, ENCFF002FAA and ENCFF002FAC (see III.1 and Figure 6 b), the majority (87%) of the overlapping candidates derive from exons. Only a minority (6,5%) originates either from intron or intergenic regions. Interestingly, approximately 35% of all candidates were previously predicted in soleus muscle data (Figure 6 a), whereas the majority of candidates (58%) were solely detected in heart. A small 6% of candidates are circular isoforms of previously discovered circRNAs from soleus muscle data.

To further categorize the corresponding host genes of the identified circRNAs, we performed a gene ontology analysis (as described in II.13) (Figure 13 b). Host genes annotate mainly to molecular function categories *binding* and *catalytic activity*, as well as *molecular function regulators for molecular function*. Regarding biological processes, the majority of the circRNA host genes is involved in *metabolic* and *cellular processes* and *biological regulation*. For cellular component, top annotations are *cellular anatomical entity, intracellular and protein containing complex*. Proteins translated from candidate host genes are mainly annotated to *gene-specific transcriptional regulators, metabolite interconversion enzyme and protein modifying enzymes*.

Expression levels of circRNAs were calculated using normalized circular read counts to the sum of circular, as well as linear reads for each candidate (as mentioned in III.1). Candidates with a predominant expression of the circular isoform have values above 0.5, whereas candidates with a higher expression of the linear isoform show values below 0.5. The resulting heat map (Figure 13 c) shows strong heterogeneity in the expression levels of the circRNAs studied in both biological replicates. Therefore, this quantification approach was not pursued further and instead qPCR of selected candidates was performed.

a

name	position	type	symbol
circGigyf2	chr1:87364104|87380008	exon	Gigyf2
circintergen1	chr9:13619990|13621675	intergen.	
circAlg12	chr15:88811297|88812159	exon	Alg12
circMboat2	chr12:24878191|24882794	exon	Mboat2
circFbxw4	chr19:45630865|45640521	exon	Fbxw4
circTulp4	chr17:6137211|6139156	intron	Tulp4
circNfkb1	chr3:135655500|135669339	exon	Nfkb1
circEefsec	chr6:88355483|88358642	exon	Eefsec
circZfp827	chr8:79118175|79136663	exon	Zfp827
circTtc3	chr16:94383912|94403368	exon	Ttc3
circCasc5	chr2:119076936|119081625	exon	Casc5
circMettl9	chr7:121047838|121057399	exon	Mettl9
circPtpn14	chr1:189786636|189798681	exon	Ptpn14
circTaok1	chr11:77571607|77585494	exon	Taok1
circPhf21a	chr2:92214049|92230724	exon	Phf21a
circEif3c	chr7:126551975|126552338	exon	Eif3c
circGm21992	chr19:4792398|4794009	intron	Gm21992
circRad52	chr6:119920110|119921028	exon	Rad52
circIgf1r	chr7:68003810|68004355	exon	Igf1r
circMlip	chr9:77173959|77217048	exon	Mlip
circMeis2	chr2:115921672|116049198	exon	Meis2
circMyocd	chr11:65218529|65233184	exon	Myocd
circTtc3	chr16:94383912|94393174	exon	Ttc3
circintergen2	chr17:81647809|81649638	intergen.	
circSmad4	chr14:47016277|47016795	exon	Samd4
circHipk3	chr2:104470749|104471847	exon	Hipk3
circOgdh	chr11:6313788|6317080	exon	Ogdh
circFhl2	chr1:43141698|43153254	exon	Fhl2
Circmt-Rnr2_2	chrMT:2162|2672	exon	mt-Rnr2
Circmt-Rnr2_1	chrMT:1623|1844	exon	mt-Rnr2
Circmt-Rnr2_3	chrMT:2295|2663	exon	mt-Rnr2

commonly identified in soleus muscle

isoform identified in soleus muscle

new circRNA candidate

b

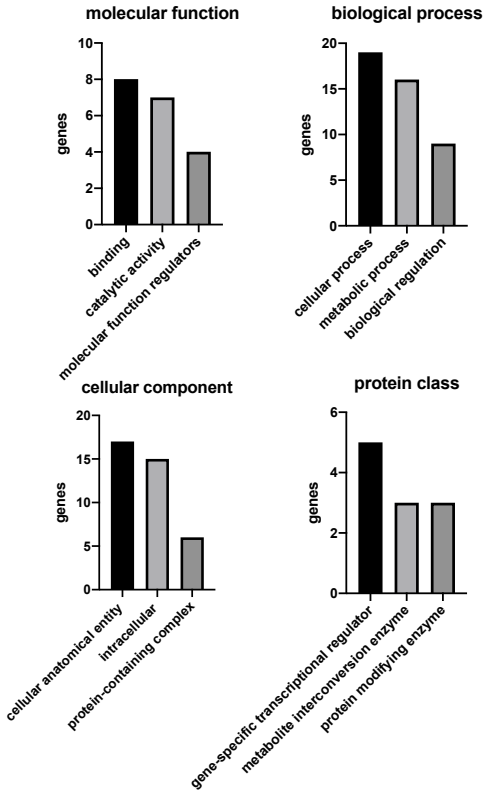

c

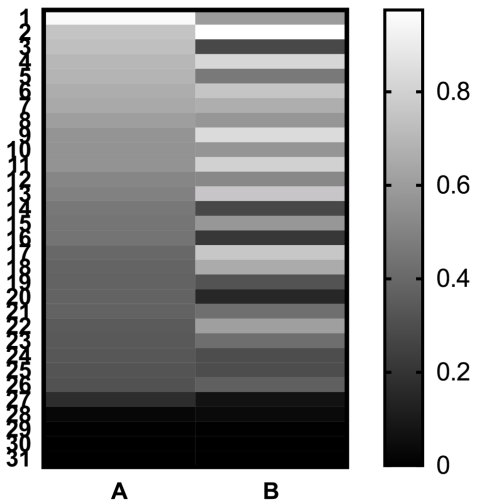

A: ENCFF002FAA
B: ENCFF002FAC

Figure 13 circRNA predictions from murine heart sequencing data

a) Compendium of the 31 predicted circRNAs identified in both heart replicates (ENCFF002FAA & ENCFF002FAC, Figure 6 b). Candidates are depicted as follows:

Name, position (chromosome: start|end), *type* (circRNA type), *symbol* (host gene symbol). b) Top 3 annotations of GO-slim analysis of host genes displaying functional classifications: Molecular function, biological process, cellular component and protein class c) Heatmap depicting the distribution of expression levels of circRNA candidates based on circular reads normalized to the sum of circular and linear reads.

III.5 Cardiac circRNA candidates are differentially expressed compared to linear counterparts

To validate predicted circRNAs deduced from heart (Figure 13 a), we selected 3 candidates, which were identified in the overlap of both replicates (circZpf827, circSmad4, circFhl2), as well as one candidate, which was uniquely detected in one of the replicates (circMmp15) for qPCR analysis (Figure 14). Since our bioinformatic quantification analysis resulted in heterogenous results, we selected candidates derived from functional relevant host genes for experimental quantification. Corresponding qPCRs were performed as described in II.8.1, primers are listed in II.14.2. CircSmad4 derives from the *SMAD family member 4* (*Smad4*) gene, which is ubiquitous expressed in mouse tissues. SMAD4 exhibits various functions by mediating transforming growth factor-β (TGF-β) and bone morphogenetic protein (BMP) signaling in cardiomyocytes, to maintain heart homeostasis (Umbarkar et al., 2019). CircFhl2 originates from the *four and a half Lim domains 2* (*Fhl2*) gene and encodes a protein involved in several signaling pathways and processes of development and cellular differentiation, including maturation and maintenance of the cardiovascular system (Kong et al., 2001). In contrast, circMmp15 was exclusively identified in the RNA sequencing sample ENCFF002FAA and the corresponding host gene *matrix metallopeptidase 15* (*Mmp15*), encodes a preprotein of the matrix metalloproteinase family, acting in the degradation of extracellular matrix, e.g., in tissue remodeling processes (O'Leary et al., 2016). CircZfp827 was originally detected in our soleus muscle data set and its host gene function was previously characterized (see III.2). To experimentally validate our candidates, we made use of qPCR based on atrial and ventricular RNA to quantify the abundance of the circular and the adjacent linear splice junctions (II.8). Figure 14 a displays the resulting relative expression levels of circRNA candidates in comparison to their linear counterparts in atrial RNA. As a result, circZfp827 and circSmad4 display no significant difference, although a trend towards increased linear expression is detectable for circSmad4.

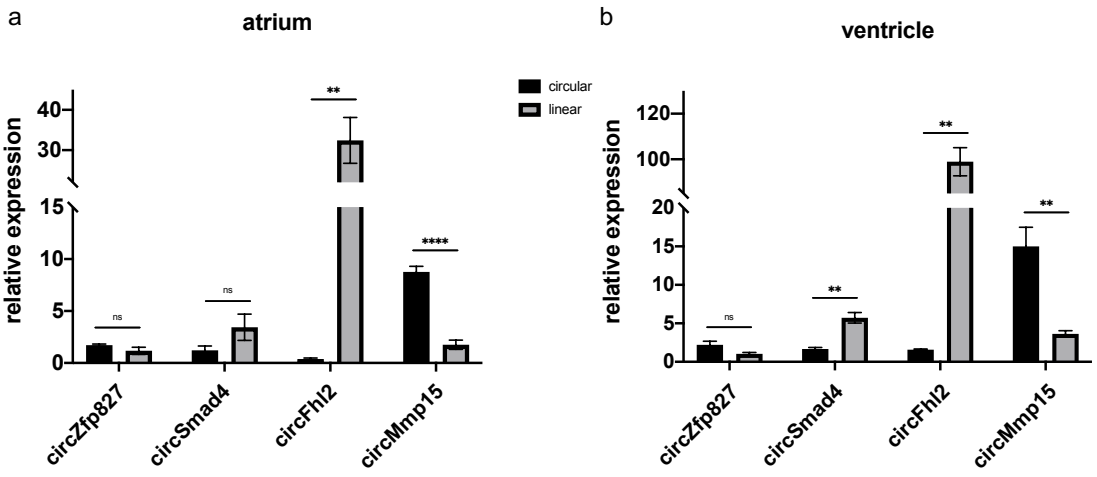

Figure 14 Expression profiles of selected circRNA candidates from murine heart RNA sequencing data in atrial and ventricular RNA

Relative expression analysis of circRNA candidates circZfp827, circSmad4, circFhl2, circMmp15 (retrieved from Figure 13) by qPCR in comparison to linear isoforms using atrial (a) and ventricular (b) RNA. For circular RNAs, the back-splice junction was amplified, whereas an adjacent linear junction was used for linear isoforms. N=4 in all experiments. All targets were normalized to GAPDH. Graphs are presented as mean ±SEM with p values *<0.05, **<0.01, ***<0.001, ****<0.0001 and ns = not significant.

Regarding *Fhl2*, the circular isoform is much less abundant compared to the linear isoform (mean linear relative expression= 32.42 vs. mean circular relative expression= 0.35). In contrast, circMmp15 displays a significant, approximately 5-fold higher expression compared to the linear counterpart. For ventricular RNA, expression patterns were similar in comparison to atrial RNA (Figure 14 b). Interestingly, the previously described trend toward higher expression of linear Smad4 in the atrium is significant with ventricular RNA. CircMmp15 displays the overall highest abundance in both, ventricular and atrial RNA, compared to the linear counterpart.

In summary, the majority of investigated circRNA candidates show a differential expression level compared to their linear counterparts, suggesting regulatory processes in circRNA biogenesis, rather than a simple co-expression of circular and linear isoforms.

III.6 circRNA expression in a murine TAC-induced hypertrophy model

The TAC surgery model is a widely used procedure to induce cardiac hypertrophy and ultimately heart failure in mice by pressure overload via constriction of the transverse aorta (see II.1). Accordingly, it is used to study pathogenesis of cardiac hypertrophy and heart failure in cardiovascular research (Bosch et al., 2020). Since multiple circRNAs are known to be involved in hypertrophy development, we hypothesized, that TAC may lead to an altered expression profile of circRNAs.

To address circRNA expression alterations in TAC-induced cardiac hypertrophy, 4 mice each were subjected to TAC and sham surgery as described in II.1. In short, TAC mice obtained a ligation between the right subclavian and the left carotid artery (displayed in Figure 15 a). As a result, the afterload increases, thereby inducing heart hypertrophy. In contrast, control mice underwent sham surgery, which was performed the same except for aortic constriction. Since cardiomyocytes in particular respond to hypertrophic stimuli, we isolated cardiomyocytes from sham control and TAC hearts for RNA isolation and subsequent circRNA profiling (see II.1.3, II.3.1).

To validate cardiac damage, expression levels of cardiac stress markers ANP and β-MHC were evaluated by qPCR (Figure 15 b). As excepted, both ANP (3.27 fold) and β-MHC (5.09 fold) are significantly upregulated in cardiomyocytes from TAC hearts.

In total, 3 TAC and 3 sham RNA samples were submitted to commercial circRNA array analysis using Arraystars' *Mouse circular RNA microarray V2.0* (as described in II.9).

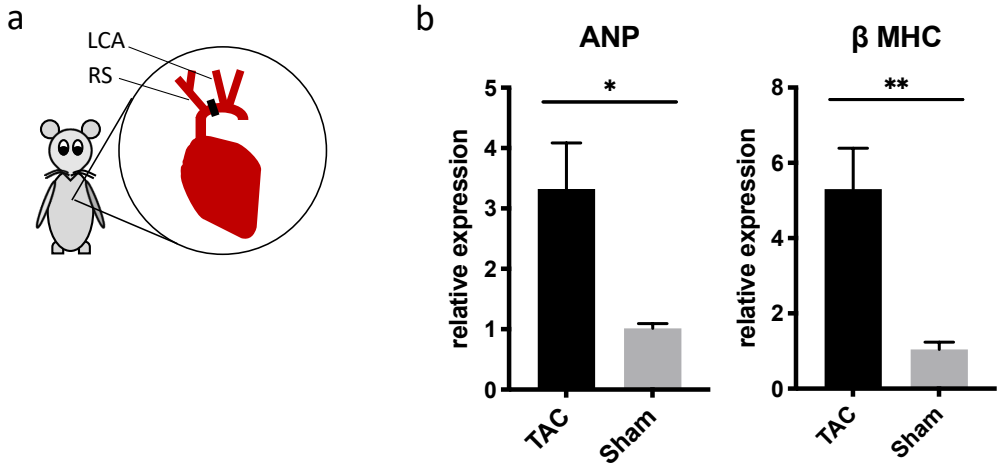

Figure 15 TAC-induced cardiac hypertrophy model

a) Schematic view of TAC-induced pressure overload resulting in ventricular hypertrophy. An aortic ligation between the right subclavian (RS) and the left carotid artery (LCA) increases the afterload, thereby generating stimuli for hypertrophy induction. In contrast, sham control underwent an equivalent surgery without ligation. b) Taq Man® assay to detect mRNA levels of cardiac stress markers ANP and β-MHC. n(TAC)=3, n(sham)= 4. Samples normalized to GAPDH. All graphs presented as mean ±SEM with p values *<0.05, **<0.01, and ns = not significant.

III.6.1 Overview of microarray-based circRNA expression profiling in TAC-induced heart hypertrophy

According to the manufactures' quality control, in total 3 TAC and 2 sham RNA samples fulfilled the criteria for microarray analysis. Raw intensities from predefined 8888 different circRNA probes were obtained and subsequently analyzed for differential expression (Figure 16).

The box plot in Figure 16 a displays the distribution of normalized intensity values for circRNAs of the dataset (TAC1-3 and SHAM1-2), thereby enabling a comparison of expression values between individual samples.

To assess circRNA expression variation of both conditions (TAC and sham), a scatter plot illustration (Figure 16 b) was used. CircRNAs were considered significantly differentially expressed with foldchanges above and below 1,5 and p-values < 0.05. These relationships for the grouped data of TAC and sham mice are well represented by volcano

plot (Figure 16 c). Here, the ratios between the p-value and FC of the individual circRNAs are shown.

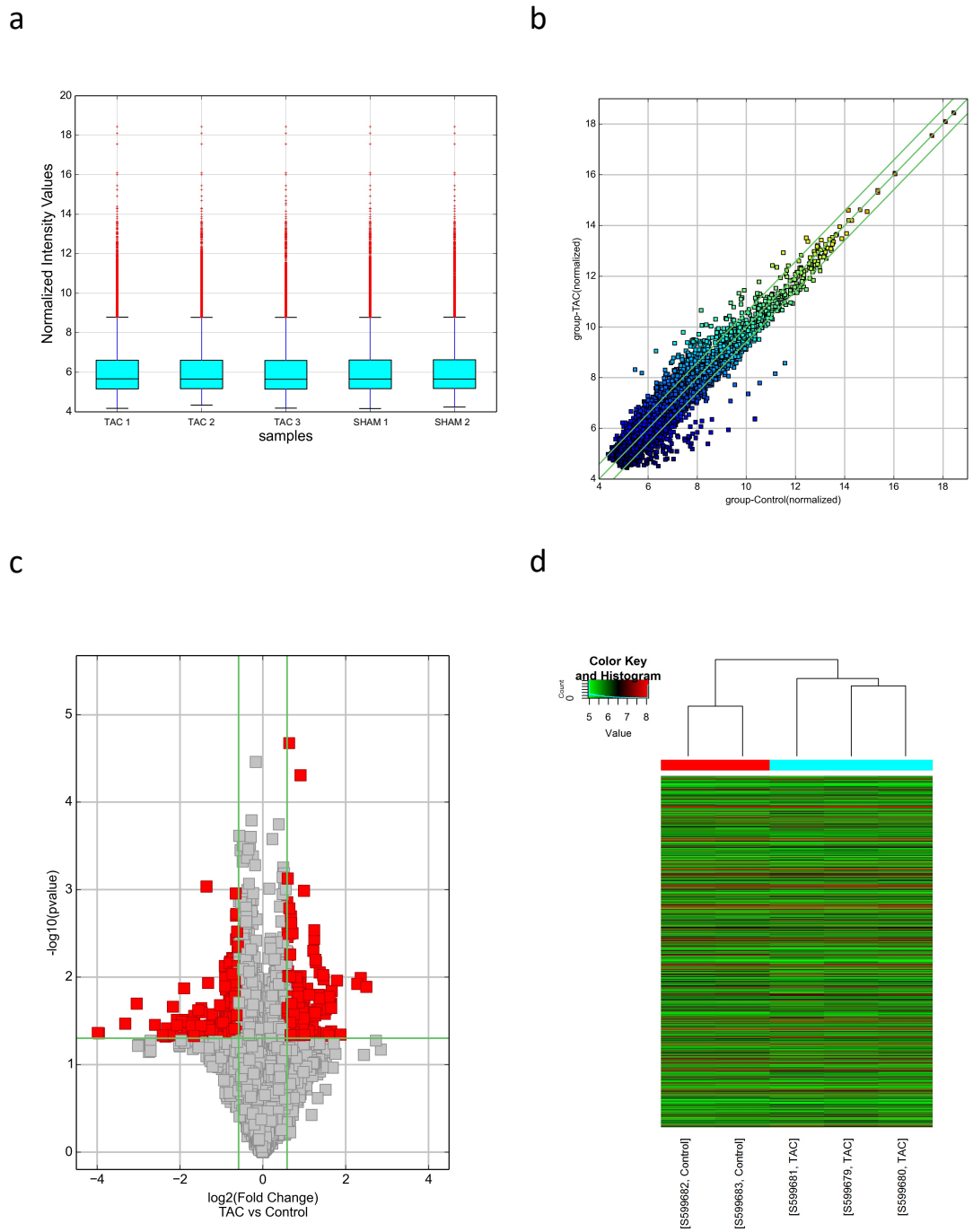

Figure 16 Altered circRNA expression in cardiomyocytes after TAC surgery

a) The box plot displays normalized intensity values of circRNA probes to compare the distribution of expression values of isolated cardiomyocytes after sham (SHAM1,2) and TAC (TAC1,2,3) surgery. b) Scatter plot demonstrating circRNA expression variation

of TAC vs. sham. Averaged normalized TAC (y-axis) and control (x-axis) signal intensity values are depicted. Green lines represent the foldchange thresholds: Top and bottom green lines indicate ≥ +1.5, respectively ≤ -1,5 foldchange threshold, whereas the center line indicates 0 foldchange. c) Volcano plot depicts the relationship between FC-values (x-axis: log2 scaled FC-values TAC vs control/sham) and statistical significance (y-axis: -log10 scaled p-values). Vertical green lines correspond to FC values +1.5 or 1.5, whereas the horizontal line indicates p-values of 0.05. As a result, red squares represent significant differentially expressed circRNAs. d) Hierarchical clustering analysis of circRNA expression levels reveals a distinct profile among samples. The dendrogram indicates related samples, expression intensity is indicated by color code.

In total, 203 up- as well as 192 downregulated circRNAs were identified with maximal FCs ranking from 5.65 fold for up-regulation to 15.82 fold for down-regulation. Finally, a hierarchical clustering analysis was performed (Figure 16 d) to analyze the expression profile of individual samples. Here, it can be well demonstrated, that circRNA expression of TAC mice is significantly different from that of sham mice.

III.6.2 Analysis of up- & downregulated circRNAs

In accordance to previous results from soleus muscle and heart, circRNAs originate predominantly from exons (81.3%), whereas a minor proportion is related to intronic (4.4%) and to sense overlapping sequences (circRNAs transcribed form same gene locus as linear transcript, but not classified into exonic or intronic, e.g. circRNAs containing introns and exons) (14.3%). Significantly upregulated circRNAs exhibit a 2-foldchange on average, with the 15 most upregulated circRNAs presented in Figure 17 a. Mmu_circRNA_25584 represents the strongest upregulated circRNA (FC= 5.65), deriving from the *aarF domain containing kinase 1* (*Adck1*) gene, which is ubiquitously expressed in various tissues (Yoon et al., 2019). GO term analysis revealed, that the host gene *Adck1* is associated with *transferase and kinase activity*, as well *as involvements in mitochondrial organization and phosphorylation.*-Recently, *Adck1* has been related with signaling pathway maintaining mitochondrial morphology and functions in *Drosophilia* muscle (Yoon et al., 2019).

a

FC (abs)	Regulation	circRNA	circRNA_type	chrom	strand	txStart	txEnd	best_transcript	GeneSymbol
5,6514069	up	mmu_circRNA_25584	exonic	chr12	+	88431020	88459203	NM_028105	Adck1
5,1384639	up	mmu_circRNA_36706	exonic	chr4	-	44133639	44159052	NM_001038993	Rnf38
4,848387	up	mmu_circRNA_42572	exonic	chr8	-	13605861	13631892	NM_009025	Rasa3
3,66423	up	mmu_circRNA_31249	intronic	chr18	-	9386734	9412753	uc012azd.1	Ccny
3,4570494	up	mmu_circRNA_27197	exonic	chr14	+	21774962	21780181	NM_026283	Samd8
3,1693968	up	mmu_circRNA_36481	exonic	chr4	+	11593620	11605005	NM_001039556	Rad54b
3,1404062	up	mmu_circRNA_31240	exonic	chr18	-	9319408	9353507	NM_026484	Ccny
3,1399348	up	mmu_circRNA_19178	sense overlapping	chr17	-	14988387	15044490	NM_011560	Tcte3
3,1325776	up	mmu_circRNA_31359	exonic	chr18	-	16627567	16629712	NM_007664	Cdh2
3,1315368	up	mmu_circRNA_002563	exonic	chr18	+	22375132	22434675	NM_001167777	Asxl3
3,098174	up	mmu_circRNA_34777	sense overlapping	chr2	+	152677541	152704941	NM_010376	H13
3,0385434	up	mmu_circRNA_004746	exonic	chr8	+	79118174	79136663	NM_178267	Zfp827
3,0162782	up	mmu_circRNA_005305	exonic	chr14	+	47016276	47016795	NM_028966	Samd4
3,0157723	up	mmu_circRNA_000610	exonic	chr8	+	79118174	79120540	NM_178267	Zfp827
2,8895869	up	mmu_circRNA_28834	exonic	chr15	-	81323609	81338087	NM_011399	Slc25a17

b

FC (abs)	circRNA	MRE1	MRE2	MRE3	MRE4	MRE5
5,6514069	mmu_circRNA_25584	mmu-miR-1966-5p	mmu-miR-1956	mmu-miR-770-3p	mmu-miR-7032-5p	mmu-miR-1199-5p
5,1384639	mmu_circRNA_36706	mmu-miR-7020-5p	mmu-miR-7076-5p	mmu-miR-7047-5p	mmu-miR-1966-5p	mmu-miR-5110
4,848387	mmu_circRNA_42572	mmu-miR-27b-3p	mmu-miR-27a-3p	mmu-miR-128-3p	mmu-miR-25-5p	mmu-miR-6953-5p
3,66423	mmu_circRNA_31249	mmu-miR-8100	mmu-miR-7661-5p	mmu-miR-7054-5p	mmu-miR-1249-5p	mmu-miR-7063-5p
3,4570494	mmu_circRNA_27197	mmu-miR-1929-5p	mmu-miR-3064-3p	mmu-miR-544-3p	mmu-miR-9768-5p	mmu-miR-1933-5p
3,1693968	mmu_circRNA_36481	mmu-miR-6951-3p	mmu-miR-7092-3p	mmu-miR-7116-3p	mmu-miR-7234-5p	mmu-miR-7012-5p
3,1404062	mmu_circRNA_31240	mmu-miR-335-5p	mmu-miR-7243-5p	mmu-miR-329-5p	mmu-miR-686	mmu-miR-3970
3,1399348	mmu_circRNA_19178	mmu-miR-5110	mmu-miR-7092-3p	mmu-miR-7116-3p	mmu-miR-7054-5p	mmu-miR-326-5p
3,1325776	mmu_circRNA_31359	mmu-miR-2136	mmu-miR-511-5p	mmu-miR-3106-3p	mmu-miR-6985-5p	mmu-miR-7018-5p
3,1315368	mmu_circRNA_002563	mmu-miR-205-5p	mmu-miR-1251-3p	mmu-miR-329-3p	mmu-miR-7004-3p	mmu-miR-7068-5p
3,098174	mmu_circRNA_34777	mmu-miR-1249-5p	mmu-miR-6931-5p	mmu-miR-5110	mmu-miR-6981-5p	mmu-miR-5107-5p
3,0385434	mmu_circRNA_004746	mmu-miR-494-5p	mmu-miR-410-5p	mmu-miR-7092-3p	mmu-miR-219b-5p	mmu-miR-875-3p
3,0162782	mmu_circRNA_005305	mmu-miR-5623-3p	mmu-miR-7058-5p	mmu-miR-423-5p	mmu-miR-7024-3p	mmu-miR-3966
3,0157723	mmu_circRNA_000610	mmu-miR-7092-3p	mmu-miR-219b-5p	mmu-miR-6896-3p	mmu-miR-3064-5p	mmu-miR-3083-5p
2,8895869	mmu_circRNA_28834	mmu-miR-1907	mmu-miR-6957-5p	mmu-miR-15a-5p	mmu-miR-15b-5p	mmu-miR-6353

c

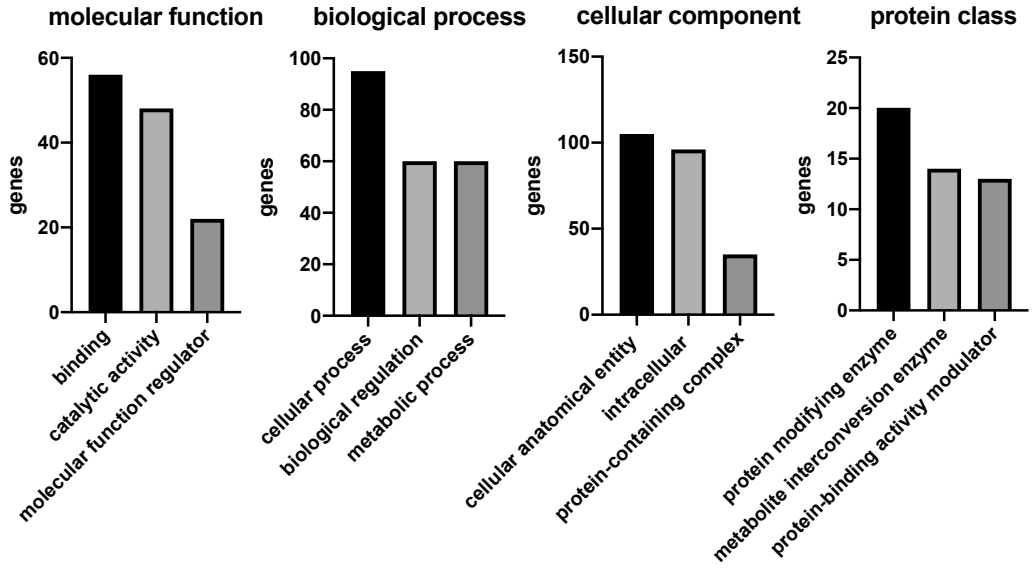

Figure 17 Selection of top upregulated circRNAs

a) Top 15 upregulated circRNAs depicted as FC(abs) = absolute foldchange, circRNA = circRNA ID, circRNAtype = exon/intron/sense overlapping, chrom = chromosome,

strand = +/- strand, txStart= start of the genomic position of the circular RNA, txEnd = end of the genomic position of the circular RNA, best_transcript = annotated linear transcript within the region of the circRNA, GeneSymbol= symbol of host gene locus b) displays top 5 predicted miRNA - miRNA responsive elements (MRE) interactions. c) Top 3 classifications of all upregulated host genes based on GO-Slim analysis for molecular and biological function, cellular component and protein class (Mi et al., 2021).

Since circRNAs are known to interfere with miRNA-mediated gene expression regulation via sequestration of miRNAs (Hansen et al., 2013), differentially expressed circRNAs were investigated for putative miRNA-circRNA interaction using Arraystars' prediction software (II.9). The resulting top 5 predicted miRNAs are displayed in Figure 17 b.
To further categorize circRNA host genes, a GO-Silm gene ontology analysis (as described in II.13) was performed (Figure 17 c). Within the top 3 highest ranking annotations, host gene transcripts encode predominantly *proteins with binding and catalytic activities*, involved in *cellular*, as well as *metabolic processes* and *biological regulations*. Concerning cellular components, they were predominantly annotated to *cellular anatomic entities*, *intracellular* and *protein-containing complexes*. The majority of host genes annotate in the category protein classes encompassing *protein modifying enzymes*, *metabolite interconversion enzymes* and *protein-binding activity modulators*.

Regarding downregulated circRNAs, mean FC amounts to 2.2. Again, the majority of circRNAs derive from exons (71%), followed by sense overlapping (13.5%), intron (9.3%), intergenic (4.2%) and antisense (2.1%) sequences. Among the top 15 downregulated circRNAs (Figure 18 a), mmu_circRNA_19997 shows the highest foldchange compared to sham condition (FC=15.8). It originates from the *POU domain, class 3, transcription factor 3 adjacent noncoding transcript 1* (*Pantr1*) gene, annotated to *regulation of gene expression* in GO terms. *Pantr1* transcript belongs to the class of long non-coding RNA, involved in carcinogenesis by promoting various cellular functions such as migration, invasion, proliferation or repression of apoptosis (Seles et al., 2020).
According to the upregulated circRNAs, potential miRNA-circRNA interactions were predicted for the downregulated circRNAs (Figure 18 b).

a

FC (abs)	Regulation	circRNA	circRNA_type	chrom	strand	txStart	txEnd	best_transcript	GeneSymbol
15,8243592	down	mmu_circRNA_19996	exonic	chr1	-	42666840	42667003	NR_027826	Pantr1
15,5464864	down	mmu_circRNA_33321	intronic	chr2	+	34419107	34435222	ENSMUST00000156967	Mapkap1
10,004746	down	mmu_circRNA_20885	sense overlapping	chr1	-	134546625	134550091	NM_001145300	Mgat4e
8,2459976	down	mmu_circRNA_29984	exonic	chr16	-	87404005	87423578	NM_001081068	Ltn1
6,0817763	down	mmu_circRNA_42050	exonic	chr7	+	107284781	107285730	uc009jaz.1	AY512917
5,3443133	down	mmu_circRNA_35732	sense overlapping	chr3	+	88207185	88209716	uc008pug.1	AK141565
5,1021939	down	mmu_circRNA_42962	exonic	chr8	-	64594896	64619547	NM_013494	Cpe
4,9793406	down	mmu_circRNA_20866	exonic	chr1	+	131928063	131929762	NM_175294	Nucks1
4,831377	down	mmu_circRNA_39531	exonic	chr5	+	135715871	135716063	NM_008898	Por
4,7353033	down	mmu_circRNA_29850	exonic	chr16	+	58424560	58463108	NM_028523	Dcbld2
4,7287323	down	mmu_circRNA_24792	exonic	chr12	+	21305302	21310284	NM_018813	Cpsf3
4,5057746	down	mmu_circRNA_29796	exonic	chr16	-	50220444	50251394	NM_027444	Bbx
4,478475	down	mmu_circRNA_30123	exonic	chr16	-	96002433	96017724	NM_145125	Brwd1
4,2121234	down	mmu_circRNA_19661	exonic	chr1	+	11545153	11596317	NM_177173	A830018L16Rik
4,2042919	down	mmu_circRNA_26264	intronic	chr13	-	45681222	45697945	ENSMUST00000167708	Atxn1

b

FC (abs)	circRNA	MRE1	MRE2	MRE3	MRE4	MRE5
15,8243592	mmu_circRNA_19996	mmu-miR-7018-5p	mmu-miR-7222-3p	mmu-miR-326-5p	mmu-miR-298-5p	mmu-miR-3154
15,5464864	mmu_circRNA_33321	mmu-miR-7092-3p	mmu-miR-5107-5p	mmu-miR-466m-3p	mmu-miR-466c-3p	mmu-miR-466b-3p
10,004746	mmu_circRNA_20885	mmu-miR-7116-3p	mmu-miR-7092-3p	mmu-miR-6984-3p	mmu-miR-7058-3p	mmu-miR-6344
8,2459976	mmu_circRNA_29984	mmu-miR-6985-5p	mmu-miR-7094-1-5p	mmu-miR-6919-3p	mmu-miR-7086-5p	mmu-miR-22-5p
6,0817763	mmu_circRNA_42050	mmu-miR-686	mmu-miR-7231-3p	mmu-miR-488-3p	mmu-miR-466i-5p	mmu-miR-7119-3p
5,3443133	mmu_circRNA_35732	mmu-miR-6975-3p	mmu-miR-6971-5p	mmu-miR-361-3p	mmu-miR-346-3p	mmu-miR-6384
5,1021939	mmu_circRNA_42962	mmu-miR-667-5p	mmu-miR-3101-3p	mmu-miR-6402	mmu-miR-6912-5p	mmu-miR-298-3p
4,9793406	mmu_circRNA_20866	mmu-miR-3966	mmu-miR-107-5p	mmu-miR-3084-3p	mmu-miR-7092-3p	mmu-miR-6896-3p
4,831377	mmu_circRNA_39531	mmu-miR-6996-3p	mmu-miR-324-3p	mmu-miR-210-5p	mmu-miR-1933-3p	mmu-miR-3058-5p
4,7353033	mmu_circRNA_29850	mmu-miR-23a-5p	mmu-miR-1903	mmu-let-7g-3p	mmu-miR-7086-3p	mmu-miR-6996-5p
4,7287323	mmu_circRNA_24792	mmu-miR-370-5p	mmu-miR-6539	mmu-miR-7019-3p	mmu-miR-128-3p	mmu-miR-1193-3p
4,5057746	mmu_circRNA_29796	mmu-miR-7116-3p	mmu-miR-6946-3p	mmu-miR-1903	mmu-miR-7678-3p	mmu-miR-432
4,478475	mmu_circRNA_30123	mmu-miR-6902-5p	mmu-miR-7094-1-5p	mmu-miR-7214-5p	mmu-miR-670-3p	mmu-miR-6946-3p
4,2121234	mmu_circRNA_19661	mmu-miR-666-3p	mmu-miR-6400	mmu-miR-7211-5p	mmu-miR-683	mmu-miR-3084-5p
4,2042919	mmu_circRNA_26264	mmu-miR-7020-5p	mmu-miR-6906-5p	mmu-miR-5110	mmu-miR-669f-3p	mmu-miR-466m-3p

c

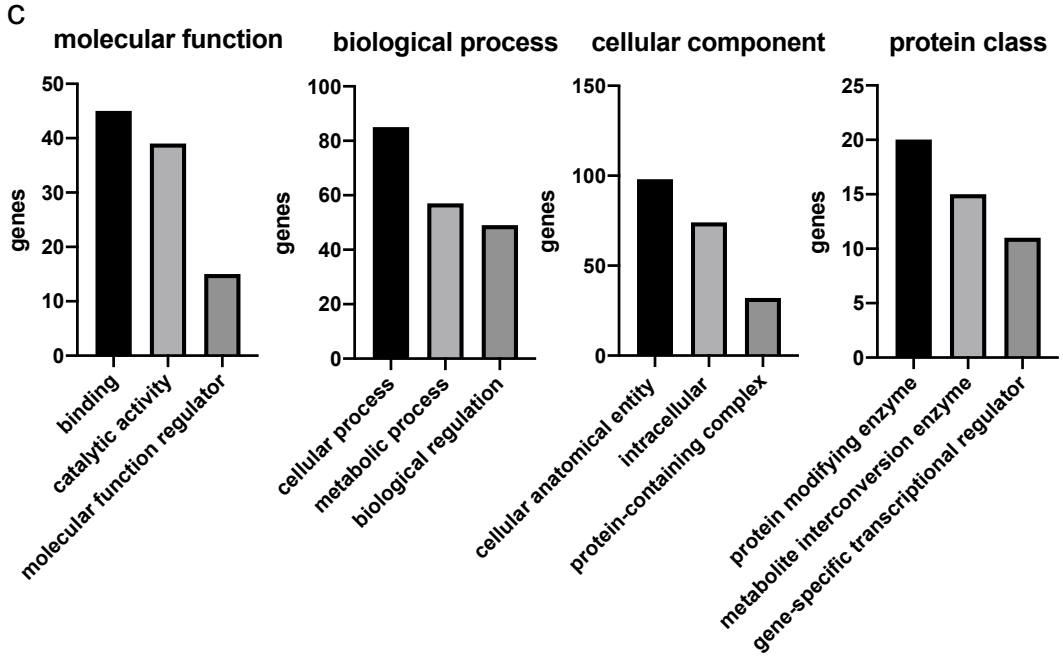

Figure 18 Selection of top downregulated circRNAs

a) Top 15 downregulated circRNAs depicted as FC(abs) = absolute foldchange, circRNA = circRNA ID, circRNAtype = exon/intron/sense overlapping, chrom =

chromosome, strand = +/- strand, txStart= start of the genomic position of the circular RNA, txEnd = end of the genomic position of the circular, best_transcript = annotated linear transcript within the region of the circRNA, GeneSymbol = symbol of host gene locus. b) Top 5 predicted miRNA - miRNA responsive elements (MRE) interactions. c) Top 3 classifications of all downregulated host genes based on GO-Slim analysis for molecular and biological function, cellular component and protein class (Mi et al., 2021).

The host genes of downregulated circRNAs display similar top 3 GO annotations for functional classifications compared to upregulated circRNAs, except for protein classes (Figure 18 c). Here, downregulated circRNAs annotate predominantly to *gene specific transcriptional regulators*.

Statistical overrepresentation of GO terms (as described in II.13) was performed on both, up- as well as downregulated circRNA host genes with statistical significance set to an overall FDR <0.05. Upregulated circRNAs display highest overrepresentation fold enrichment (38.58) in the category *production of miRNAs involved in gene silencing by miRNA* (with host genes *Pum1* and *Pum2*, *Zc3h7b*) and approximately 18-fold for *regulation of mRNA stability* (with host genes *Pum1* and *2*, *Fxr2* and *Smad4*). However, downregulated host genes show no statistically significant overrepresentation.

Interestingly, the majority of altered expressed circRNAs host genes encode only a single circRNA (89%). Accordingly, a minority (11%) produce multiple circRNA isoforms. For example, host genes *Zfp827*, *Zfp532*, *Tt3*, *Usp3*, *Actr2*, *Akap7* and *Debld2* generate at least 3 circRNAs. In comparison to our detected circRNAs in heart using RNA seq data from the publicly available ENCODE library (Figure 6 b and Figure 13 a), 85% of differentially expressed circRNAs in TAC condition were *de novo* identified. Accordingly, 5% represent identical circRNAs from heart, whereas 10% were circRNA isoforms from the same host genes.
In summary, our microarray results display significantly altered circRNA expression in cardiomyocytes after TAC surgery. This dataset will provide us with a new starting point to study the role of differentially expressed circRNAs in the pathogenesis of cardiac hypertrophy. For this purpose, a comprehensive list, including all differentially expressed circRNAs and their predicted MREs, is provided in the appendix XI.2.

IV DISCUSSION

Although single-stranded, covalently closed circular RNA molecules in viroid have been described decades ago (Sanger et al., 1976), research has focused predominantly on the splicing mechanisms of linear rather than circular RNAs.

In the following years, non-canonically spliced, so called “scrambled” transcripts from the endogenous DCC and EST-1 loci were described (Cocquerelle et al., 1992; Nigro et al., 1991), postulating, that their biogenesis is associated with large flanking introns (Cocquerelle et al., 1992). Subsequently, the covalently closed circular structure, stability and cytoplasmic localization of the scrambled DCC and EST-1 transcripts was experimentally validated (Cocquerelle et al., 1993). Likewise, the predominantly cytoplasmatically localized scrambled RNA transcripts of the SRY gene were shown to have a circular structure and to be expressed in a tissue-specific manner. (Capel et al., 1993).

In the following years, additional studies hypothesized various mechanisms by which circRNAs are formed via altered splicing processes.

In respect to the circular SRY transcript, it was demonstrated, that a 400 nucleotide long sequence, consisting of inverted repeats, flanking the SRY gene, is required to mediate circularization (Dubin et al., 1995). In addition, *in vitro* circularization studies performed in mammalian nuclear extracts, which contain all basic components of the splicing machinery, indicated, that these processes were more efficient using small exon lengths, as well as intronic complementary sequences flanking the circularized exon (Pasman et al., 1996; Schindewolf et al., 1996).

Within the late 1990s and early 2000s, various additional circRNAs were identified, although their functional capabilities were not evaluated at that time.

Recent improvements in RNA next generation sequencing and consecutive bioinformatic analysis in the last decade resulted in a massive increase in circRNA research. Hence, thousands of circRNAs were *de novo* identified in numerous organisms and cell-types. These circular RNAs are generally expressed at low levels compared to the linear isoforms, although in few cases, the circRNA isoforms are highly abundant, e.g., for SRY, where the circular transcript represents the predominant isoform (Hansen et al., 2013; Jeck et al., 2013; Memczak et al., 2013; Salzman et al., 2012). Interestingly, several circRNAs, e.g. circSRY and CDR1as, have multiple miRNA binding sites, enabling them

the ability to bind miRNAs and thereby modulate their activity (Hansen et al., 2013; Memczak et al., 2013). Moreover, these and other studies in several organisms demonstrated, that circRNA levels alter during development and within different tissues (Gruner et al., 2016; Rybak-Wolf et al., 2015; Westholm et al., 2014).

Ashwal-Fluss and colleagues provided evidence for co-transcriptional biogenesis of circRNAs, which compete with linear splicing of mRNAs within the locus (Ashwal-Fluss et al., 2014), indicating that circRNA formation can act as a trap for mRNA biogenesis. Until now, the process of circRNA biogenesis is not entirely understood, however, specific sequences for circularization within flanking introns of a circularizable exon were identified (Ashwal-Fluss et al., 2014; Jeck et al., 2013; Rybak-Wolf et al., 2015; Y. Zhang et al., 2016). In recent years, numerous RBPs including MBL, ADAR and QKI, were described to regulate circRNA formation in different organisms (Conn et al., 2015; Ivanov et al., 2015; Rybak-Wolf et al., 2015).

Alongside the growing interest in circRNAs, bioinformatics detection methods, as well as sequencing protocols, improved significantly. Hereby, the exonuclease RNAse R-mediated enrichment for circRNAs, is one major technological progress (Jeck et al., 2013; Memczak et al., 2013).

Nowadays, numerous bioinformatic pipelines for circRNA identification, based on the specific characteristics of the circular junction, as well as circRNA databases encompassing information of previously identified circRNAs, are publicly available.

However, specific knowledge about the molecular function of certain circRNAs is still limited. The initial assumption, that most circRNAs function primarily as miRNA sponges, has not proven to be true. Instead, the class of circular RNAs seems to exert several individual biological functions apart from modulating miRNAs, e.g., acting as scaffolds of RBPs (William W Du et al., 2017) or encoding translational potential (Yang et al., 2018).

Since circular RNAs are widely expressed in human tissues, there is increasing evidence regarding potential roles of circRNAs in pathogenesis of diseases, as well as potential therapeutic targets. The vast majority of studies focuses on malignant tumors and implemented circRNAs acting either as oncogenes, e.g., circPVT1 in squamous cell carcinoma of the head and neck (Verduci et al., 2017) and CDR1as in colorectal cancer (Weng et al., 2017), or as tumor suppressor genes, e.g., circSMARCA5 in glioblastoma (Barbagallo et al., 2018). However, circRNAs in diseases such as diabetes, chronic inflammatory diseases, neurological disorders, as well as cardiovascular disease are still

in research focus and might provide promising approaches to better understand the pathology and provide novel therapeutic targets.

In this study, we made use of an in-house-developed circRNA detection pipeline, which was first applied to identify circRNAs derived from soleus muscle. Selected candidates were thereafter validated in various mouse tissues including soleus muscle. Subsequently, we transferred this approach to the adult mouse heart and analyzed the expression of selected circRNA candidates. Additionally, an established circRNA microarray was used to identify differentially expressed circRNAs in a TAC-induced heart hypertrophy mouse model.

Accurate predictions of circRNAs from soleus muscle based on the in-house pipeline

CircRNAs emerge as important players in diverse cellular processes, such as cell proliferation, survival, as well as cell differentiation. However, their function in the skeletal muscle is a topic of ongoing research.

Skeletal muscles, such as the soleus muscle, play a crucial role in promoting locomotion, thermal homeostasis and metabolism. They mainly consist of contractile myofibers, generated by fusion of mononuclear myofibroblasts by process called myogenesis (Okazaki & Holtzer, 1966). During embryogenesis, myogenic progenitor cells (MPCs) differentiate to myofibers, whereas in adult muscle, stem cells referred to as satellite cells, are the major source to regenerate damage of skeletal muscle. Myogenesis is regulated transcriptionally via myogenic regulatory factors (MRFs) such as Myf5 (Braun et al., 1989; Braun et al., 1992), as well as post-transcriptionally via RBPs and ncRNAs (Apponi et al., 2011; Hagan et al., 2017).

Recent studies have indicated, that circRNAs are involved in regulation of gene expression during myogenesis. Differential expression of circular RNAs has been demonstrated in prenatal compared to postnatal muscle (C. Li et al., 2017), in differentiating myoblasts (Chen et al., 2018), as well as in the aging skeletal muscle (Abdelmohsen et al., 2015). Meanwhile, some studies have provided insights into the functional mechanisms of how circRNAs regulate gene expression. For example, circZfp609 inhibits myoblast differentiation by sponging miR-194-5p, thereby resulting in an increased expression of the miR-194-5p target Bcl associated factor 1 (BCLAF1), which acts as a transcription factor (Wang et al., 2019).

In addition, circLMO7, a highly abundant circRNA in bovine muscle tissue, which originates from the LIM domain only protein 7 (*LMO7*) gene locus, is strongly reduced in proliferating myoblast. Functionally, circLMO7 inhibits apoptosis and myogenesis by binding miR-378a-3p (Wei et al., 2017).
Furthermore, circFGFR4 represents another highly abundant circRNA in bovine muscle, promoting muscle fiber formation by inhibiting miR-107-mediated suppression of *WNT3A* expression (H. Li, X. Wei, et al., 2018). Additionally, overexpression of circFUT10 inhibits myoblast proliferation, while enhancing differentiation mediated by an increased expression of serum response factor (SRF) (H. Li, J. Yang, et al., 2018).

In this study, we made use of an in-house circRNA detection pipeline to identify novel circRNAs in soleus muscle RNA. A total of approximately 3.300 circRNA candidates per sample were predicted for rRNA and poly-A depleted RNA in the two studied conditions comparing *Mettl21c* knockout and wildtype with two biological replicates each.
Interestingly, about 96% of candidates are exclusively identified in individual samples, whereas for both conditions, a minority of averagely 4% is commonly detected in each biological replicate. The overlap of identified circRNA candidates between all samples, on the other hand, is still significantly lower. To date, the effects of *Mettl21c* knockout on circRNA formation have not been studied. However, we do not expect significant alterations on overall circRNA expression, since METTL21C is a skeletal muscle-specific lysine methyltransferase, acting by modulating protein degradation and has no known interactions with DNA or RNA (Wiederstein et al., 2018).
In accordance to previously published data, the vast majority of detected candidates derive from exonic sequences (Jeck et al., 2013). In total, 4 circRNA candidates from the overlap of all samples were selected for validation: CircZfp827, circNeb, circSec24b and circNfix. For each individual candidate, we successfully detected a characteristic back-splice junction using a back-splice-specific RT-PCR. The sequencing analysis of the full-length RT-PCR products revealed, that all 4 selected circRNAs derive from exonic sequences and can therefore be categorized as exonic circRNAs. Among them, circZfp827 and circNeb encode multiple exons, whereas circNfix includes exclusively the circularized exon. Sequencing of CircSec24b was only partially possible, therefore no conclusions can be made about the complete sequence.

Interestingly, the full-length PCR of circZfp827 detected an additional weaker band with unknown composition at approximately 340bp length, which was not further investigated by direct sequencing. Since it is well known, that a single host gene locus can generate multiple circRNA isoforms (Y. Li et al., 2017; X. O. Zhang et al., 2016), the shorter PCR product might reflect a smaller circZfp827 isoform containing fewer exons. However, other reasons, such as non-specific PCR products or amplification of non-circular back-splice junction-containing products, e.g., observed by template switching during cDNA preparation or trans-splicing, might also happen.

Since the back-splice junction is not a unique characteristic of circRNAs (Lasda & Parker, 2014), an additional validation method was implemented to proof the circularity of the selected candidates. To achieve this aim, RNAse R treatment is a useful tool to asses circularity by measuring the RNA resistance to degradation (Jeck et al., 2013; Suzuki & Tsukahara, 2014). Therefore, RNAse R resistance was validated by relative enrichment of the selected circRNAs compared to selected linear transcripts (HPRT and β-actin mRNA) in RNAse R and mock-treated RNA normalized to GAPDH.
CircZfp827, circSec24b and circNfix are characterized by explicit high relative enrichments, indicating a stability towards RNAse R digestion, whereas linear HPRT and β-actin transcripts demonstrate minor enrichments. Interestingly, circNeb shows only a moderate enrichment compared to the other circRNAs. Werfel and colleagues argue, that larger circRNAs display lower enrichment due to endonuclease contamination or small degree of cellular RNAse degradation during RNA isolation (Werfel et al., 2016). Most likely, variable resistance against RNAse R treatment is caused by methodical constrains such as RNAse R activity, different expression levels of targets and the normalization to GAPDH.
Surprisingly, all investigated targets, circular, as well as linear, demonstrate enrichment scores above 1, implying increased stability to RNAse R degradation in comparison to GAPDH. These findings indicate, that GAPDH is degraded more efficiently than HPRT and β-actin. To overcome this problem, future analyses should implement a comparison of the degradation of circular RNAs and the corresponding linear mRNA of the same host gene.

In summary, the randomly selected circRNAs candidates circZfp827, circNeb, circSec24b and circNfix, identified de novo in RNAseq of soleus muscle, contain a back-

splice junction, encode exclusively exonic sequences of the corresponding host gene and are enriched in RNAse R treated RNA samples. Therefore, we predict a circular structure of our studied circRNA candidates. Accordingly, the presented data demonstrate, that our in-house circRNA detection pipeline provides circRNAs reliably and comparably to common published pipelines (Hansen et al., 2016; Jeck & Sharpless, 2014; Salzman et al., 2012; Xiangxiang Zeng et al., 2017). To support this finding, further studies with a higher number of circRNA candidates are needed.

Selected soleus muscle circRNAs are differentially expressed in murine tissue

Previous studies indicate conservation of homologous circRNAs across various species (Jeck et al., 2013) and differential expression in a cell-type, developmental stage and tissue-specific manner (Jakobi, Czaja-Hasse, Reinhardt, & Dieterich, 2016; Y. Li et al., 2017; Memczak et al., 2013; Xu et al., 2017).

Interestingly, reported circRNA expression profiles are heterogenous compared with their coresponding linear counterparts. There is evidance indicating, that circRNA expression does not necessarily correlate with linear expression (Memczak et al., 2013; Salzman et al., 2012) and that biogenesis of the majority of circRNAs is independent from expression of the linear isoform of the host gene (Y. Li et al., 2017). In fact, a recent study has shown evidence for circRNA expression to even exceed the expression of the corresponding linear isoform (Siede et al., 2017).

In this study, circRNA expression was evaluated by a semiquantitive RT-PCR analysis using cDNA from various mouse tissues including heart, lung, soleus muscle, extensor digitorum longus muscle, kidney and aorta, as well as by a qRT-PCR using cDNA from cardiomyocytes and non-cardiomyocytes. Our results indicate, that all investigated circRNAs are co-expressed with the coresponding linear isoforms. This finding is consistent with a co-transcriptional biogenesis of circRNAs, in which back-splicing competes with linear splicing of the same transcript - a process described as mRNA-trapping (Ashwal-Fluss et al., 2014).

Two of our candidates, circZfp827 and circNfix, are ubiquitous expressed in all selected tissues, whereas circNeb and circSec24b display a tissue-specific expression. CircNeb is exclusively detected in muscle tissues in accordance with the transcription of the linear *Neb* mRNA, whereas circSec24b is solely detectable in soleus and extensor digitorum longus muscle.

Interestingly, Sec24b represents the only target displaying a non-concomittant expression of linear and circular RNAs. In heart, lung and aorta tissue, exclusively the linear Sec24b isofrom is detected, whereas circular transcripts are soley discovered in soleus and extensor digitorum longus muscle alongside the linear isoform. This finding suggests a differential, tissue-specific regulation of circRNA expression.

In all other examples, circular RNAs, as well as the linear counterparts, are concomittantly expressed.

However, the information value of these findings is limited due to the low sample number and the semiquantitive RT-PCR validation. Further quantification studies with larger biological replicate numbers are needed to confirm these preliminary findings.

To overcome these limitations, tissue-specific circRNA expression was also studied by qPCR in diffferent cellular subtypes of the heart, namely cardiomyocytes and non-cardiomyocytes.

Here, circZfp827, as well as circNeb, are significantly lower expressed in cardiomyocytes, whereas circNfix expression is highly abundant. These findings are consistent with recently published data, demonstrating an enrichment of circNfix in cardiomyocytes. Here, circNfix was shown to sponge mir-214, thereby promoting glycogen synthase kinase 3 beta (GSK3β) and inhibiting β-catenin activity. Furthermore, circNfix is involved in sponging RBPs repressing Cyclin B1 and A1 (Huang et al., 2019). Consecutively, circNfix loss-of-function increases proliferation of cardiomyocytes, angiogenesis and acts protective against ischemia myocardial infarction models. Vice-versa, gain-of-function experiments result in diminished cardiomyocyte proliferation (Huang et al., 2019).

Moreover, according to qPCR, circSec24b is not detectable in cardiomyocytes or non-cardiomyocytes, which is consistent with the results of RT-PCR in heart.

In conclusion, the presented results of circRNAs from soleus muscle support previously published data on tissue- and cell type-specific expression of circRNAs. Accordingly, we hypothesize a regulatory process in circRNA formation for the circRNAs presented.

Interestingly, all explored circRNAs were co-expressed with their linear counterpart, implying an interdependent biogenesis of both RNA types.

Differential expression of circRNAs and linear isoforms in heart predicted from in-house bioinformatics analysis

Along with the growing interest in circular RNAs, more and more studies have been published in recent years addressing their expression and functions in the heart.
Jakobi and colleagues detected 575 distinct circRNAs in RNAse R enriched, rRNA depleted RNA seq data sets of the adult murine heart, among which multiple host genes were linked to cardiovascular diseases (Jakobi et al., 2016).
Furthermore, over 9000 circRNAs were detected in mouse and rat hearts, indicating a differential expression of those circRNAs during cardiac development and in cardiac disease conditions such as hypertrophy (Werfel et al., 2016).
Complementary, differentially expressed circRNA profiles have been reported in human heart during multiple stages of heart development (Y. Li et al., 2017).
In our study, circRNA detection using the in-house bioinformatics approach revealed 31 robust expressed circRNA candidates in rRNA depleted total RNA from the heart. This strikingly lower number could result from methodological differences, including omitted RNAse R enrichment, bioinformatic processing of sequencing data such as downsampling, sample size and different stringency settings.
Interestingly, circRNAs from host genes generating multiple, partly differentially regulated, circRNAs in heart like *titin* (*Ttn*) or *ryanodine 2 receptor (Ryr2)* (Werfel et al., 2016), are only detected in either one of the two biological replicates in our bioinformatics analysis.
GO analysis revealed, that the majority of circRNA host genes are annotated to *function in metabolic and cellular processes*, as well as *biological regulation* in functional classifications. Since our analysis exclusively focuses on GO annotations of the host genes encoding circRNAs, annotated terms are non-specific and provide a restricted overview of known functionalities. However, a sub-fraction of the detected host genes, e.g., *Smad4* and *Fhl2*, are correlated to more specific functions such as "Maintaining heart function". *Fhl2* plays a significant role in modifying the hypertrophic response to β-adrenergic stimulation in the heart (Kong et al., 2001). On the other hand, *Smad4* regulates cardiomyocyte proliferation during embryonic heart development (Qi et al.,

2007), as well as homeostasis of the heart via TGF-β signaling (Umbarkar et al., 2019) and targeted disruption of *Smad4* leads to a hypertrophy phenotype (Wang et al., 2005).

In total, 4 candidates were selected for further validation by qRT-PCR. The previously characterized circZfp827, which we also detected in soleus muscle, circSmad4 – generated from *Smad4* host gene, circFhl2 originating of the *Fhl2* locus and circMmp15 processed from *Mmp15*. CircRNA expression was studied in comparison to a linear isoform via back-splice-specific qPCR in atrial and ventricular RNA.
In the case of cicZfp827, no significant differences in respect to expression levels in atrial and ventricular RNA were observed compared to the linear control. In contrast, *Smad4* shows a statistically significant predominant linear expression in ventricle, which is not significant in atria.
Interestingly, circFhl2 and circMmp15 expression varies significantly compared to the linear isoform. The linear *Fhl2* transcript is approximately 100 times more abundant than the circular isoform in atria, as well as in ventricle. In contrast, circMmp15 is significantly more abundant in atria and ventricle than linear *Mmp15*.
Taken together, these findings indicate a specific expression pattern of selected circRNA candidates in atrial and ventricular heart.
Recently, Li and colleagues investigated the expression patterns of circRNAs and their host genes in human cardiomyocytes during various differentiation stages. The majority of circRNAs were co-expressed with the corresponding linear isoforms. Interestingly, few circRNAs from host genes that encode multiple circRNAs, such as *TTN* and *SLC8A1*, were shown to display distinct expression patterns of the linear transcript, indicating potential independent functions (Y. Li et al., 2017).
In summary, multiple circRNAs were identified in the heart using our in-house detection pipeline. Several of these circRNAs were demonstrated to exhibit different expression levels compared to their corresponding linear isoforms in atrial and ventricular fractions, suggesting complex underlying regulatory mechanisms and possibly relevant biological functions in the heart.

circRNAs are differentially expressed in a TAC-induced hypertrophy model

Pathological cardiac hypertrophy is a significant problem in modern medicine, because it leads to cardiac arrhythmias and ultimately heart failure – one of the leading causes of morbidity and mortality throughout the world with increasing incidence (Bui et al., 2011;

Roger, 2013). Etiologically, hypertension, valvular dysfunctions, as well as ischemia of the heart, storage diseases or hereditary cardiomyopathies are common causes of pathologic hypertrophy. As a result of the increased workload, the ventricle undergoes concentric growth, leading to a thinning of the walls, as well as a dilation of both chambers and ultimately to a decrease in ejection fraction and heart failure (Schiattarella & Hill, 2015).

A variety of different molecular pathways are involved in the development of pathological hypertrophy of the heart. Cardiomyocytes are mainly affected via an increased β-adrenergic receptor activity (Lymperopoulos et al., 2013) and altered mTOR signaling (Laplante & Sabatini, 2012). Cytokines, FGF and CTRP9 mediate pathological pathways in non-myocytes such as immune cells, adipocytes and fibroblasts (Frieler & Mortensen, 2015). Altered activity of TGFβ - SMAD2/3 signaling is another cause leading to hypertrophy (Kuwahara et al., 2002), as well as altered functions of mechanosensors of the heart (Correll et al., 2015).

Contrary to linear RNA products, the research on circular RNAs in the pathogenesis of pathological heart hypertrophy is still in its infancy.

Until now, differential expression of circRNAs in cardiac hypertrophy models has been inconsistently reported. Compared to cardiac development, alterations in heart hypertrophy are significantly smaller (Tan et al., 2017; Werfel et al., 2016). However, Li and Yang provide evidence of a significantly altered circRNA transcriptome in TAC-induced hypertrophy model using a microarray approach (X. Li et al., 2022), as well as in an isoproterenol-induced heart failure model based on RNAseq (M. H. Yang et al., 2020). In contrast, other studies detect no significant differential circRNA expression in TAC mice by RNAseq (Tan et al., 2017) or only a tendency towards increased expression (Werfel et al., 2016). These inconsistencies might be related to different forms of heart hypertrophy related to various disease models (TAC vs. isoproterenol), as well as diverging time points of tissue isolation and experimental evaluation techniques (RNAseq vs. microarray).

So far, only a limited number of circRNAs with specific functions in pathogenesis of heart hypertrophy were reported.

HRCR represents a circRNA encoding 6 miR-233 binding sites, thereby attenuating cardiac hypertrophy via sponging of miR-233 (Wang et al., 2016). In contrast, CircSlc8a1 is one of the most abundant circRNAs identified in heart (Lim et al., 2019), acting as a

miR-133a sponge – a miRNA involved in regulation of cardiac hypertrophy (Care et al., 2007; Lim et al., 2019).

In order to study the pathogenesis of cardiac hypertrophy, the TAC model, firstly introduced in 1991, is broadly used (H. A. Rockman et al., 1991). The induced pressure overload results in hypertrophy and heart failure, but also in limited fibrosis, inflammation, and cardiac dilatation (Xia et al., 2009).

Up to date, circRNA studies in cardiac hypertrophy models have been performed predominantly using RNAseq analysis of circRNA expression alterations compared to sham controls (Tan et al., 2017; Werfel et al., 2016; M.H. Yang et al., 2022).

In this study, I performed one of the first microarray-based analyses detecting differentially expressed circRNAs in a TAC-induced hypertrophy model.

RNAseq-based transcriptome profiling has become an increasingly popular method over the past 10 years due to several distinct advantages. It provides detection of novel, previously unknown splice junctions, has a broad dynamic range depending on the sequencing depth and can generate expression profiles of non-reference organisms. In contrast, microarray-based transcriptome profiling provides higher reliability and is therefore still widely used (Mantione et al., 2014). The circRNA junction microarray used in this study offers several additional advantages, as it is well established for various tissues (Guo et al., 2014; Memczak et al., 2013; You et al. 2015; Zhang et al., 2017) and disease models, including cardiovascular (Wu et al., 2016) and based on previously annotated, detected and verified circRNAs. Additionally, specific microarrays exhibit a higher efficiency in circRNA profiling compared to RNA sequencing (S. Li et al., 2019). Furthermore, the microarray-based approach was favored, since our bioinformatics pipeline had issues to reliably calculate circRNA expression levels from the RNA sequencing data.

In this study, circRNA microarray analysis of cardiomyocytes isolated from TAC and sham mouse hearts revealed differential expression of circRNAs. In total, about 200 significantly up- and 190 significantly downregulated circRNAs are detected.

Interestingly, the published RNAseq data from TAC and sham hearts do not fully support this result, as noted above. Werfel and co-workers report over 650 differentially expressed circRNAs in rRNA depleted, RNAse R enriched RNA sequencing of TAC vs. sham mouse hearts, however only the minority was statistically significant (Werfel et al., 2016). In their study, the authors describe a tendency towards an increased circRNA formation in TAC mice 3 weeks after surgery. Approximately 25% of the host genes of these

differentially expressed circRNAs were detected in our microarray-based circRNA study using TAC mice sacrificed approximately 4 weeks after surgery. Li and colleagues investigated the circRNA transcriptome at 3 different time points after TAC surgery and performed circRNA microarray transcriptome profiling, revealing 554 significantly differential expressed circRNAs at 2 weeks, 127 at 4 weeks and 186 at 8 weeks postoperatively (X. Li et al., 2022). Of these, only 11 upregulated and 3 downregulated circRNAs were altered in expression at all time points examined.

Competing endogenous RNA network analysis based on circRNA – miRNA - mRNA interaction prediction, revealed specific target pathways of differentially expressed cricRNAs. After 2 weeks, mRNAs encoding adrenergic signaling, pyruvate metabolism, metabolic regulators and matrix metallopeptidases were targeted. In contrast, after 4 weeks collagens and matrix regulators, as well as adipokines and after 8 weeks regulators of inflammatory response and mitochondrial enzymes were affected. Although a similar approach was used in our study, namely a microarray-based analysis of circRNA expression in mice 4 weeks after TAC surgery, the data did not show similarities in terms of the most differentially expressed circRNAs. This discrepancy could be due to different surgical techniques or variations in the expression of the hypertrophy phenotype.

In contrast, an additional study using RNA sequencing from rRNA depleted, RNAse R enriched RNAs from isolated hearts of TAC and sham mice did not reveal significant differences in circRNA expression (Tan et al., 2017).

As previously reported in the circRNA profiling for soleus muscle, the majority of differentially expressed circRNAs detected in TAC vs. sham microarray, originate from exonic loci.

Based on GO term analysis, host genes encoding up- or downregulated circRNAs are mainly annotated to *binding and catalytic activities* in molecular function category and were involved in *cellular*, as well as *metabolic processes* and *biological regulations for biologic functions*. Concerning cellular components, the majority is linked to *cellular anatomic entities*, *intracellular* and *protein-containing complexes*.

Annotations for protein classes differ slightly between up- & downregulated circRNAs. *Protein modifying enzymes* and *metabolite interconversion enzymes* are detected for both groups, however downregulated circRNAs demonstrate an annotation for *gene-specific transcriptional regulators*.

GO analysis for overrepresented GO terms could only find significant overrepresentation in the category *biological process* for upregulated circRNAs.

Overrepresented host genes annotate to GO terms *production of miRNAs involved in gene silencing by miRNA*, as well as *regulation of mRNA stability*.

This finding is of particular interest, since circRNAs are well known to interact with miRNAs and repress their function in the mRNA degradation and/or silencing pathways (Memczak et al., 2013).

Generally, the annotated GO terms are rather unspecific, which might be related to the heterogenous pool of circRNAs probe sets predefined in the commercially available circRNA microarray. These probes detect previously annotated circRNAs deriving from various pathologies, tissues and organs including the heart (Guo et al., 2014; Memczak et al., 2013; You et al., 2015).This heterogeneity in the origin of circRNA probes was a fundamental limitation of our microarray-based study on circRNA expression alteration in a specific pathology such as heart hypertrophy.

Nevertheless, multiple promising candidates for further functional studies were identified by GO term overrepresentation analysis of upregulated circRNA host genes in the category *biological function*.

Among these, *Pumilio RNA-binding family member 1 and* 2 (*Pum1* and *2*), as well as *zinc finger CCCH type containing 7B* (*Zc3h7b*), are host genes annotated to the GO term *Production of miRNAs involved in gene silencing*.

Pum1 and *2* are post-transcriptional regulators, widely expressed in various tissues. Both repress and promote translation as well as modify target mRNA stability and thereby exhibiting an important role in embryogenesis and pluripotency of embryonic stem cells (Uyhazi et al., 2020). Since circRNAs can influence miRNAs function via miRNA-sponging (Hansen et al., 2013; Memczak et al., 2013), a circRNA-miRNA interaction prediction analysis for potential miRNA binding sites of circPum1 and 2 was performed. Several potential miRNA interaction partners were identified, however none of them has been previously linked to the pathogenesis of cardiovascular diseases.

ZC3H7B on the other hand, is an ubiquitously expressed RBP, that binds to miRNAs involved in heart disease, such as miR7-1 (Geng et al., 2016) and miR29a (Zhang et al., 2019), via a zinc finger domain. Furthermore, it acts as a specific regulator of miRNA biogenesis (Treiber et al., 2017). The cicRNA-miRNA interaction predictions provided several potential targets, which have not been associated with cardiovascular disease.

In conclusion, *Pum 1* & 2- and *Zc3h7b*-derived circRNAs might represent promising candidates for further studies.

The other GO term, which is overrepresented in upregulated circRNAs, encompasses *regulators of mRNA stability* including *Smad family member 4* (*Smad4*) and *Fragile X mental retardation, autosomal homolog 2* (*Fxr2*).

The *Smad4* host gene originates mmu_circRNA_005305, which is 3-fold upregulated in TAC mice. *Smad4* was previously reported as a central mediator in transforming growth factor β (TGF-β) signaling, a cytokine involved in various physiological, as well as pathological processes, including heart development (Qi et al., 2007) and induction of hypertrophy (Nakajima et al., 2000). *Smad4*-specific deletion in cardiomyocytes leads to cardiac hypertrophy and heart failure presumably via an altered cellular response to TGF-β (Wang et al., 2005). In our study, up-regulation of circular *Smad4* transcript is evident under TAC conditions, which might cause a reduction of the linear *Smad4* transcript via mRNA trapping and consecutively a decline of SMAD4 protein level. In addition, circular Smad4 might also act as a miRNA sponge, indicated by predicted miRNA interaction with miR-423-5p, a miRNA involved in down-regulation of 2 ion channels, hyperpolarization-activated cyclic nucleotide gated channel 4 (HCN4) and funny current (If) (D'Souza et al., 2017), in the sinus node and in exercise-induced bradycardia. Furthermore, miR-423-5p is upregulated in left-ventricular remodeling after infarction (Bauters et al., 2013).

FXR2 represents a ubiquitously expressed RNA-binding protein, which transports specific mRNAs to cellular compartments and inhibits protein translation of targets. So far, neither FXR2, nor the predicted miRNA targets of the circular isoform, have been associated with cardiovascular diseases.

In addition to these candidates from the overrepresentation analysis, the highest upregulated circRNAs under TAC conditions encompasses additional promising candidates for future functional studies.

Mmu_circRNA_25584 originates from the *Adck1* gene locus and is 7-times upregulated in TAC condition. *Adck1* mRNA is ubiquitously expressed in various mouse tissues and GO annotations indicate *protein kinase activity* and *involvement in mitochondrial organization and positive regulation of christae formation*. Recently, *Adck1* has been described in a mitochondrial pathway consisting of YME-like ATPase (YME1L1), OPA1 mitochondrial dynamin like GTPase (OPA1) and inner membrane mitochondrial protein (IMMT), thereby maintaining structures and functions in Drosophila muscle (Yoon et al., 2019). The miRNA interaction prediction revealed a potential interaction with miRNA-

1966-5p, a validated target of several circRNAs in an isoproterenol hydrochloride hypertrophy model (M.-H. Yang et al., 2020).
Furthermore, mmu_circRNA_31359 represents an additional circRNA candidate, which is approximately 3 times upregulated in TAC hearts. The host gene *cadherin 2* (*Cdh2*) represent a member of the calcium-dependent glycoproteins family cadherin, involved in cell adhesion and is wildly expressed in various tissues, especially in brain and heart.
In cardiomyocytes, *Cdh2* maintains structural and functional integrity and is part of the adherence junctions, essential for electric coupling. Depletion of *Cdh2* leads to dilated cardiomyopathy, arrythmias, as well as damaged function of the heart (Kostetskii et al., 2005; Li et al., 2005; Mayosi et al., 2017). Interestingly, *Cdh2* is linked to the development of heart failure in a cardiac hypertrophy rat model (dos Santos et al., 2016). Furthermore, CDH2 is involved in numerous signaling pathways mediating cell differentiation and proliferation, apoptosis and angiogenesis (Ishimine et al., 2013). Of note, none of the predicted miRNA interaction partners of the circular Cdh2 isoform have been previously described in the context of cardiovascular diseases.
In addition, mmu_circRNA_002563 represents an additional circRNA, which is 3-fold upregulated in TAC mice and originates from *Asxl transcriptional regulator 3* (*Asxl3*) gene. ASXL3 exhibits an important function during cardiac development, most likely by influencing mRNAs associated with apoptosis and cell proliferation (Fu et al., 2021).
In contrast to the host genes of the highest upregulated circRNAs, the host genes of the downregulated cirRNAs were not associated with cardiac disease pathogenesis so far.

Interestingly, circSlc8a1, one of the most abundant circRNAs in human and mouse cardiomyocytes (Y. Li et al., 2017; Werfel et al., 2016), is not differentially expressed in our microarray-based analysis of TAC vs. sham cardiomyocytes. In a parallel approach, circSlc8a1 was recently reported to sponge hypertrophy related miRNA miR-133a (Lim et al., 2019). However, altered expression level of circSlc8a1 during cardiac stress was not observed (Lim et al., 2019; Werfel et al., 2016; Wu et al., 2016), which is in line with our observation. However, it is assumed, that the amount of sequestered miR-133a increases during cardiac stress (Lim et al., 2019).

To date, circRNA-miRNA interactions are the best-investigated functions of circRNAs. In this study, no functional experiments were performed to investigate potential mechanistic processes; however, our circRNA microarray analysis provided several

potential circRNA-miRNA interactions, as discussed previously. Nevertheless, mRNA trapping, translation into proteins, transcriptional regulators or RBP sponges may represent additional functions of circRNAs in the pathogenesis of cardiac hypertrophy.

In summary, this study provides evidence of altered circRNA expression in a TAC-induced, murine heart hypertrophy model. Several novel circRNAs were discovered, that may exert important functions in the pathogenesis of cardiac hypertrophy.
However, subsequent analysis will be necessary including validation of differential expression using qRT-PCR quantification, as well as bioinformatics-based selection approaches. Therefore, a comprehensive list, containing all differentially expressed circRNAs, is added in the appendix. In a second step, promising circRNAs need to be functionally tested, e.g., using shRNA-mediated knockdown and overexpression approaches.

IV.1 Conclusion

In this study, we made use of an in-house circRNA detection pipeline to identify numerous novel circRNA candidates in mouse soleus muscle and heart. These predictions were experimentally verified for randomly selected candidates, including circZfp827, circNeb, circSec24b, circNfix, circSmad4, circFhl2 and circMmp15, indicating a high accuracy of our pipeline.
The circRNAs studied show tissue and cell-type specificity and are co-expressed with their linear counterparts. These findings suggest distinct biological functions and regulatory processes for circRNA formation. Here, further studies are needed to verify our preliminary findings.
Additionally, this study provides further evidence for alteration of circRNA expression in heart hypertrophy. Gene ontology analysis and miRNA interaction prediction revealed, host genes and potential miRNA targets of numerous differentially expressed circRNAs are involved in cardiovascular disease pathways. Accordingly, these circRNAs might exert important functions in the pathogenesis of heart hypertrophy, however, more detailed studies are necessary to verify the differential expression.
In the future, our findings may result in a better understanding of the pathogenesis of cardiac hypertrophy and thereby lead to therapeutic targets, as well as in the identification of novel biomarkers.

V ZUSAMMENFASSUNG

Zirkuläre RNAs stellen eine Untergruppe der RNAs dar, welche sich durch eine ringförmige Struktur und hohe Stabilität auszeichnen. Kürzlich veröffentlichte Studien zeigen, dass circRNAs eine entscheidende Rolle in der Pathogenese von Erkrankungen spielen, unter anderem indem sie regulatorische miRNAs puffern und dadurch eine post-transkriptionelle Genkontrolle ausüben. Pathologische Herzhypertrophie ist ein maladaptiver Prozess des Herzens, der zu einer Reduktion der Ejektionsfraktion und damit zu Arrhythmien, Herzversagen und Tod führt. Bislang wurde die Rolle von circRNAs hierbei kaum charakterisiert. In dieser Studie wurde eine hausinterne circRNA Detektionspipeline angewendet, um neue circRNAs im Soleus Muskel, sowie im Herzen der Maus zu identifizieren. Kandidaten wurden mittels RT-PCR, Sanger-Sequenzierung in Kombination mit RNAse R Behandlung validiert und charakterisiert, sowie deren Expressionsprofile in verschiedenen Geweben durch semi- & quantitative PCR analysiert. Des Weiteren wurde die Veränderung der circRNA Expression in einem TAC-induzierten Herzhypertrophie-Modell der Maus mittels Microarray untersucht. Als Ergebnis konnten zahlreiche neue circRNA Kandidaten im Soleus Muskel und im Herzen identifiziert werden. Von diesen wurden 4 ausgewählt, circZfp287, circNeb, circSec24b und circNfix und experimentell als circRNAs bestätigt, wodurch die Genauigkeit der Detektionspipeline belegt wurde. Die untersuchten circRNAs zeigten eine Koexpression mit ihren linearen Transkripten, sowie eine Gewebs- & Zelltypspezifität, was auf Regulationsmechanismen bei der circRNA Bildung, sowie potentielle biologische Funktionen hinweist. Im Herzen konnten signifikante Expressionsunterschiede zwischen circRNAs und deren linearen Isoformen gezeigt werden. Die Mikroarray Untersuchung wies fast 400 signifikant differentiell exprimierte circRNAs unter Hypertrophie-Konditionen nach. Nur ein Teil dieser circRNAs stammt entweder von Wirtsgenen ab, oder interagiert potentiell mit miRNAs, die bekannterweise in der Pathogenese der Herzhypertrophie involviert sind. Bisherige Arbeiten hierzu lieferten uneindeutige Daten zu Veränderungen der circRNA Expression unter Herzhypertrophie-Konditionen. Die dargestellten circRNA Transkriptomdaten dienen als Ausgangspunkt für zukünftige Studien, bei denen differentiell exprimierte circRNAs validiert und im Anschluss funktionell getestet werden sollten. Das daraus resultierende Wissen könnte neue Einblicke in post-transkriptionelle Regulationsnetzwerke bei Herzhypertrophie geben und möglicherweise Ziele für Therapieansätze oder Biomarker Entwicklung liefern.

VI SUMMARY

Circular RNAs represent a subclass of RNAs characterized by a loop structure and high stability in various environments. Recently, numerous circRNAs were demonstrated to play crucial roles in disease pathways, amongst others by sponging regulatory miRNAs and thereby regulating post-transcriptional gene control. Pathological cardiac hypertrophy is a process, in which the heart undergoes various adaptive processes leading to a reduced ejection fraction and subsequently to arrhythmias, heart failure and death. To date, the role of circRNAs in this pathology has been poorly characterized. In this study, we made use of an in-house circRNA detection pipeline to identify novel circRNA candidates in soleus muscle and heart. Candidates were validated and characterized by RT-PCR, as well as Sanger sequencing combined with RNAse R enrichment assays. Subsequently, expression profiles were investigated by quantitative and semi-quantitative RT-PCRs in various tissues. Ultimately, altered circRNA expression was studied in a TAC heart hypertrophy mouse model using a microarray-based transcriptome profiling. As a result, numerous de novo circRNA candidates were identified in soleus muscle, as well as in the heart. In total, 4 selected circRNA candidates from soleus muscle, including circZfp827, circNeb, circSec24b and circNfix, were experimentally verified, demonstrating the accuracy of the in-house circRNA detection pipeline. All investigated circRNAs are co-expressed with their linear counterparts and display tissue- and cell-type-specificity, indicating regulatory mechanisms in circRNA formation and potential biological functions. Quantification of circRNAs identified in heart revealed significant differential expression of selected circRNAs compared to their linear counterparts. Additionally, microarray analysis detected a significantly altered expression of nearly 400 circRNAs in a murine heart hypertrophy model. Interestingly, a subset of these circRNAs either derive from host genes, or are predicted to interact with miRNAs, involved in essential signaling pathways of hypertrophy pathogenesis. Until now, our approach provides one of the first microarray-based studies of differentially expressed circRNAs in a TAC-induced hypertrophy model. Previous reports, based on RNA sequencing data, did not provide conclusive data on altered circRNA expression. In the future, validation of differential expression of these circRNA candidates by qRT-PCR and Sanger sequencing of the back-splice junction in combination with functional assays may provide new insights into post-transcriptional regulatory networks involved in cardiac hypertrophy and may offer new biomarkers.

VII ABBREVIATIONS

A	Adenosine
ACR	Apoptosis repressor with CARD domain
Actr2	Actin Related Protein 2
ADAR1	RNA editing enzyme adenosine deaminase acting on RNA 1
Adck1	AarF domain containing kinase 1
Akap7	A-Kinase Anchoring Protein 7
Amotl1	*Angiomotin-like Protein 1*
AMPK	AMP-activated protein kinase K
ANP	Natriuretic peptide A
ANP	Atrial natriuretic peptide
Approx.	Approximately
Asxl3	Asxl transcriptional regulator 3
BCLAF1	Bcl associated factor 1
BMP	Bone morphogenetic protein
BNP	Natriuretic peptide B
Bp	Base pair
C	Cytosine
CaMKII	Ca^{2+}/calmodulin-dependent protein kinase II
cAMP	Cyclic adenosine monophosphate
Cdh2	Cadherin 2
cDNA	Complementary DNA
CDR1	Cerebellar Degeneration Related Protein 1
CDR1as	CDR1 antisense RNA
cGMP	Cyclic guanosine monophosphate
circRNA	Circular RNA
ciRNA	Intron-containing circular RNA
cm	Cardiomyocyte
Ct	Cycle threshold

CTRP9	C1q/TNF-related protein 9
DCC	DCC Netrin 1 Receptor
DDX39A	DExD-Box Helicase 39A
DDX39B	DExD-Box Helicase 39B
DNA	Desoxyribonucleic acid
E2F1	E2F transcription factor
EDL	Extensor digitorum longus muscle
EIcircRNA	Exon-intron-containing circular RNA
EPACs	Exchange proteins directly activated by cAMP
EtOH	Ethanol
FAK	Focal Adhesion Kinase
FC	Foldchange
FDR	False discovery rate
FGF	Fibroblast growth factor
FGFR4	Fibroblast Growth Factor Receptor 4
Fhl2	Four And A Half LIM Domains 2
Foxo3	Forkhead Box O 3
FUT10	Fucosyltransferase 10
Fxr2	FMR1 Autosomal Homolog 2
G	Guanine
g	G-force
GAPDH	Glyceraldehyde-3-phosphate dehydrogenase
Gata4	GATA Binding Protein 4
GO	Gene Ontology
GSK3β	Gylcogen synthas kinase 3 beta
HCN4	Hyperpolarization-activated cyclic nucleotide gated channel 4
HIF-α	Hypoxia Inducible Subunit Alpha
HPRT	Hypoxanthine Phosphoribosyltransferase 1
HRCR	Heart-related circRNA
HUR	Hu-antigen R

I	Inosin
Id-1	Inhibitor of DNA-binding 1
IGF1	Insulin-like growth factor 1
IMMT	Inner membrane mitochondrial protein
IP3	Inositol triphosphate
IRES	Internal ribosome entry sites
LMO7	LIM domain only protein 7
MBL	Muscleblind
Mettl21c	Methyltransferase like 21c
min	Minutes
miRISC	MiRNA-induced RNA silencing complex
miRNA	MicroRNA
ml	Milliliters
Mmp15	Matrix Metallopeptidase 15
MPC	Myogenic progenitor cell
MRE	MiRNA responsive element
MRF	Myogenic regulatory factor
mRNA	Messenger RNA
Mt	Knock out
mTOR	Mechanistic target of rapamycin
Myf5	Myogenic Factor 5
MYH7	Myosin 7
Myo9a	*Myosin IXA*
ncRNA	Non-coding RNA
ncRNA	Non-coding RNA
Neb	Nebulin
NFAT	Nuclear factor of activated T cells
Nfix	Nuclear factor I/X
NGS	Next-generation sequencing
NO	Nitric oxide
Non-cm	Non-cardiomyocyte
Nt	nucleotide
OPA1	OPA1 mitochondrial dynamin like GTPase

ORF	Open reading frames
PABPN1	poly(A) binding protein nuclear 1
Pantr1	POU domain, class 3, transcription factor 3 adjacent noncoding transcript 1
PBS	Phosphate buffered saline
PCR	Polymerase chain reaction
PDGF	Platelet-derived growth factor
PDK1	Pyruvat Dehydrogenase Liponamide Kinase Isoenzym 1
PGC1α	Peroxisome proliferator-activated receptor-ɣ co-activator 1 α
PKB	Protein Kinase B
Pol II	Polymerase II
Poly-A	Polyadenylation
Pre-mRNA	Precursor mRNA
Pum1	Pumilio RNA Binding Family Member 1
Pum2	Pumilio RNA Binding Family Member 2
PVT1	Pvt1 Oncogen
QK1	Quaking 1
qPCR	Quantitative PCR
RBM20	RNA binding motif protein 20
RBP	RNA binding protein
rcf	Relative centrifugal force
RNA	Ribonucleic acid
RNA-seq	RNA sequencing
RNAse R	Ribonuclease R
rRNA	Ribosomal RNA
RT	Room temperature
RYR2	Ryanodine 2 receptor
Sec	seconds
Sec24b	Sec24 related gene family, member B
SEM	Standard error of mean
SLC8A1	Solute Carrier Family 8 Member A1

SM	Soleus muscle
SMAD 2/3	SMAD family member 2 & 3
Smad4	SMAD family member 4
SMARCA5	SWI/SNF Related, Matrix Associated, Actin Dependent Regulator Of Chromatin, Subfamily A, Member 5
snRNP	Small nuclear ribonucleoportein
SRF	Serum response factor
SRY	Sex determining region Y
STIM1	Stromal interaction molecule 1
T	Thymine
TA	Tibialis anterior muscle
TAC	Transverse aortic constriction
TET1	Ten-eleven translocation methylcytosine dioxygenase 1
TFG β	Transforming growth factor β
TGF-β	Transforming growth factor-β
Tm	Primer melting temperature
TRPC	Transient receptor potential channels
TTN	Titin
U	Uracil
U	Unit
Usp3	Ubiquitin Specific Peptidase 3
UTR	Untranslated regions
UV	Ultraviolet
VEGF	Vascular endothelial growth factor
Wnt3a	Wnt Family Member 3A
Wt	Wild-type
YME1L1	YME-like ATPase
Zc3h7b	Zinc Finger CCCH-Type Containing 7B
Zfp532	Zinc Finger Protein 532
Zfp609	Zinc Finger Protein 609
Zfp827	Zinc finger protein 827

ZNF 609	Zinc Finger Protein 609
β-actin	Actin beta
β-MHC	Beta myosin heavy chain
µg	Microgram
µl	Microliters

VIII LIST OF FIGURES

IX LIST OF TABLES

X REFERENCES

Abdelmohsen, K., Panda, A. C., De, S., Grammatikakis, I., Kim, J., Ding, J., . . . Gorospe, M. (2015). Circular RNAs in monkey muscle: age-dependent changes. *Aging (Albany NY)*, *7*(11), 903-910. https://doi.org/10.18632/aging.100834

Abdelmohsen, K., Panda, A. C., Munk, R., Grammatikakis, I., Dudekula, D. B., De, S., . . . Gorospe, M. (2017). Identification of HuR target circular RNAs uncovers suppression of PABPN1 translation by CircPABPN1. *RNA Biol*, *14*(3), 361-369. https://doi.org/10.1080/15476286.2017.1279788

Abe, N., Matsumoto, K., Nishihara, M., Nakano, Y., Shibata, A., Maruyama, H., . . . Abe, H. (2015). Rolling Circle Translation of Circular RNA in Living Human Cells. *Sci Rep*, *5*, 16435. https://doi.org/10.1038/srep16435

Ahmed, I., Karedath, T., Andrews, S. S., Al-Azwani, I. K., Mohamoud, Y. A., Querleu, D., . . . Malek, J. A. (2016). Altered expression pattern of circular RNAs in primary and metastatic sites of epithelial ovarian carcinoma. *Oncotarget*, *7*(24), 36366-36381. https://doi.org/10.18632/oncotarget.8917

Altesha, M. A., Ni, T., Khan, A., Liu, K., & Zheng, X. (2019). Circular RNA in cardiovascular disease. *J Cell Physiol*, *234*(5), 5588-5600. https://doi.org/10.1002/jcp.27384

Apponi, L. H., Corbett, A. H., & Pavlath, G. K. (2011). RNA-binding proteins and gene regulation in myogenesis. *Trends Pharmacol Sci*, *32*(11), 652-658. https://doi.org/10.1016/j.tips.2011.06.004

Arnberg, A. C., Van Ommen, G. J., Grivell, L. A., Van Bruggen, E. F., & Borst, P. (1980). Some yeast mitochondrial RNAs are circular. *Cell*, *19*(2), 313-319. https://doi.org/10.1016/0092-8674(80)90505-x

Ashwal-Fluss, R., Meyer, M., Pamudurti, N. R., Ivanov, A., Bartok, O., Hanan, M., . . . Kadener, S. (2014). circRNA biogenesis competes with pre-mRNA splicing. *Mol Cell*, *56*(1), 55-66. https://doi.org/10.1016/j.molcel.2014.08.019

Barbagallo, D., Caponnetto, A., Cirnigliaro, M., Brex, D., Barbagallo, C., D'Angeli, F., . . . Purrello, M. (2018). CircSMARCA5 Inhibits Migration of Glioblastoma Multiforme Cells by Regulating a Molecular Axis Involving Splicing Factors SRSF1/SRSF3/PTB. *Int J Mol Sci*, *19*(2). https://doi.org/10.3390/ijms19020480

Barrett, S. P., & Salzman, J. (2016). Circular RNAs: analysis, expression and potential functions. *Development*, *143*(11), 1838-1847.

Barrett, S. P., Wang, P. L., & Salzman, J. (2015). Circular RNA biogenesis can proceed through an exon-containing lariat precursor. *Elife*, *4*, e07540. https://doi.org/10.7554/eLife.07540

Bauters, C., Kumarswamy, R., Holzmann, A., Bretthauer, J., Anker, S. D., Pinet, F., & Thum, T. (2013). Circulating miR-133a and miR-423-5p fail as biomarkers for left ventricular remodeling after myocardial infarction. *International journal of cardiology*, *168*(3), 1837-1840.

Behjati, S., & Tarpey, P. S. (2013). What is next generation sequencing? *Archives of Disease in Childhood-Education and Practice*, *98*(6), 236-238.

Behm-Ansmant, I., Rehwinkel, J., Doerks, T., Stark, A., Bork, P., & Izaurralde, E. (2006). mRNA degradation by miRNAs and GW182 requires both CCR4: NOT deadenylase and DCP1: DCP2 decapping complexes. *Genes & development*, *20*(14), 1885-1898.

Bosch, L., de Haan, J. J., Bastemeijer, M., van der Burg, J., van der Worp, E., Wesseling, M., . . . Pasterkamp, G. (2020). The transverse aortic constriction heart failure animal model: a systematic review and meta-analysis. *Heart failure reviews*, 1-10.

Braun, T., Buschhausen-Denker, G., Bober, E., Tannich, E., & Arnold, H. H. (1989). A novel human muscle factor related to but distinct from MyoD1 induces myogenic conversion in 10T1/2 fibroblasts. *EMBO J*, *8*(3), 701-709. https://doi.org/10.1002/j.1460-2075.1989.tb03429.x

Braun, T., Rudnicki, M. A., Arnold, H. H., & Jaenisch, R. (1992). Targeted inactivation of the muscle regulatory gene Myf-5 results in abnormal rib development and perinatal death. *Cell*, *71*(3), 369-382. https://doi.org/10.1016/0092-8674(92)90507-9

Broughton, J. P., Lovci, M. T., Huang, J. L., Yeo, G. W., & Pasquinelli, A. E. (2016). Pairing beyond the seed supports microRNA targeting specificity. *Molecular cell*, *64*(2), 320-333.

Bui, A. L., Horwich, T. B., & Fonarow, G. C. (2011). Epidemiology and risk profile of heart failure. *Nat Rev Cardiol*, *8*(1), 30-41. https://doi.org/10.1038/nrcardio.2010.165

Burset, M., Seledtsov, I. A., & Solovyev, V. V. (2000). Analysis of canonical and non-canonical splice sites in mammalian genomes. *Nucleic Acids Res*, *28*(21), 4364-4375. https://doi.org/10.1093/nar/28.21.4364

Calvert, J. W., Condit, M. E., Aragón, J. P., Nicholson, C. K., Moody, B. F., Hood, R. L., . . . Barouch, L. A. (2011). Exercise protects against myocardial ischemia–reperfusion injury via stimulation of β3-adrenergic receptors and increased nitric oxide signaling: role of nitrite and nitrosothiols. *Circulation research*, *108*(12), 1448-1458.

Capel, B., Swain, A., Nicolis, S., Hacker, A., Walter, M., Koopman, P., . . . Lovell-Badge, R. (1993). Circular transcripts of the testis-determining gene Sry in adult mouse testis. *Cell*, *73*(5), 1019-1030. https://doi.org/10.1016/0092-8674(93)90279-y

Care, A., Catalucci, D., Felicetti, F., Bonci, D., Addario, A., Gallo, P., . . . Dalton, N. D. (2007). MicroRNA-133 controls cardiac hypertrophy. *Nature medicine*, *13*(5), 613-618.

Carmeliet, P., Ng, Y.-S., Nuyens, D., Theilmeier, G., Brusselmans, K., Cornelissen, I., . . . Mattot, V. (1999). Impaired myocardial angiogenesis and ischemic cardiomyopathy in mice lacking the vascular endothelial growth factor isoforms VEGF 164 and VEGF 188. *Nature medicine*, *5*(5), 495-502.

Chandler, D. S. (2011). Pre-mRNA Splicing. In M. Schwab (Ed.), *Encyclopedia of Cancer* (pp. 2972-2977). Springer Berlin Heidelberg. https://doi.org/10.1007/978-3-642-16483-5_4711

Chen, C. Y., & Sarnow, P. (1995). Initiation of protein synthesis by the eukaryotic translational apparatus on circular RNAs. *Science*, *268*(5209), 415-417. https://doi.org/10.1126/science.7536344

Chen, R., Jiang, T., Lei, S., She, Y., Shi, H., Zhou, S., . . . Liu, Y. (2018). Expression of circular RNAs during C2C12 myoblast differentiation and prediction of coding potential based on the number of open reading frames and N6-methyladenosine motifs. *Cell Cycle*, *17*(14), 1832-1845. https://doi.org/10.1080/15384101.2018.1502575

Chen, X., Han, P., Zhou, T., Guo, X., Song, X., & Li, Y. (2016). circRNADb: A comprehensive database for human circular RNAs with protein-coding annotations. *Scientific Reports*, *6*(1), 34985. https://doi.org/10.1038/srep34985

Cheng, J., Metge, F., & Dieterich, C. (2016). Specific identification and quantification of circular RNAs from sequencing data. *Bioinformatics*, *32*(7), 1094-1096.

Chintalgattu, V., Ai, D., Langley, R. R., Zhang, J., Bankson, J. A., Shih, T. L., . . . Pati, S. (2010). Cardiomyocyte PDGFR-β signaling is an essential component of the mouse cardiac response to load-induced stress. *The Journal of clinical investigation*, *120*(2), 472-484.

Cocquerelle, C., Daubersies, P., Majerus, M. A., Kerckaert, J. P., & Bailleul, B. (1992). Splicing with inverted order of exons occurs proximal to large introns. *Embo j*, *11*(3), 1095-1098.

Cocquerelle, C., Mascrez, B., Hétuin, D., & Bailleul, B. (1993). Mis-splicing yields circular RNA molecules. *FASEB J*, *7*(1), 155-160. https://doi.org/10.1096/fasebj.7.1.7678559

Conn, S. J., Pillman, K. A., Toubia, J., Conn, V. M., Salmanidis, M., Phillips, C. A., . . . Goodall, G. J. (2015). The RNA binding protein quaking regulates formation of circRNAs. *Cell*, *160*(6), 1125-1134. https://doi.org/10.1016/j.cell.2015.02.014

Correll, R. N., Goonasekera, S. A., van Berlo, J. H., Burr, A. R., Accornero, F., Zhang, H., . . . Chen, X. (2015). STIM1 elevation in the heart results in aberrant Ca2+ handling and cardiomyopathy. *Journal of molecular and cellular cardiology*, *87*, 38-47.

Davis, C. A., Hitz, B. C., Sloan, C. A., Chan, E. T., Davidson, J. M., Gabdank, I., . . . Narayanan, A. K. (2018). The Encyclopedia of DNA elements (ENCODE): data portal update. *Nucleic acids research*, *46*(D1), D794-D801.

Di, Y. F., Li, D. C., Shen, Y. Q., Wang, C. L., Zhang, D. Y., Shang, A. Q., & Hu, T. (2017). MiR-146b protects cardiomyocytes injury in myocardial ischemia/reperfusion by targeting Smad4. *Am J Transl Res*, *9*(2), 656-663.

dos Santos, D. O., Blefari, V., Prado, F. P., Silva, C. A., Fazan Jr, R., Salgado, H. C., . . . Prado, C. M. (2016). Reduced expression of adherens and gap junction proteins can have a fundamental role in the development of heart failure following cardiac hypertrophy in rats. *Experimental and molecular pathology*, *100*(1), 167-176.

Du, W. W., Fang, L., Yang, W., Wu, N., Awan, F. M., Yang, Z., & Yang, B. B. (2017). Induction of tumor apoptosis through a circular RNA enhancing Foxo3 activity. *Cell Death Differ*, *24*(2), 357-370. https://doi.org/10.1038/cdd.2016.133

Du, W. W., Yang, W., Chen, Y., Wu, Z. K., Foster, F. S., Yang, Z., . . . Yang, B. B. (2017). Foxo3 circular RNA promotes cardiac senescence by modulating multiple factors associated with stress and senescence responses. *Eur Heart J*, *38*(18), 1402-1412. https://doi.org/10.1093/eurheartj/ehw001

Du, W. W., Zhang, C., Yang, W., Yong, T., Awan, F. M., & Yang, B. B. (2017). Identifying and characterizing circRNA-protein interaction. *Theranostics*, *7*(17), 4183.

Dubin, R. A., Kazmi, M. A., & Ostrer, H. (1995). Inverted repeats are necessary for circularization of the mouse testis Sry transcript. *Gene*, *167*(1-2), 245-248. https://doi.org/10.1016/0378-1119(95)00639-7

Dudekula, D. B., Panda, A. C., Grammatikakis, I., De, S., Abdelmohsen, K., & Gorospe, M. (2016). CircInteractome: a web tool for exploring circular RNAs and their interacting proteins and microRNAs. *RNA biology*, *13*(1), 34-42.

D'Souza, A., Pearman, C. M., Wang, Y., Nakao, S., Logantha, S. J. R., Cox, C., . . . Linscheid, N. (2017). Targeting miR-423-5p reverses exercise training–induced HCN4 channel remodeling and sinus bradycardia. *Circulation research*, *121*(9), 1058-1068.

Enright, A. J., John, B., Gaul, U., Tuschl, T., Sander, C., & Marks, D. S. (2003). MicroRNA targets in Drosophila. *Genome Biol*, *5*(1), R1. https://doi.org/10.1186/gb-2003-5-1-r1

Fica, S. M., Tuttle, N., Novak, T., Li, N. S., Lu, J., Koodathingal, P., . . . Piccirilli, J. A. (2013). RNA catalyses nuclear pre-mRNA splicing. *Nature*, *503*(7475), 229-234. https://doi.org/10.1038/nature12734

Friedman, R. C., Farh, K. K.-H., Burge, C. B., & Bartel, D. P. (2009). Most mammalian mRNAs are conserved targets of microRNAs. *Genome research*, *19*(1), 92-105.

Frieler, R. A., & Mortensen, R. M. (2015). Immune cell and other noncardiomyocyte regulation of cardiac hypertrophy and remodeling. *Circulation*, *131*(11), 1019-1030.

Fu, F., Li, R., Lei, T.-y., Wang, D., Yang, X., Han, J., . . . Li, F.-t. (2021). Compound heterozygous mutation of the ASXL3 gene causes autosomal recessive congenital heart disease. *Human Genetics*, *140*(2), 333-348.

Gaudet, P., Livstone, M. S., Lewis, S. E., & Thomas, P. D. (2011). Phylogenetic-based propagation of functional annotations within the Gene Ontology consortium. *Briefings in bioinformatics*, *12*(5), 449-462.

Geng, H.-H., Li, R., Su, Y.-M., Xiao, J., Pan, M., Cai, X.-X., & Ji, X.-P. (2016). The circular RNA Cdr1as promotes myocardial infarction by mediating the regulation of miR-7a on its target genes expression. *PLoS One*, *11*(3), e0151753.

Gerstberger, S., Hafner, M., & Tuschl, T. (2014). A census of human RNA-binding proteins. *Nature Reviews Genetics*, *15*(12), 829-845.

Ghosal, S., Das, S., Sen, R., Basak, P., & Chakrabarti, J. (2013). Circ2Traits: a comprehensive database for circular RNA potentially associated with disease and traits. *Frontiers in genetics*, *4*, 283.

Gruner, H., Cortés-López, M., Cooper, D. A., Bauer, M., & Miura, P. (2016). CircRNA accumulation in the aging mouse brain. *Sci Rep*, *6*, 38907. https://doi.org/10.1038/srep38907

Guo, J. U., Agarwal, V., Guo, H., & Bartel, D. P. (2014). Expanded identification and characterization of mammalian circular RNAs. *Genome Biol*, *15*(7), 409. https://doi.org/10.1186/s13059-014-0409-z

Gupta, S. K., Garg, A., Bar, C., Chatterjee, S., Foinquinos, A., Milting, H., . . . Thum, T. (2018). Quaking Inhibits Doxorubicin-Mediated Cardiotoxicity Through Regulation of Cardiac Circular RNA Expression. *Circ Res*, *122*(2), 246-254. https://doi.org/10.1161/CIRCRESAHA.117.311335

Hagan, M., Zhou, M., Ashraf, M., Kim, I. M., Su, H., Weintraub, N. L., & Tang, Y. (2017). Long noncoding RNAs and their roles in skeletal muscle fate determination. *Noncoding RNA Investig*, *1*. https://doi.org/10.21037/ncri.2017.12.01

Hansen, T. B., Jensen, T. I., Clausen, B. H., Bramsen, J. B., Finsen, B., Damgaard, C. K., & Kjems, J. (2013). Natural RNA circles function as efficient microRNA sponges. *Nature*, *495*(7441), 384-388. https://doi.org/10.1038/nature11993

Hansen, T. B., Venø, M. T., Damgaard, C. K., & Kjems, J. (2016). Comparison of circular RNA prediction tools. *Nucleic acids research*, *44*(6), e58-e58.

Hansen, T. B., Wiklund, E. D., Bramsen, J. B., Villadsen, S. B., Statham, A. L., Clark, S. J., & Kjems, J. (2011). miRNA-dependent gene silencing involving Ago2-mediated cleavage of a circular antisense RNA. *Embo j*, *30*(21), 4414-4422. https://doi.org/10.1038/emboj.2011.359

Holtwick, R., van Eickels, M., Skryabin, B. V., Baba, H. A., Bubikat, A., Begrow, F., . . . Kuhn, M. (2003). Pressure-independent cardiac hypertrophy in mice with

cardiomyocyte-restricted inactivation of the atrial natriuretic peptide receptor guanylyl cyclase-A. *The Journal of clinical investigation*, *111*(9), 1399-1407.

Huang, C., Liang, D., Tatomer, D. C., & Wilusz, J. E. (2018). A length-dependent evolutionarily conserved pathway controls nuclear export of circular RNAs. *Genes & development*, *32*(9-10), 639-644.

Huang, S., Li, X., Zheng, H., Si, X., Li, B., Wei, G., . . . Liao, W. (2019). Loss of super-enhancer-regulated circRNA Nfix induces cardiac regeneration after myocardial infarction in adult mice. *Circulation*, *139*(25), 2857-2876.

Ishimine, H., Yamakawa, N., Sasao, M., Tadokoro, M., Kami, D., Komazaki, S., . . . Kuno, S. (2013). N-Cadherin is a prospective cell surface marker of human mesenchymal stem cells that have high ability for cardiomyocyte differentiation. *Biochemical and biophysical research communications*, *438*(4), 753-759.

Ivanov, A., Memczak, S., Wyler, E., Torti, F., Porath, H. T., Orejuela, M. R., . . . Rajewsky, N. (2015). Analysis of intron sequences reveals hallmarks of circular RNA biogenesis in animals. *Cell Rep*, *10*(2), 170-177. https://doi.org/10.1016/j.celrep.2014.12.019

Izumiya, Y., Shiojima, I., Sato, K., Sawyer, D. B., Colucci, W. S., & Walsh, K. (2006). Vascular endothelial growth factor blockade promotes the transition from compensatory cardiac hypertrophy to failure in response to pressure overload. *Hypertension*, *47*(5), 887-893.

Izumo, S., Lompre, A., Matsuoka, R., Koren, G., Schwartz, K., Nadal-Ginard, B., & Mahdavi, V. (1987). Myosin heavy chain messenger RNA and protein isoform transitions during cardiac hypertrophy. Interaction between hemodynamic and thyroid hormone-induced signals. *The Journal of clinical investigation*, *79*(3), 970-977.

Jakobi, T., Czaja-Hasse, L. F., Reinhardt, R., & Dieterich, C. (2016). Profiling and Validation of the Circular RNA Repertoire in Adult Murine Hearts. *Genomics Proteomics Bioinformatics*, *14*(4), 216-223. https://doi.org/10.1016/j.gpb.2016.02.003

James, M. A., Saadeh, A. M., & Jones, J. V. (2000). Wall stress and hypertension. *Journal of cardiovascular risk*, *7*(3), 187–190. https://doi.org/10.1177/204748730000700304

Jeck, W. R., & Sharpless, N. E. (2014). Detecting and characterizing circular RNAs. *Nat Biotechnol*, *32*(5), 453-461. https://doi.org/10.1038/nbt.2890

Jeck, W. R., Sorrentino, J. A., Wang, K., Slevin, M. K., Burd, C. E., Liu, J., . . . Sharpless, N. E. (2013). Circular RNAs are abundant, conserved, and associated with ALU repeats. *RNA*, *19*(2), 141-157. https://doi.org/10.1261/rna.035667.112

Jo, M. H., Shin, S., Jung, S.-R., Kim, E., Song, J.-J., & Hohng, S. (2015). Human Argonaute 2 has diverse reaction pathways on target RNAs. *Molecular cell*, *59*(1), 117-124.

Jonas, S., & Izaurralde, E. (2015). Towards a molecular understanding of microRNA-mediated gene silencing. *Nature Reviews Genetics*, *16*(7), 421-433.

Kelly, S., Greenman, C., Cook, P. R., & Papantonis, A. (2015). Exon Skipping Is Correlated with Exon Circularization. *J Mol Biol*, *427*(15), 2414-2417. https://doi.org/10.1016/j.jmb.2015.02.018

Khan, M. A., Reckman, Y. J., Aufiero, S., van den Hoogenhof, M. M., van der Made, I., Beqqali, A., . . . Pinto, Y. M. (2016). RBM20 Regulates Circular RNA Production From the Titin Gene. *Circ Res*, *119*(9), 996-1003. https://doi.org/10.1161/CIRCRESAHA.116.309568

Kong, Y., Shelton, J. M., Rothermel, B., Li, X., Richardson, J. A., Bassel-Duby, R., & Williams, R. S. (2001). Cardiac-specific LIM protein FHL2 modifies the hypertrophic response to β-adrenergic stimulation. *Circulation*, *103*(22), 2731-2738.

Kostetskii, I., Li, J., Xiong, Y., Zhou, R., Ferrari, V. A., Patel, V. V., . . . Radice, G. L. (2005). Induced deletion of the N-cadherin gene in the heart leads to dissolution of the intercalated disc structure. *Circulation research*, *96*(3), 346-354.

Kozak, M. (1979). Inability of circular mRNA to attach to eukaryotic ribosomes. *Nature*, *280*(5717), 82-85. https://doi.org/10.1038/280082a0

Kuwahara, F., Kai, H., Tokuda, K., Kai, M., Takeshita, A., Egashira, K., & Imaizumi, T. (2002). Transforming growth factor-β function blocking prevents myocardial fibrosis and diastolic dysfunction in pressure-overloaded rats. *Circulation*, *106*(1), 130-135.

Labeit, S., Ottenheijm, C. A., & Granzier, H. (2011). Nebulin, a major player in muscle health and disease. *The FASEB journal*, *25*(3), 822-829.

Laplante, M., & Sabatini, D. M. (2012). mTOR signaling in growth control and disease. *Cell*, *149*(2), 274-293.

Lasda, E., & Parker, R. (2014). Circular RNAs: diversity of form and function. *RNA*, *20*(12), 1829-1842. https://doi.org/10.1261/rna.047126.114

Lasda, E., & Parker, R. (2016). Circular RNAs co-precipitate with extracellular vesicles: a possible mechanism for circRNA clearance. *PLoS One*, *11*(2), e0148407.

Lavenniah, A., Luu, T. D. A., Li, Y. P., Lim, T. B., Jiang, J., Ackers-Johnson, M., & Foo, R. S. (2020). Engineered Circular RNA Sponges Act as miRNA Inhibitors to Attenuate Pressure Overload-Induced Cardiac Hypertrophy. *Mol Ther*, *28*(6), 1506-1517. https://doi.org/10.1016/j.ymthe.2020.04.006

Legnini, I., Di Timoteo, G., Rossi, F., Morlando, M., Briganti, F., Sthandier, O., . . . Bozzoni, I. (2017). Circ-ZNF609 Is a Circular RNA that Can Be Translated and Functions in Myogenesis. *Mol Cell*, *66*(1), 22-37 e29. https://doi.org/10.1016/j.molcel.2017.02.017

Li, C., Li, X., Yao, Y., Ma, Q., Ni, W., Zhang, X., . . . Hu, S. (2017). Genome-wide analysis of circular RNAs in prenatal and postnatal muscle of sheep. *Oncotarget*, *8*(57), 97165-97177. https://doi.org/10.18632/oncotarget.21835

Li, H., Li, K., Lai, W., Li, X., Wang, H., Yang, J., . . . Qiu, Y. (2018). Comprehensive circular RNA profiles in plasma reveals that circular RNAs can be used as novel biomarkers for systemic lupus erythematosus. *Clinica Chimica Acta*, *480*, 17-25.

Li, H., Wei, X., Yang, J., Dong, D., Hao, D., Huang, Y., . . . Chen, H. (2018). circFGFR4 Promotes Differentiation of Myoblasts via Binding miR-107 to Relieve Its Inhibition of Wnt3a. *Mol Ther Nucleic Acids*, *11*, 272-283. https://doi.org/10.1016/j.omtn.2018.02.012

Li, H., Xu, J. D., Fang, X. H., Zhu, J. N., Yang, J., Pan, R., . . . Shan, Z. X. (2020). Circular RNA circRNA_000203 aggravates cardiac hypertrophy via suppressing miR-26b-5p and miR-140-3p binding to Gata4. *Cardiovasc Res*, *116*(7), 1323-1334. https://doi.org/10.1093/cvr/cvz215

Li, H., Yang, J., Wei, X., Song, C., Dong, D., Huang, Y., . . . Chen, H. (2018). CircFUT10 reduces proliferation and facilitates differentiation of myoblasts by sponging miR-133a. *J Cell Physiol*, *233*(6), 4643-4651. https://doi.org/10.1002/jcp.26230

Li, J., Patel, V. V., Kostetskii, I., Xiong, Y., Chu, A. F., Jacobson, J. T., . . . Radice, G. L. (2005). Cardiac-specific loss of N-cadherin leads to alteration in connexins with conduction slowing and arrhythmogenesis. *Circulation research*, *97*(5), 474-481.

Li, J.-H., Liu, S., Zhou, H., Qu, L.-H., & Yang, J.-H. (2014). starBase v2. 0: decoding miRNA-ceRNA, miRNA-ncRNA and protein–RNA interaction networks from large-scale CLIP-Seq data. *Nucleic acids research*, *42*(D1), D92-D97.

Li, S., Teng, S., Xu, J., Su, G., Zhang, Y., Zhao, J., . . . Lu, Z. J. (2019). Microarray is an efficient tool for circRNA profiling. *Briefings in bioinformatics*, *20*(4), 1420-1433.

Li, X., Liu, C. X., Xue, W., Zhang, Y., Jiang, S., Yin, Q. F., . . . Chen, L. L. (2017). Coordinated circRNA Biogenesis and Function with NF90/NF110 in Viral Infection. *Mol Cell*, *67*(2), 214-227 e217. https://doi.org/10.1016/j.molcel.2017.05.023

Li, X., Liu, J., Lu, Q., Ren, D., Sun, X., Rousselle, T., . . . Li, J. (2019). AMPK: a therapeutic target of heart failure—not only metabolism regulation. *Bioscience reports*, *39*(1).

Li, X., Tan, W., Zheng, S., Pyle, W. G., Zhu, C., Chen, H., Kang, L., Wu, J., Zou, Y., Backx, P. H., & Yang, F. H. (2022). Differential mRNA Expression and Circular RNA-Based Competitive Endogenous RNA Networks in the Three Stages of Heart Failure in Transverse Aortic Constriction Mice. *Frontiers in physiology*, *13*, 777284.

Li, Y., Zhang, J., Huo, C., Ding, N., Li, J., Xiao, J., . . . Xu, J. (2017). Dynamic Organization of lncRNA and Circular RNA Regulators Collectively Controlled Cardiac Differentiation in Humans. *EBioMedicine*, *24*, 137-146. https://doi.org/10.1016/j.ebiom.2017.09.015

Li, Z., Huang, C., Bao, C., Chen, L., Lin, M., Wang, X., . . . Shan, G. (2015). Exon-intron circular RNAs regulate transcription in the nucleus. *Nat Struct Mol Biol*, *22*(3), 256-264. https://doi.org/10.1038/nsmb.2959

Liang, D., & Wilusz, J. E. (2014). Short intronic repeat sequences facilitate circular RNA production. *Genes Dev*, *28*(20), 2233-2247. https://doi.org/10.1101/gad.251926.114

Lim, T. B., Aliwarga, E., Luu, T. D. A., Li, Y. P., Ng, S. L., Annadoray, L., . . . Foo, R. S.-Y. (2019). Targeting the highly abundant circular RNA circSlc8a1 in cardiomyocytes attenuates pressure overload induced hypertrophy. *Cardiovascular research*, *115*(14), 1998-2007.

Ling, H., Zhang, T., Pereira, L., Means, C. K., Cheng, H., Gu, Y., . . . Bers, D. (2009). Requirement for Ca 2+/calmodulin–dependent kinase II in the transition from pressure overload–induced cardiac hypertrophy to heart failure in mice. *The Journal of clinical investigation*, *119*(5), 1230-1240.

Liu, Y.-C., Li, J.-R., Sun, C.-H., Andrews, E., Chao, R.-F., Lin, F.-M., . . . Cheng, C. (2016). CircNet: a database of circular RNAs derived from transcriptome sequencing data. *Nucleic acids research*, *44*(D1), D209-D215.

Lodish H., B. A., Matsudaira P., Krieger M., Scott MP., Zipursky SL., Darnell J. (2004). *Molecular Cell Biology* (Vol. 8th ed.). W. H. Freeman.

Lukiw, W. (2013). Circular RNA (circRNA) in Alzheimer's disease (AD). *Frontiers in genetics*, *4*, 307.

Lymperopoulos, A., Rengo, G., & Koch, W. J. (2013). Adrenergic nervous system in heart failure: pathophysiology and therapy. *Circulation research*, *113*(6), 739-753.

Maillet, M., Van Berlo, J. H., & Molkentin, J. D. (2013). Molecular basis of physiological heart growth: fundamental concepts and new players. *Nature reviews Molecular cell biology*, *14*(1), 38-48.

Mantione, K. J., Kream, R. M., Kuzelova, H., Ptacek, R., Raboch, J., Samuel, J. M., & Stefano, G. B. (2014). Comparing bioinformatic gene expression profiling methods: microarray and RNA-Seq. *Medical science monitor basic research*, *20*, 138.

Mayosi, B. M., Fish, M., Shaboodien, G., Mastantuono, E., Kraus, S., Wieland, T., . . . Ntusi, N. B. (2017). Identification of cadherin 2 (CDH2) mutations in arrhythmogenic right ventricular cardiomyopathy. *Circulation: Cardiovascular Genetics*, *10*(2), e001605.

Memczak, S., Jens, M., Elefsinioti, A., Torti, F., Krueger, J., Rybak, A., . . . Rajewsky, N. (2013). Circular RNAs are a large class of animal RNAs with regulatory potency. *Nature*, *495*(7441), 333-338. https://doi.org/10.1038/nature11928

Mi, H., Ebert, D., Muruganujan, A., Mills, C., Albou, L. P., Mushayamaha, T., & Thomas, P. D. (2021). PANTHER version 16: a revised family classification, tree-based classification tool, enhancer regions and extensive API. *Nucleic Acids Res*, *49*(D1), D394-D403. https://doi.org/10.1093/nar/gkaa1106

Mi, H., Muruganujan, A., Huang, X., Ebert, D., Mills, C., Guo, X., & Thomas, P. D. (2019). Protocol Update for large-scale genome and gene function analysis with the PANTHER classification system (v.14.0). *Nat Protoc*, *14*(3), 703-721. https://doi.org/10.1038/s41596-019-0128-8

Molkentin, J. D., Lu, J.-R., Antos, C. L., Markham, B., Richardson, J., Robbins, J., . . . Olson, E. N. (1998). A calcineurin-dependent transcriptional pathway for cardiac hypertrophy. *Cell*, *93*(2), 215-228.

Métrich, M., Lucas, A., Gastineau, M., Samuel, J.-L., Heymes, C., Morel, E., & Lezoualc'h, F. (2008). Epac mediates β-adrenergic receptor–induced cardiomyocyte hypertrophy. *Circulation research*, *102*(8), 959-965.

Nakajima, H., Nakajima, H. O., Salcher, O., Dittiè, A. S., Dembowsky, K., Jing, S., & Field, L. J. (2000). Atrial but not ventricular fibrosis in mice expressing a mutant transforming growth factor-β1 transgene in the heart. *Circulation research*, *86*(5), 571-579.

Nigro, J. M., Cho, K. R., Fearon, E. R., Kern, S. E., Ruppert, J. M., Oliner, J. D., . . . Vogelstein, B. (1991). Scrambled exons. *Cell*, *64*(3), 607-613. https://doi.org/10.1016/0092-8674(91)90244-s

Nishida, W., Nakamura, M., Mori, S., Takahashi, M., Ohkawa, Y., Tadokoro, S., . . . Sobue, K. (2002). A triad of serum response factor and the GATA and NK families governs the transcription of smooth and cardiac muscle genes. *J Biol Chem*, *277*(9), 7308-7317. https://doi.org/10.1074/jbc.M111824200

O'Leary, N. A., Wright, M. W., Brister, J. R., Ciufo, S., Haddad, D., McVeigh, R., . . . Ako-Adjei, D. (2016). Reference sequence (RefSeq) database at NCBI: current status, taxonomic expansion, and functional annotation. *Nucleic acids research*, *44*(D1), D733-D745.

Okazaki, K., & Holtzer, H. (1966). Myogenesis: fusion, myosin synthesis, and the mitotic cycle. *Proc Natl Acad Sci U S A*, *56*(5), 1484-1490. https://doi.org/10.1073/pnas.56.5.1484

Pamudurti, N. R., Bartok, O., Jens, M., Ashwal-Fluss, R., Stottmeister, C., Ruhe, L., . . . Kadener, S. (2017). Translation of CircRNAs. *Mol Cell*, *66*(1), 9-21 e27. https://doi.org/10.1016/j.molcel.2017.02.021

Pan, Q., Shai, O., Lee, L. J., Frey, B. J., & Blencowe, B. J. (2008). Deep surveying of alternative splicing complexity in the human transcriptome by high-throughput sequencing. *Nat Genet*, *40*(12), 1413-1415. https://doi.org/10.1038/ng.259

Panda, A. C., De, S., Grammatikakis, I., Munk, R., Yang, X., Piao, Y., . . . Gorospe, M. (2017). High-purity circular RNA isolation method (RPAD) reveals vast collection of intronic circRNAs. *Nucleic acids research*, *45*(12), e116-e116.

Panni, S., Lovering, R. C., Porras, P., & Orchard, S. (2020). Non-coding RNA regulatory networks. *Biochimica et Biophysica Acta (BBA)-Gene Regulatory Mechanisms*, *1863*(6), 194417.

Pantos, C., Mourouzis, I., & Cokkinos, D. V. (2011). New insights into the role of thyroid hormone in cardiac remodeling: time to reconsider? *Heart failure reviews*, *16*(1), 79-96.

Pasman, Z., Been, M. D., & Garcia-Blanco, M. A. (1996). Exon circularization in mammalian nuclear extracts. *RNA*, *2*(6), 603-610.

Pasquinelli, A. E. (2012). MicroRNAs and their targets: recognition, regulation and an emerging reciprocal relationship. *Nature Reviews Genetics*, *13*(4), 271-282.

Patel, A. A., & Steitz, J. A. (2003). Splicing double: insights from the second spliceosome. *Nature reviews Molecular cell biology*, *4*(12), 960-970.

Pereira, L., Cheng, H., Lao, D. H., Na, L., Van Oort, R. J., Brown, J. H., . . . Bers, D. M. (2013). Epac2 mediates cardiac β1-adrenergic–dependent sarcoplasmic reticulum Ca2+ leak and arrhythmia. *Circulation*, *127*(8), 913-922.

Preußer, C., Hung, L.-H., Schneider, T., Schreiner, S., Hardt, M., Moebus, A., . . . Bindereif, A. (2018). Selective release of circRNAs in platelet-derived extracellular vesicles. *Journal of extracellular vesicles*, *7*(1), 1424473.

Qi, X., Yang, G., Yang, L., Lan, Y., Weng, T., Wang, J., . . . Yang, X. (2007). Essential role of Smad4 in maintaining cardiomyocyte proliferation during murine embryonic heart development. *Developmental biology*, *311*(1), 136-146.

Qu, S., Zhong, Y., Shang, R., Zhang, X., Song, W., Kjems, J., & Li, H. (2017). The emerging landscape of circular RNA in life processes. *RNA Biol*, *14*(8), 992-999. https://doi.org/10.1080/15476286.2016.1220473

Rainer, P. P., & Kass, D. A. (2016). Old dog, new tricks: novel cardiac targets and stress regulation by protein kinase G. *Cardiovascular research*, *111*(2), 154–162. https://doi.org/10.1093/cvr/cvw107

Rockman, H. A., Ross, R. S., Harris, A. N., Knowlton, K. U., Steinhelper, M. E., Field, L. J., . . . Chien, K. R. (1991). Segregation of atrial-specific and inducible expression of an atrial natriuretic factor transgene in an in vivo murine model of cardiac hypertrophy. *Proceedings of the National Academy of Sciences*, *88*(18), 8277-8281.

Rockman, H. A., Ross, R. S., Harris, A. N., Knowlton, K. U., Steinhelper, M. E., Field, L. J., . . . Chien, K. R. (1991). Segregation of atrial-specific and inducible expression of an atrial natriuretic factor transgene in an in vivo murine model of cardiac hypertrophy. *Proc Natl Acad Sci U S A*, *88*(18), 8277-8281. https://doi.org/10.1073/pnas.88.18.8277

Roger, V. L. (2013). Epidemiology of heart failure. *Circulation research*, *113*(6), 646-659.

Rybak-Wolf, A., Stottmeister, C., Glažar, P., Jens, M., Pino, N., Giusti, S., . . . Ashwal-Fluss, R. (2015). Circular RNAs in the mammalian brain are highly abundant, conserved, and dynamically expressed. *Molecular cell*, *58*(5), 870-885.

Salgado-Somoza, A., Zhang, L., Vausort, M., & Devaux, Y. (2017). The circular RNA MICRA for risk stratification after myocardial infarction. *Int J Cardiol Heart Vasc*, *17*, 33-36. https://doi.org/10.1016/j.ijcha.2017.11.001

Saltiel, A. R., & Kahn, C. R. (2001). Insulin signalling and the regulation of glucose and lipid metabolism. *Nature*, *414*(6865), 799-806.

Salzman, J., Gawad, C., Wang, P. L., Lacayo, N., & Brown, P. O. (2012). Circular RNAs are the predominant transcript isoform from hundreds of human genes in diverse cell types. *PLoS One*, *7*(2), e30733. https://doi.org/10.1371/journal.pone.0030733

Sanger, H. L., Klotz, G., Riesner, D., Gross, H. J., & Kleinschmidt, A. K. (1976). Viroids are single-stranded covalently closed circular RNA molecules existing as highly base-paired rod-like structures. *Proc Natl Acad Sci U S A*, *73*(11), 3852-3856. https://doi.org/10.1073/pnas.73.11.3852

Sato, P. Y., Chuprun, J. K., Schwartz, M., & Koch, W. J. (2015). The evolving impact of g protein-coupled receptor kinases in cardiac health and disease. *Physiological reviews*, *95*(2), 377-404.

Schiattarella, G. G., & Hill, J. A. (2015). Inhibition of hypertrophy is a good therapeutic strategy in ventricular pressure overload. *Circulation*, *131*(16), 1435-1447.

Schindewolf, C., Braun, S., & Domdey, H. (1996). In vitro generation of a circular exon from a linear pre-mRNA transcript. *Nucleic Acids Res*, *24*(7), 1260-1266. https://doi.org/10.1093/nar/24.7.1260

Schneider, T., & Bindereif, A. (2017). Circular RNAs: Coding or noncoding? *Cell Res*, *27*(6), 724-725. https://doi.org/10.1038/cr.2017.70

Seles, M., Hutterer, G. C., Foßelteder, J., Svoboda, M., Resel, M., Barth, D. A., . . . Pichler, M. (2020). Long Non-Coding RNA PANTR1 is Associated with Poor Prognosis and Influences Angiogenesis and Apoptosis in Clear-Cell Renal Cell Cancer. *Cancers (Basel)*, *12*(5). https://doi.org/10.3390/cancers12051200

Selvetella, G., Hirsch, E., Notte, A., Tarone, G., & Lembo, G. (2004). Adaptive and maladaptive hypertrophic pathways: points of convergence and divergence. *Cardiovascular research*, *63*(3), 373–380. https://doi.org/10.1016/j.cardiores.2004.04.031

Shen, T., Han, M., Wei, G., & Ni, T. (2015). An intriguing RNA species--perspectives of circularized RNA. *Protein Cell*, *6*(12), 871-880. https://doi.org/10.1007/s13238-015-0202-0

Shioi, T., McMullen, J. R., Tarnavski, O., Converso, K., Sherwood, M. C., Manning, W. J., & Izumo, S. (2003). Rapamycin attenuates load-induced cardiac hypertrophy in mice. *Circulation*, *107*(12), 1664-1670.

Siede, D., Rapti, K., Gorska, A. A., Katus, H. A., Altmuller, J., Boeckel, J. N., . . . Dieterich, C. (2017). Identification of circular RNAs with host gene-independent expression in human model systems for cardiac differentiation and disease. *J Mol Cell Cardiol*, *109*, 48-56. https://doi.org/10.1016/j.yjmcc.2017.06.015

Starke, S., Jost, I., Rossbach, O., Schneider, T., Schreiner, S., Hung, L. H., & Bindereif, A. (2015). Exon circularization requires canonical splice signals. *Cell Rep*, *10*(1), 103-111. https://doi.org/10.1016/j.celrep.2014.12.002

Su, A. I., Wiltshire, T., Batalov, S., Lapp, H., Ching, K. A., Block, D., . . . Hogenesch, J. B. (2004). A gene atlas of the mouse and human protein-encoding transcriptomes. *Proc Natl Acad Sci U S A*, *101*(16), 6062-6067. https://doi.org/10.1073/pnas.0400782101

Surono, A., Takeshima, Y., Wibawa, T., Ikezawa, M., Nonaka, I., & Matsuo, M. (1999). Circular dystrophin RNAs consisting of exons that were skipped by alternative splicing. *Hum Mol Genet*, *8*(3), 493-500. https://doi.org/10.1093/hmg/8.3.493

Suzuki, H., & Tsukahara, T. (2014). A view of pre-mRNA splicing from RNase R resistant RNAs. *Int J Mol Sci*, *15*(6), 9331-9342. https://doi.org/10.3390/ijms15069331

Tan, K. E., & Lim, Y. Y. (2020). Viruses join the circular RNA world. *The FEBS Journal*.

Tan, W. L., Lim, B. T., Anene-Nzelu, C. G., Ackers-Johnson, M., Dashi, A., See, K., . . . Luu, T. D. (2017). A landscape of circular RNA expression in the human heart. *Cardiovascular research*, *113*(3), 298-309.

Tatomer, D. C., & Wilusz, J. E. (2017). An Unchartered Journey for Ribosomes: Circumnavigating Circular RNAs to Produce Proteins. *Mol Cell*, *66*(1), 1-2. https://doi.org/10.1016/j.molcel.2017.03.011

Tham, Y. K., Bernardo, B. C., Ooi, J. Y., Weeks, K. L., & McMullen, J. R. (2015). Pathophysiology of cardiac hypertrophy and heart failure: signaling pathways and novel therapeutic targets. *Archives of toxicology*, *89*(9), 1401-1438.

Treiber, T., Treiber, N., Plessmann, U., Harlander, S., Daiß, J.-L., Eichner, N., . . . Meister, G. (2017). A compendium of RNA-binding proteins that regulate microRNA biogenesis. *Molecular cell*, *66*(2), 270-284. e213.

Trivieri, M. G., Oudit, G. Y., Sah, R., Kerfant, B.-G., Sun, H., Gramolini, A. O., . . . De Escobar, G. M. (2006). Cardiac-specific elevations in thyroid hormone enhance contractility and prevent pressure overload-induced cardiac dysfunction. *Proceedings of the National Academy of Sciences*, *103*(15), 6043-6048.

Umbarkar, P., Singh, A. P., Gupte, M., Verma, V. K., Galindo, C. L., Guo, Y., . . . Lal, H. (2019). Cardiomyocyte SMAD4-dependent TGF-β signaling is essential to maintain adult heart homeostasis. *JACC: Basic to Translational Science*, *4*(1), 41-53.

Uyhazi, K. E., Yang, Y., Liu, N., Qi, H., Huang, X. A., Mak, W., . . . Song, X. (2020). Pumilio proteins utilize distinct regulatory mechanisms to achieve complementary functions required for pluripotency and embryogenesis. *Proceedings of the National Academy of Sciences*, *117*(14), 7851-7862.

Vasudevan, S., & Steitz, J. A. (2007). AU-rich-element-mediated upregulation of translation by FXR1 and Argonaute 2. *Cell*, *128*(6), 1105-1118.

Vega, R. B., Konhilas, J. P., Kelly, D. P., & Leinwand, L. A. (2017). Molecular mechanisms underlying cardiac adaptation to exercise. *Cell metabolism*, *25*(5), 1012-1026.

Verduci, L., Ferraiuolo, M., Sacconi, A., Ganci, F., Vitale, J., Colombo, T., . . . Blandino, G. (2017). The oncogenic role of circPVT1 in head and neck squamous cell carcinoma is mediated through the mutant p53/YAP/TEAD transcription-competent complex. *Genome Biol*, *18*(1), 237. https://doi.org/10.1186/s13059-017-1368-y

Vincent, H. A., & Deutscher, M. P. (2006). Substrate recognition and catalysis by the exoribonuclease RNase R. *Journal of Biological Chemistry*, *281*(40), 29769-29775.

Wang, D., Oparil, S., Feng, J. A., Li, P., Perry, G., Chen, L. B., . . . Chen, Y.-F. (2003). Effects of pressure overload on extracellular matrix expression in the heart of the atrial natriuretic peptide–null mouse. *Hypertension*, *42*(1), 88-95.

Wang, J., Song, Y., Zhang, Y., Xiao, H., Sun, Q., Hou, N., . . . Zhan, D. (2012). Cardiomyocyte overexpression of miR-27b induces cardiac hypertrophy and dysfunction in mice. *Cell research*, *22*(3), 516-527.

Wang, J., Xu, N., Feng, X., Hou, N., Zhang, J., Cheng, X., . . . Yang, X. (2005). Targeted disruption of Smad4 in cardiomyocytes results in cardiac hypertrophy and heart failure. *Circulation research*, *97*(8), 821-828.

Wang, K., Long, B., Liu, F., Wang, J. X., Liu, C. Y., Zhao, B., . . . Li, P. F. (2016). A circular RNA protects the heart from pathological hypertrophy and heart failure by targeting miR-223. *Eur Heart J*, *37*(33), 2602-2611. https://doi.org/10.1093/eurheartj/ehv713

Wang, Y., Li, M., Liu, J., Zhang, M., Fang, X., Chen, H., & Zhang, C. (2019). A Zfp609 circular RNA regulates myoblast differentiation by sponging miR-194-5p. *Int J Biol Macromol*, *121*, 1308-1313. https://doi.org/10.1016/j.ijbiomac.2018.09.039

Wei, X., Li, H., Yang, J., Hao, D., Dong, D., Huang, Y., . . . Chen, H. (2017). Circular RNA profiling reveals an abundant circLMO7 that regulates myoblasts differentiation and survival by sponging miR-378a-3p. *Cell Death Dis*, *8*(10), e3153. https://doi.org/10.1038/cddis.2017.541

Weng, W., Wei, Q., Toden, S., Yoshida, K., Nagasaka, T., Fujiwara, T., . . . Goel, A. (2017). Circular RNA ciRS-7-A Promising Prognostic Biomarker and a Potential Therapeutic Target in Colorectal Cancer. *Clin Cancer Res*, *23*(14), 3918-3928. https://doi.org/10.1158/1078-0432.CCR-16-2541

Werfel, S., Nothjunge, S., Schwarzmayr, T., Strom, T. M., Meitinger, T., & Engelhardt, S. (2016). Characterization of circular RNAs in human, mouse and rat hearts. *J Mol Cell Cardiol*, *98*, 103-107. https://doi.org/10.1016/j.yjmcc.2016.07.007

Westholm, J. O., Miura, P., Olson, S., Shenker, S., Joseph, B., Sanfilippo, P., . . . Lai, E. C. (2014). Genome-wide analysis of drosophila circular RNAs reveals their structural and sequence properties and age-dependent neural accumulation. *Cell Rep*, *9*(5), 1966-1980. https://doi.org/10.1016/j.celrep.2014.10.062

Wiederstein, J. L., Nolte, H., Günther, S., Piller, T., Baraldo, M., Kostin, S., Bloch, W., Schindler, N., Sandri, M., Blaauw, B., Braun, T., Hölper, S., & Krüger, M. (2018). Skeletal Muscle-Specific Methyltransferase METTL21C Trimethylates p97 and Regulates Autophagy-Associated Protein Breakdown. *Cell reports*, *23*(5), 1342–1356. https://doi.org/10.1016/j.celrep.2018.03.136

Wu, T. D., & Nacu, S. (2010). Fast and SNP-tolerant detection of complex variants and splicing in short reads. *Bioinformatics (Oxford, England)*, *26*(7), 873–881. https://doi.org/10.1093/bioinformatics/btq057

Wu, H.-J., Zhang, C.-Y., Zhang, S., Chang, M., & Wang, H.-Y. (2016). Microarray expression profile of circular RNAs in heart tissue of mice with myocardial infarction-induced heart failure. *Cellular Physiology and Biochemistry*, *39*(1), 205-216.

Wu, T. Y., Zhang, T. H., Qu, L. M., Feng, J. P., Tian, L. L., Zhang, B. H., . . . Liu, M. (2014). MiR-19a is correlated with prognosis and apoptosis of laryngeal squamous cell carcinoma by regulating TIMP-2 expression. *Int J Clin Exp Pathol*, *7*(1), 56-63.

Xia, Y., Lee, K., Li, N., Corbett, D., Mendoza, L., & Frangogiannis, N. G. (2009). Characterization of the inflammatory and fibrotic response in a mouse model of cardiac pressure overload. *Histochem Cell Biol*, *131*(4), 471-481. https://doi.org/10.1007/s00418-008-0541-5

Xu, T., Wu, J., Han, P., Zhao, Z., & Song, X. (2017). Circular RNA expression profiles and features in human tissues: a study using RNA-seq data. *BMC Genomics*, *18*(Suppl 6), 680. https://doi.org/10.1186/s12864-017-4029-3

Yang, M. H., Wang, H., Han, S. N., Jia, X., Zhang, S., Dai, F. F., . . . Xue, L. X. (2020). Circular RNA expression in isoproterenol hydrochloride-induced cardiac hypertrophy. *Aging (Albany NY)*, *12*(3), 2530-2544. https://doi.org/10.18632/aging.102761

Yang, Y., Fan, X., Mao, M., Song, X., Wu, P., Zhang, Y., . . . Wang, Z. (2017). Extensive translation of circular RNAs driven by N(6)-methyladenosine. *Cell Res*, *27*(5), 626-641. https://doi.org/10.1038/cr.2017.31

Yang, Y., Gao, X., Zhang, M., Yan, S., Sun, C., Xiao, F., . . . Zhou, H. (2018). Novel role of FBXW7 circular RNA in repressing glioma tumorigenesis. *JNCI: Journal of the National Cancer Institute*, *110*(3), 304-315.

Yoon, W., Hwang, S.-H., Lee, S.-H., & Chung, J. (2019). Drosophila ADCK1 is critical for maintaining mitochondrial structures and functions in the muscle. *PLoS genetics*, *15*(5), e1008184.

You, X., Vlatkovic, I., Babic, A., Will, T., Epstein, I., Tushev, G., . . . Chen, W. (2015). Neural circular RNAs are derived from synaptic genes and regulated by development and plasticity. *Nat Neurosci*, *18*(4), 603-610. https://doi.org/10.1038/nn.3975

Zaphiropoulos, P. G. (1996). Circular RNAs from transcripts of the rat cytochrome P450 2C24 gene: correlation with exon skipping. *Proc Natl Acad Sci U S A*, *93*(13), 6536-6541. https://doi.org/10.1073/pnas.93.13.6536

Zeng, X., Lin, W., Guo, M., & Zou, Q. (2017). A comprehensive overview and evaluation of circular RNA detection tools. *PLoS Comput Biol*, *13*(6), e1005420. https://doi.org/10.1371/journal.pcbi.1005420

Zeng, Y., Du, W. W., Wu, Y., Yang, Z., Awan, F. M., Li, X., . . . Yang, B. B. (2017). A Circular RNA Binds To and Activates AKT Phosphorylation and Nuclear Localization Reducing Apoptosis and Enhancing Cardiac Repair. *Theranostics*, *7*(16), 3842-3855. https://doi.org/10.7150/thno.19764

Zhang, S., Yin, Z., Dai, F. F., Wang, H., Zhou, M. J., Yang, M. H., . . . Zang, M. X. (2019). miR-29a attenuates cardiac hypertrophy through inhibition of PPARδ expression. *Journal of cellular physiology*, *234*(8), 13252-13262.

Zhang, X. O., Dong, R., Zhang, Y., Zhang, J. L., Luo, Z., Zhang, J., . . . Yang, L. (2016). Diverse alternative back-splicing and alternative splicing landscape of circular RNAs. *Genome Res*, *26*(9), 1277-1287. https://doi.org/10.1101/gr.202895.115

Zhang, X. O., Wang, H. B., Zhang, Y., Lu, X., Chen, L. L., & Yang, L. (2014). Complementary sequence-mediated exon circularization. *Cell*, *159*(1), 134-147. https://doi.org/10.1016/j.cell.2014.09.001

Zhang, Y., Xue, W., Li, X., Zhang, J., Chen, S., Zhang, J. L., . . . Chen, L. L. (2016). The Biogenesis of Nascent Circular RNAs. *Cell Rep*, *15*(3), 611-624. https://doi.org/10.1016/j.celrep.2016.03.058

Zhang, Y., Zhang, X. O., Chen, T., Xiang, J. F., Yin, Q. F., Xing, Y. H., . . . Chen, L. L. (2013). Circular intronic long noncoding RNAs. *Mol Cell*, *51*(6), 792-806. https://doi.org/10.1016/j.molcel.2013.08.017

Zhang, Y., Zhang, Y., Li, X., Zhang, M., & Lv, K. (2017). Microarray analysis of circular RNA expression patterns in polarized macrophages. *International journal of molecular medicine*, *39*(2), 373-379.

Zou, M., Huang, C., Li, X., He, X., Chen, Y., Liao, W., . . . Bin, J. (2017). Circular RNA expression profile and potential function of hsa_circRNA_101238 in human thoracic aortic dissection. *Oncotarget*, *8*(47), 81825-81837. https://doi.org/10.18632/oncotarget.18998

XI SUPPLEMENTS

XI.1 Whole circle sequencing results

circZfp827

P1:

CTGGAGCAGACACTCTTCCGTGCAGCACAGATTCACCAGGCAGCAGATCTT
TTGAATTGGAGGTGAATGGTGATTGTCTAAATGTGTCTTCTGAAAAGAAAG
GGCTGGTGGTTGTCCGCATTGCGTTTTCTTTCGTGTGATTGTGTTCTTTGCTC
ACTTTTTCCGAGAGCTGAAAAAGCAGCTCAGAAGCCATCTTCACAGAGATG
TCCTGGCTGAAGAGATTTCTCTCTGGGGGAACTCGACCTTCTGGCAGCTTCT
GTAAGGGTTCAGTTTTCTCTCGCCCCATTAAAGTGCTGTAGCCAATGTTCCG
GCTGGG

P2:

CCCTTACAGAAGCTGCCAGAAGGTCGAGTTCCCCCAGAGAGAAATCTCTTC
AGCCAGGACATCTCTGTGAAGATGGCTTCTGAGCTGCTTTTTCAGCTCTCGG
AAAAAGTGAGCAAAGAACACAATCACACGAAAGAAAACGCAATGCGGACA
ACCACCAGCCCTTTCTTTTCAGAAGACACATTTAGACAATCACCATTCACCT
CCAATTCAAAAGATCTGCTGCCTGGTGAATCTGTGCTGCACGGAAGAGTGT
CTGCTCCAGCGGAAAGCTACAAGGAGACGCAGGCGGTGACGGTTAAAGAA
GAACCCATGGAGGTGGACATCCAGGACTCCCCAGCCTCCATATCA

circNeb

P1:

TAATCGCTTGTTCATGTTGAGGGCGTNGCTCTTGGCCAGCACCTGCTCCAGA
GAATCAGTCACACTGGTGAACTTAAACTTGTTTGGAGGCTGGCGATAGATG
TTGTCGCTCAGGATCTCTGCAGCTCTCTTACACTTGACCACATCCAGAGACC
CGATGGGRACCCAGCCAATGCCTCTCATCCACTGGAGATCTGACTTGTACAC
ATTATCACTCTGGAGATCATAGGCCTGCCGAGCGTGGATGACATCATTCTGG
TCAGGTAGACATGTCCACTGGTGTAGGNANTTCCTGTAGTCCACATCGCTGA
CCAAGGTCTGGCACTTCTTGGCCAATACCACCCCCAGCATGTCCACTGGGCT
GCTATACTTAGTCTTCCATTTCTCAAAGTCCTTCTTGTACTCCCTGTCACTCT
GGATCTTGGCCACGTGCATGGACCACATCATCTTGGGGTCATCTTCAATGTT
GCGGGCTCCAATGTGGTGTCCCAGCTGCTTACGGTAGCCAACTTTGTATTTG

TAGTCACTGGCAATATCTCTGGAGGCCTTGGCCGCCACAATGGGGATAGCA
TCGACACGCAGGTCATAGCCTTTCTTCTTTGCTTCTTCATTGGCCAGTTTATA
TAGACTCTCGCTGTAGTTGATTCTGTTCTGCCTTTGCCAG
P2:
ANAGGCTATGACCTGCGTGTCGATGCTATCCCCATTGTGGCGGCCAAGGCCT
CCAGAGATATTGCCAGTGACTACAAATACAAAGTTGGCTACCGTAAGCAGC
TGGGACACCACATTGGAGCCCGCAACATTGAAGATGACCCCAAGATGATGT
GGTCCATGCACGTGGCCAAGATCCAGAGTGACAGGGAGTACAAGAAGGAC
TTTGAGAAATGGAA
GACTAAGTATAGCAGCCCAGTGGACATGCTGGGGGTGGTATTGGCCAAGAA
GTGCCAGACCTTGGTCAGCGATGTGGACTACAGGAACTACCTACACCAGTG
GACATGTCTRCCTGACCAGAATGATGTCATCCACGCTCGGCAGGCCTATGAT
CTCCAGAGTGATAATGTGTACAAGTCAGATCTCCAGTGGATGAGAGGCATT
GGCTGGGTYCCCATCGGGTCTCTGGATGTGGTCAAGTGTAAGAGAGCTGCA
GAGATCCTGAGCGACAACATCTATCGCCAGCCTCCAAACAAGTTTAAGTTC
ACCAGTGTGACTGATTCTCTGGAGCAGGTGCTGGCCAAGAGCAACGCCCTC
AACATGAACAAGCGATTATACACAGAGGCCTGGGACAAAGACAAGATTCA
AATTCATGTAATGCCTGATACACCGGAGAATTATGCTG

circSec24b:
P1:
GGAGGATGAGGAAGCAGGTGTTGACAGCTCTTCCACCACCAGCAGTGCTTC
GCCCTTGCCCAACAGTTACGATGCCTTGGAAGGAGGCAGCTACCCAGNTAT
GCATTCTNSTNCNTNNNGCAGCCCTGTTCCTGACCATGCCCTGGAACCCAGT
CCCACCCTCGCCCAGGCTCTGTCTGCAGCCCCCACTCCCCCTGCAGCTCANC
CAGCCAAGGTGGCAAAGCCTTTTGGCTATGGCTACCCAGCTCTGCAGCCTGC
CTATCAGAACGCAGCACCACCACCCATGCCCGCAGCACATCCCAGCGGCCC
AGCGTACACTGGATATCCTCAGNATTACCCAGGTGTGAACCAGCTGTCCTCN
GGTCTCGGAGGACTAAGCCTGCANAGTTCTCCACAGCCAGAAAGCCTAAGA
CCTGNCAACCTCACCCAGGAGAAAAANATTTTACCTCCAACTCCTA

circNfix:
P1:

TTGGAGTACTGATGGGGAGCGGCTCTACAAGTCGCCCCAGTGCTCGAACCC
CGGCCTGTGTGTCCAGCCACATCACATTGGAGTCACAATCAAAGAACTGGA
CCTTTATCTGGCTTACTTTGTCCACACTCCGGGATGAGTTCCACCCGTTTATC
GAGGCGCTGCTGCCTCACGTCCGAGCCTTCTCCTACACCTGGTTCAACCTGC
AGGCGCGGAAGCGCAAGTACTTCAAGAAGCACGAGAAGCGGATGTCAAAG
GACGAGGAGCGCGCAGTGAAGGACGAGCTGCTGGGCGAGAAGCCTGAGAT
CAAGCAGAAGTGGGCATCCCGGCTGTTGGCAAAGCTGCGCNNCTCGTCCTT
TGACATCCGCTTCTCGTGCTTCTTGAAGTANTTGCGCTTCCGCNCCTGCAGG

XI.2 Differentially expressed circRNAs from microarray TAC vs. sham cardiomyocytes

Table 20 Differentially expressed circRNAs in TAC vs sham cardiomyocytes

FC (abs)	Reg	circRNA	Symbol	MRE1	MRE2	MRE3	MRE4	MRE5
1,6789252	up	mmu_circRNA_38777	Ociad1	mmu-miR-467a-5p	mmu-miR-6984-3p	mmu-miR-290a-3p	mmu-miR-5114	mmu-miR-107-5p
1,583554	up	mmu_circRNA_29981	App	mmu-miR-7661-3p	mmu-miR-181b-5p	mmu-miR-6952-3p	mmu-miR-3077-3p	mmu-miR-1912-3p
1,5081375	up	mmu_circRNA_32228	Hnrnpul2	mmu-miR-365-1-5p	mmu-miR-320-5p	mmu-miR-365-2-5p	mmu-miR-1903	mmu-miR-7117-3p
1,5321375	up	mmu_circRNA_39954	Tnpo3	mmu-miR-7218-3p	mmu-miR-6411	mmu-miR-1929-5p	mmu-miR-1934-3p	mmu-miR-6372
1,6490524	up	mmu_circRNA_009035	Cacul1	mmu-miR-96-5p	mmu-miR-6940-5p	mmu-miR-466i-3p	mmu-miR-669c-3p	mmu-miR-466m-3p
3,0157723	up	mmu_circRNA_000610	Zfp827	mmu-miR-7092-3p	mmu-miR-219b-5p	mmu-miR-6896-3p	mmu-miR-3064-5p	mmu-miR-3083-5p
2,097898	up	mmu_circRNA_31207	Zeb1	mmu-miR-7065-3p	mmu-miR-489-5p	mmu-miR-7688-5p	mmu-miR-6338	mmu-miR-20a-5p
1,5635966	up	mmu_circRNA_20588	Pam	mmu-miR-1966-5p	mmu-miR-7231-3p	mmu-miR-145a-5p	mmu-miR-670-3p	mmu-miR-7089-3p
1,7010349	up	mmu_circRNA_33053	Mllt10	mmu-miR-145a-3p	mmu-miR-7116-3p	mmu-miR-7059-3p	mmu-miR-691	mmu-miR-103-1-5p
1,5697717	up	mmu_circRNA_19242	Strbp	mmu-miR-7007-5p	mmu-miR-7092-3p	mmu-miR-7016-5p	mmu-miR-149-3p	mmu-miR-880-5p
3,1399348	up	mmu_circRNA_19178	Tcte3	mmu-miR-5110	mmu-miR-7092-3p	mmu-miR-7116-3p	mmu-miR-7054-5p	mmu-miR-326-5p
2,5925784	up	mmu_circRNA_34264	Fam98b	mmu-miR-421-5p	mmu-miR-7065-3p	mmu-miR-7215-5p	mmu-miR-883b-5p	mmu-miR-6974-3p
1,667383	up	mmu_circRNA_19383	Atp2a2	mmu-miR-1195	mmu-miR-10b-5p	mmu-miR-10a-5p	mmu-miR-706	mmu-miR-709
1,6078692	up	mmu_circRNA_19196	Gm5815	mmu-miR-134-5p	mmu-miR-692	mmu-miR-5101	mmu-miR-7053-3p	mmu-miR-190b-5p
1,6907984	up	mmu_circRNA_20855	Pfkfb2	mmu-miR-141-5p	mmu-miR-182-5p	mmu-miR-3475-5p	mmu-miR-6769b-3p	mmu-miR-7680-5p
1,6563034	up	mmu_circRNA_010146	Mpp6	mmu-miR-7211-3p	mmu-miR-7660-3p	mmu-miR-15b-3p	mmu-miR-3473b	mmu-miR-3473e
1,9209643	up	mmu_circRNA_38020	Ankib1	mmu-miR-7030-5p	mmu-miR-3547-5p	mmu-miR-665-5p	mmu-miR-7076-5p	mmu-miR-680
1,7170579	up	mmu_circRNA_36024	Agl	mmu-miR-3058-5p	mmu-miR-145a-3p	mmu-miR-669e-3p	mmu-miR-7028-5p	mmu-miR-6911-5p
1,6970251	up	mmu_circRNA_42531	Efnb2	mmu-miR-6377	mmu-miR-6916-3p	mmu-miR-7115-3p	mmu-miR-7663-5p	mmu-miR-3112-3p
1,6310137	up	mmu_circRNA_19105	Zswim6	mmu-miR-15b-5p	mmu-miR-541-5p	mmu-miR-6419	mmu-miR-195b	mmu-miR-6407
1,9107751	up	mmu_circRNA_37844	Capzb	mmu-miR-377-3p	mmu-miR-141-5p	mmu-miR-7005-5p	mmu-miR-7657-3p	mmu-miR-3095-5p
1,8356491	up	mmu_circRNA_19064	Fam177a	mmu-miR-6946-5p	mmu-miR-5110	mmu-miR-7035-5p	mmu-miR-6976-5p	mmu-miR-667-5p
2,1587155	up	mmu_circRNA_32761	Rbm20	mmu-miR-3064-5p	mmu-miR-3085-3p	mmu-miR-7679-5p	mmu-miR-664-5p	mmu-miR-7087-3p
1,5310945	up	mmu_circRNA_45832	Huwe1	mmu-miR-1903	mmu-miR-6937-3p	mmu-miR-320-5p	mmu-miR-152-5p	mmu-miR-7087-5p

1,5918158	up	mmu_circRNA_009487	Cacna1c	mmu-miR-6981-5p	mmu-miR-7013-5p	mmu-miR-6965-5p	mmu-miR-8104	mmu-miR-672-5p
1,525043	up	mmu_circRNA_010314	Trappc11	mmu-miR-7028-3p	mmu-miR-500-5p	mmu-miR-190b-3p	mmu-miR-3101-3p	mmu-miR-351-3p
1,6098124	up	mmu_circRNA_45348	Med14	mmu-miR-3103-5p	mmu-miR-216c-5p	mmu-miR-7081-5p	mmu-miR-7087-5p	mmu-miR-6982-5p
1,5992599	up	mmu_circRNA_44092	Sik3	mmu-miR-215-3p	mmu-miR-743a-5p	mmu-miR-871-5p	mmu-miR-320-5p	mmu-miR-743b-5p
2,3636872	up	mmu_circRNA_18937	Hecw2	mmu-miR-467h	mmu-miR-7092-3p	mmu-miR-6976-5p	mmu-miR-7665-5p	mmu-miR-574-5p
1,5758966	up	mmu_circRNA_35719	Lrba	mmu-miR-499-3p	mmu-miR-7021-3p	mmu-miR-7649-3p	mmu-miR-7226-5p	mmu-miR-127-5p
1,6249014	up	mmu_circRNA_19247	Tlk1	mmu-miR-7661-5p	mmu-miR-7665-5p	mmu-miR-6418-5p	mmu-miR-7047-5p	mmu-miR-6976-5p
1,6638366	up	mmu_circRNA_24758	Lpin1	mmu-miR-433-3p	mmu-miR-216a-3p	mmu-miR-7670-3p	mmu-miR-204-5p	mmu-miR-6994-5p
1,8453982	up	mmu_circRNA_015633	Hist1h4f	mmu-miR-7092-3p	mmu-miR-7116-3p	mmu-miR-7054-5p	mmu-miR-466k	mmu-miR-7026-3p
1,6472433	up	mmu_circRNA_39086	Zfp326	mmu-miR-6516-5p	mmu-miR-344e-5p	mmu-miR-344h-5p	mmu-miR-106a-3p	mmu-miR-6902-3p
1,6814792	up	mmu_circRNA_017077	Mga	mmu-miR-6916-3p	mmu-miR-6344	mmu-miR-1964-5p	mmu-miR-6403	mmu-miR-3059-5p
1,9081684	up	mmu_circRNA_18941	Creb1	mmu-miR-7650-3p	mmu-miR-326-5p	mmu-miR-5110	mmu-miR-6981-5p	mmu-miR-7210-3p
1,6403709	up	mmu_circRNA_34970	Arfgef2	mmu-miR-450a-2-3p	mmu-miR-330-5p	mmu-miR-326-3p	mmu-miR-7065-3p	mmu-miR-329-5p
1,531536	up	mmu_circRNA_22927	Actr2	mmu-miR-6971-3p	mmu-miR-6340	mmu-miR-6931-3p	mmu-miR-7008-3p	mmu-miR-5125
1,5048522	up	mmu_circRNA_006404	Bbs9	mmu-miR-7007-5p	mmu-miR-7049-5p	mmu-miR-7653-5p	mmu-miR-3084-5p	mmu-miR-294-5p
1,7723098	up	mmu_circRNA_000340	Amotl1	mmu-miR-7056-5p	mmu-miR-7010-3p	mmu-miR-5110	mmu-miR-7023-5p	mmu-miR-6971-5p
1,800026	up	mmu_circRNA_014015	Arhgap12	mmu-miR-30c-1-3p	mmu-miR-450a-5p	mmu-miR-30c-2-3p	mmu-miR-592-5p	mmu-miR-320-5p
1,518482	up	mmu_circRNA_37407	Nrd1	mmu-miR-1903	mmu-miR-598-3p	mmu-miR-6344	mmu-miR-877-3p	mmu-miR-320-5p
1,8931693	up	mmu_circRNA_017328	Enah	mmu-miR-183-5p	mmu-miR-21b	mmu-miR-6936-5p	mmu-miR-7668-5p	mmu-miR-7222-5p
1,8870902	up	mmu_circRNA_001848	Rabep1	mmu-miR-107-5p	mmu-miR-7015-5p	mmu-miR-6400	mmu-miR-7649-3p	mmu-miR-20a-3p
1,8023846	up	mmu_circRNA_010383	Akap7	mmu-miR-1903	mmu-miR-135b-5p	mmu-miR-135a-5p	mmu-miR-106a-5p	mmu-miR-93-5p
1,5132409	up	mmu_circRNA_34281	Bahd1	mmu-miR-6954-5p	mmu-miR-7069-5p	mmu-miR-326-5p	mmu-miR-7081-5p	mmu-miR-7087-5p
1,6452697	up	mmu_circRNA_20261	Creb1	mmu-miR-6911-5p	mmu-miR-96-5p	mmu-miR-378b	mmu-miR-1934-3p	mmu-miR-6913-3p
3,4570494	up	mmu_circRNA_27197	Samd8	mmu-miR-1929-5p	mmu-miR-3064-3p	mmu-miR-544-3p	mmu-miR-9768-5p	mmu-miR-1933-5p
1,7189006	up	mmu_circRNA_30953	Crim1	mmu-miR-7218-5p	mmu-miR-5134-5p	mmu-miR-383-3p	mmu-miR-6923-3p	mmu-miR-377-3p
1,7238491	up	mmu_circRNA_012490	Rad52	mmu-miR-152-5p	mmu-miR-3084-5p	mmu-miR-188-3p	mmu-miR-7068-5p	mmu-miR-1904
1,5542152	up	mmu_circRNA_39532	Mdh2	mmu-miR-29b-2-5p	mmu-miR-7017-5p	mmu-miR-1231-5p	mmu-miR-6905-5p	mmu-miR-29b-1-5p
1,570066	up	mmu_circRNA_33622	Pkp4	mmu-miR-667-5p	mmu-miR-344i	mmu-miR-6992-5p	mmu-miR-365-2-5p	mmu-miR-468-5p
3,1693968	up	mmu_circRNA_36481	Rad54b	mmu-miR-6951-3p	mmu-miR-7092-3p	mmu-miR-7116-3p	mmu-miR-7234-5p	mmu-miR-7012-5p
3,1404062	up	mmu_circRNA_31240	Ccny	mmu-miR-335-5p	mmu-miR-7243-5p	mmu-miR-329-5p	mmu-miR-686	mmu-miR-3970
1,5029718	up	mmu_circRNA_28645	Asap1	mmu-miR-7008-5p	mmu-miR-6935-5p	mmu-miR-7087-5p	mmu-miR-374c-3p	mmu-miR-29b-2-5p
1,6025641	up	mmu_circRNA_19442	Lrp6	mmu-miR-8100	mmu-miR-7665-5p	mmu-miR-6925-5p	mmu-miR-1249-5p	mmu-miR-7007-5p
3,66423	up	mmu_circRNA_31249	Ccny	mmu-miR-8100	mmu-miR-7661-5p	mmu-miR-7054-5p	mmu-miR-1249-5p	mmu-miR-7063-5p
1,5273591	up	mmu_circRNA_39668	Usp12	mmu-miR-7214-5p	mmu-miR-1903	mmu-miR-669b-5p	mmu-miR-29b-2-5p	mmu-miR-6946-3p
1,5672136	up	mmu_circRNA_21046	Stx6	mmu-miR-666-3p	mmu-miR-467a-5p	mmu-miR-6908-5p	mmu-miR-7116-3p	mmu-miR-5616-3p
1,6599931	up	mmu_circRNA_32069	Zfp236	mmu-miR-717	mmu-miR-6987-5p	mmu-miR-6992-5p	mmu-miR-6940-3p	mmu-miR-6937-5p
1,575001	up	mmu_circRNA_30426	Zfand3	mmu-miR-3064-5p	mmu-miR-181b-5p	mmu-miR-181d-5p	mmu-miR-181a-5p	mmu-miR-3074-5p
1,7504356	up	mmu_circRNA_30513	Rcan2	mmu-miR-143-3p	mmu-miR-30b-3p	mmu-miR-7054-5p	mmu-miR-1224-5p	mmu-miR-3112-3p
1,7884291	up	mmu_circRNA_24457	Cyth1	mmu-miR-6949-3p	mmu-miR-873a-5p	mmu-miR-298-3p	mmu-miR-7220-3p	mmu-miR-6372
1,6979243	up	mmu_circRNA_007127	Kmt2a	mmu-miR-6988-5p	mmu-miR-7006-5p	mmu-miR-330-5p	mmu-miR-6931-5p	mmu-miR-5130
2,0334868	up	mmu_circRNA_23884	Taf15	mmu-miR-6905-3p	mmu-miR-669b-5p	mmu-miR-7094-3p	mmu-miR-7650-3p	mmu-miR-7683-5p
1,5220437	up	mmu_circRNA_003987	Chd9	mmu-miR-5110	mmu-miR-7081-5p	mmu-miR-5128	mmu-miR-191-3p	mmu-miR-7230-3p

1,6362681	up	mmu_circRNA_002148	Ezh2	mmu-miR-30d-3p	mmu-miR-3074-2-3p	mmu-miR-30a-3p	mmu-miR-30e-3p	mmu-miR-452-3p
1,6490757	up	mmu_circRNA_000595	Smox	mmu-miR-6954-3p	mmu-miR-671-5p	mmu-miR-15a-3p	mmu-miR-6919-5p	mmu-miR-1291
1,6024943	up	mmu_circRNA_44088	Sidt2	mmu-miR-7677-5p	mmu-miR-761	mmu-miR-7093-5p	mmu-miR-8104	mmu-miR-6997-5p
1,8131625	up	mmu_circRNA_22265	Trappc10	mmu-miR-15b-3p	mmu-miR-8100	mmu-miR-7035-5p	mmu-miR-6999-5p	mmu-miR-320-5p
1,5014433	up	mmu_circRNA_42492	Nap1l4	mmu-miR-693-3p	mmu-miR-7686-5p	mmu-miR-1983	mmu-miR-7649-3p	mmu-miR-6999-3p
1,6469517	up	mmu_circRNA_37851	Iffo2	mmu-miR-1942	mmu-miR-7658-3p	mmu-miR-470-5p	mmu-miR-6946-3p	mmu-miR-423-3p
2,1594886	up	mmu_circRNA_24050	Dynll2	mmu-miR-1955-5p	mmu-miR-676-5p	mmu-miR-6361	mmu-miR-344d-1-5p	mmu-miR-5124b
1,9855948	up	mmu_circRNA_32587	Sorbs1	mmu-miR-6904-5p	mmu-miR-7003-5p	mmu-miR-3083-5p	mmu-miR-6940-5p	mmu-miR-7052-5p
1,7646524	up	mmu_circRNA_44178	Acat1	mmu-miR-107-5p	mmu-miR-103-1-5p	mmu-miR-103-2-5p	mmu-miR-7031-5p	mmu-miR-135b-5p
1,6406213	up	mmu_circRNA_43674	Cwf19l2	mmu-miR-7092-3p	mmu-miR-6984-3p	mmu-miR-26b-3p	mmu-miR-877-3p	mmu-miR-1903
1,5446789	up	mmu_circRNA_29464	Lpp	mmu-miR-698-5p	mmu-miR-23a-5p	mmu-miR-7080-3p	mmu-miR-3079-3p	mmu-miR-7026-3p
1,9332439	up	mmu_circRNA_42279	Tnrc6a	mmu-miR-3064-5p	mmu-miR-6932-3p	mmu-miR-6928-3p	mmu-miR-7672-3p	mmu-miR-5620-5p
2,0877731	up	mmu_circRNA_36813	Rad23b	mmu-miR-7085-5p	mmu-miR-762	mmu-miR-7648-3p	mmu-miR-1962	mmu-miR-6993-5p
1,6097503	up	mmu_circRNA_26301	Fam120a	mmu-miR-6359	mmu-miR-677-3p	mmu-let-7b-5p	mmu-let-7a-5p	mmu-let-7c-5p
1,506972	up	mmu_circRNA_40200	Braf	mmu-miR-7649-3p	mmu-miR-3473c	mmu-miR-7226-5p	mmu-miR-7019-5p	mmu-miR-138-5p
1,8739957	up	mmu_circRNA_24167	Mir5119	mmu-miR-6953-5p	mmu-miR-1249-5p	mmu-miR-6980-5p	mmu-miR-5110	mmu-miR-7092-3p
2,1953596	up	mmu_circRNA_29852	St3gal6	mmu-miR-7688-5p	mmu-miR-6981-5p	mmu-miR-6916-5p	mmu-miR-7081-5p	mmu-miR-320-3p
1,8780485	up	mmu_circRNA_38350	Lmbr1	mmu-miR-6981-5p	mmu-miR-6965-5p	mmu-miR-703	mmu-miR-674-5p	mmu-miR-6901-3p
1,668546	up	mmu_circRNA_26251	Jarid2	mmu-miR-7000-5p	mmu-miR-6946-3p	mmu-miR-7074-3p	mmu-miR-511-5p	mmu-miR-7006-3p
1,5066558	up	mmu_circRNA_27740	Dpysl2	mmu-miR-133b-5p	mmu-miR-7019-5p	mmu-miR-3073a-3p	mmu-miR-673-5p	mmu-miR-7077-3p
1,5293254	up	mmu_circRNA_20674	Clasp1	mmu-miR-19b-1-5p	mmu-miR-669e-5p	mmu-miR-432	mmu-miR-6400	mmu-miR-544-3p
1,6345783	up	mmu_circRNA_007731	St13	mmu-miR-7116-3p	mmu-miR-6946-3p	mmu-miR-7234-5p	mmu-miR-6950-3p	mmu-miR-7049-3p
1,6472639	up	mmu_circRNA_19110	Gng2	mmu-miR-6909-5p	mmu-miR-7686-5p	mmu-miR-7664-3p	mmu-miR-7016-5p	mmu-miR-6967-5p
2,3280514	up	mmu_circRNA_27519	Samd4	mmu-miR-5627-3p	mmu-miR-667-5p	mmu-miR-6937-5p	mmu-miR-6914-5p	mmu-miR-6931-5p
1,614225	up	mmu_circRNA_44052	Ddx6	mmu-miR-1930-5p	mmu-miR-6938-3p	mmu-miR-3110-5p	mmu-miR-1958	mmu-miR-6962-3p
1,6067986	up	mmu_circRNA_006741	Cacna1c	mmu-miR-29b-2-5p	mmu-miR-5126	mmu-miR-6914-5p	mmu-miR-135a-2-3p	mmu-miR-669a-5p
2,3781443	up	mmu_circRNA_008117	Mettl9	mmu-miR-551b-5p	mmu-miR-7079-3p	mmu-miR-1903	mmu-miR-7093-5p	mmu-miR-664-3p
2,2118515	up	mmu_circRNA_37351	Zyg11b	mmu-miR-7094-1-5p	mmu-miR-7013-5p	mmu-miR-7216-5p	mmu-miR-7065-3p	mmu-miR-7002-5p
2,535435	up	mmu_circRNA_38919	Slc4a4	mmu-miR-7116-3p	mmu-miR-6899-3p	mmu-miR-6946-3p	mmu-miR-6975-3p	mmu-miR-5099
1,524911	up	mmu_circRNA_27407	Sh3bp5	mmu-miR-22-5p	mmu-miR-207	mmu-miR-6938-3p	mmu-miR-877-3p	mmu-miR-484
1,5917358	up	mmu_circRNA_013002	Ttc3	mmu-miR-7661-5p	mmu-miR-7092-3p	mmu-miR-466c-5p	mmu-miR-7012-5p	mmu-miR-3473d
1,7457644	up	mmu_circRNA_22786	Atp5b	mmu-miR-1896	mmu-miR-3065-3p	mmu-miR-3074-5p	mmu-miR-500-5p	mmu-miR-7237-5p
2,7678793	up	mmu_circRNA_19172	Ttc3	mmu-miR-1187	mmu-miR-669f-5p	mmu-miR-465d-5p	mmu-miR-466i-5p	mmu-miR-6974-5p
2,8895869	up	mmu_circRNA_28834	Slc25a17	mmu-miR-1907	mmu-miR-6957-5p	mmu-miR-15a-5p	mmu-miR-15b-5p	mmu-miR-6353
1,6214975	up	mmu_circRNA_21668	Utrn	mmu-miR-6938-3p	mmu-miR-7033-3p	mmu-miR-7033-5p	mmu-miR-7059-3p	mmu-miR-7669-3p
1,5420237	up	mmu_circRNA_20543	Ndufa10	mmu-miR-7044-5p	mmu-miR-7019-3p	mmu-miR-5615-5p	mmu-miR-384-3p	mmu-miR-7033-5p
2,0141343	up	mmu_circRNA_19353	Ankib1	mmu-miR-7092-3p	mmu-miR-669p-5p	mmu-miR-669a-5p	mmu-miR-1249-5p	mmu-miR-6899-3p
1,5626344	up	mmu_circRNA_19168	Dcbld2	mmu-miR-5110	mmu-miR-6982-5p	mmu-miR-669c-3p	mmu-miR-466o-3p	mmu-miR-6973b-5p
2,3626345	up	mmu_circRNA_003698	Hecw2	mmu-miR-9-5p	mmu-miR-770-3p	mmu-miR-7682-3p	mmu-miR-326-5p	mmu-miR-365-1-5p
3,1315368	up	mmu_circRNA_002563	Asxl3	mmu-miR-205-5p	mmu-miR-1251-3p	mmu-miR-329-3p	mmu-miR-7004-3p	mmu-miR-7068-5p
2,6037459	up	mmu_circRNA_19490	Zfp827	mmu-miR-466q	mmu-miR-466i-3p	mmu-miR-297a-3p	mmu-miR-297c-3p	mmu-miR-297b-3p
1,8720104	up	mmu_circRNA_34096	Ttc17	mmu-miR-1904	mmu-miR-207	mmu-miR-6961-3p	mmu-miR-448-3p	mmu-miR-6912-3p

2,0562907	up	mmu_circRNA_32011	Atp5a1	mmu-miR-6953-5p	mmu-miR-6382	mmu-miR-7663-5p	mmu-miR-452-3p	mmu-miR-5618-5p
1,526098	up	mmu_circRNA_19252	Phf21a	mmu-miR-466q	mmu-miR-466i-3p	mmu-miR-466o-3p	mmu-miR-467a-3p	mmu-miR-669f-3p
1,7412145	up	mmu_circRNA_27181	Kat6b	mmu-miR-5620-5p	mmu-miR-7016-3p	mmu-miR-7054-5p	mmu-miR-149-3p	mmu-miR-5110
3,098174	up	mmu_circRNA_34777	H13	mmu-miR-1249-5p	mmu-miR-6931-5p	mmu-miR-5110	mmu-miR-6981-5p	mmu-miR-5107-5p
5,1384639	up	mmu_circRNA_36706	Rnf38	mmu-miR-7020-5p	mmu-miR-7076-5p	mmu-miR-7047-5p	mmu-miR-1966-5p	mmu-miR-5110
1,7921272	up	mmu_circRNA_43956	Kirrel3	mmu-miR-667-5p	mmu-miR-7231-5p	mmu-miR-5618-5p	mmu-miR-6994-5p	mmu-miR-344b-5p
2,0685558	up	mmu_circRNA_015661	Ttc3	mmu-miR-141-5p	mmu-miR-335-3p	mmu-miR-30d-3p	mmu-miR-217-5p	mmu-miR-7077-3p
2,8173886	up	mmu_circRNA_18944	Wdfy1	mmu-miR-7010-5p	mmu-miR-6946-5p	mmu-miR-7027-5p	mmu-miR-6925-5p	mmu-miR-466k
2,8695395	up	mmu_circRNA_19470	Trim12a	mmu-miR-7092-3p	mmu-miR-7116-3p	mmu-miR-6984-3p	mmu-miR-6344	mmu-miR-1187
1,5047467	up	mmu_circRNA_24148	Socs7	mmu-miR-6940-5p	mmu-miR-320-3p	mmu-miR-6918-5p	mmu-miR-3064-5p	mmu-miR-7679-5p
1,5560003	up	mmu_circRNA_23423	Mprip	mmu-miR-337-3p	mmu-miR-5046	mmu-miR-6999-3p	mmu-miR-93-3p	mmu-miR-138-5p
3,0385434	up	mmu_circRNA_004746	Zfp827	mmu-miR-494-5p	mmu-miR-410-5p	mmu-miR-7092-3p	mmu-miR-219b-5p	mmu-miR-875-3p
1,9220234	up	mmu_circRNA_40039	Chchd3	mmu-miR-6958-3p	mmu-miR-6998-3p	mmu-miR-344d-2-5p	mmu-miR-6991-3p	mmu-miR-653-3p
2,3003666	up	mmu_circRNA_30386	Nudt3	mmu-miR-6919-3p	mmu-miR-484	mmu-miR-3572-3p	mmu-miR-3064-3p	mmu-miR-7013-3p
2,2974148	up	mmu_circRNA_42849	Sorbs2	mmu-miR-3085-5p	mmu-miR-7030-5p	mmu-miR-7076-5p	mmu-miR-7682-3p	mmu-miR-1954
1,6010897	up	mmu_circRNA_31931	Mbd2	mmu-miR-3066-5p	mmu-miR-6390	mmu-miR-203-5p	mmu-miR-7235-3p	mmu-miR-29a-5p
1,5243798	up	mmu_circRNA_40806	Zfand4	mmu-miR-7038-3p	mmu-miR-20a-3p	mmu-miR-145a-3p	mmu-miR-346-3p	mmu-miR-149-5p
1,5943556	up	mmu_circRNA_005799	Fxr2	mmu-miR-7081-5p	mmu-miR-6950-3p	mmu-miR-1933-3p	mmu-miR-665-3p	mmu-miR-3475-3p
1,5740644	up	mmu_circRNA_000427	Mark3	mmu-miR-6537-5p	mmu-miR-19a-5p	mmu-miR-6992-5p	mmu-miR-212-3p	mmu-miR-339-3p
1,7864098	up	mmu_circRNA_010567	Zswim6	mmu-miR-669d-5p	mmu-miR-141-3p	mmu-miR-200a-3p	mmu-miR-124-5p	mmu-miR-326-5p
1,788712	up	mmu_circRNA_29553	Fyttd1	mmu-miR-145a-3p	mmu-miR-7116-3p	mmu-miR-19b-2-5p	mmu-miR-7231-3p	mmu-miR-7227-5p
1,7323073	up	mmu_circRNA_20805	Rab3gap1	mmu-miR-6344	mmu-miR-207	mmu-miR-667-5p	mmu-miR-211-5p	mmu-miR-6919-3p
4,848387	up	mmu_circRNA_42572	Rasa3	mmu-miR-27b-3p	mmu-miR-27a-3p	mmu-miR-128-3p	mmu-miR-25-5p	mmu-miR-6953-5p
2,0354646	up	mmu_circRNA_24117	Phospho1	mmu-miR-207	mmu-miR-1903	mmu-miR-7235-3p	mmu-miR-6898-3p	mmu-miR-544-3p
1,8107949	up	mmu_circRNA_25527	Nek9	mmu-miR-693-3p	mmu-miR-3060-5p	mmu-miR-497b	mmu-miR-7048-3p	mmu-miR-320-5p
2,1455146	up	mmu_circRNA_43389	Cbfb	mmu-miR-6896-3p	mmu-miR-7017-3p	mmu-miR-370-3p	mmu-miR-26b-3p	mmu-miR-6976-3p
1,5502396	up	mmu_circRNA_24813	Kidins220	mmu-miR-3089-3p	mmu-miR-136-5p	mmu-miR-452-3p	mmu-miR-7223-5p	mmu-miR-181b-1-3p
1,9877948	up	mmu_circRNA_31221	Arhgap12	mmu-miR-6925-5p	mmu-miR-30c-1-3p	mmu-miR-665-3p	mmu-miR-6899-3p	mmu-miR-450a-5p
1,6134873	up	mmu_circRNA_18970	Akap7	mmu-miR-669b-3p	mmu-miR-466m-3p	mmu-miR-466e-3p	mmu-miR-466a-3p	mmu-miR-466i-3p
2,4678614	up	mmu_circRNA_001832	Hk2	mmu-miR-1249-3p	mmu-miR-6990-5p	mmu-miR-7033-5p	mmu-miR-6942-5p	mmu-miR-761
1,7428779	up	mmu_circRNA_22888	Ogdh	mmu-miR-7232-5p	mmu-miR-344d-1-5p	mmu-miR-6335	mmu-miR-6931-5p	mmu-miR-7087-5p
2,4361333	up	mmu_circRNA_001096	Zfp532	mmu-miR-6397	mmu-miR-667-5p	mmu-miR-6539	mmu-miR-6954-5p	mmu-miR-759
1,6073632	up	mmu_circRNA_29049	Ccnt1	mmu-miR-5615-5p	mmu-miR-698-5p	mmu-miR-7029-3p	mmu-miR-466k	mmu-miR-3108-5p
1,5119937	up	mmu_circRNA_003540	Usp13	mmu-miR-3063-3p	mmu-miR-345-5p	mmu-miR-365-2-5p	mmu-miR-378a-5p	mmu-miR-6979-3p
2,5705795	up	mmu_circRNA_41204	Calm3	mmu-miR-194-2-3p	mmu-miR-1955-5p	mmu-miR-27a-3p	mmu-miR-27b-3p	mmu-miR-7055-5p
3,0162782	up	mmu_circRNA_005305	Samd4	mmu-miR-5623-3p	mmu-miR-7058-5p	mmu-miR-423-5p	mmu-miR-7024-3p	mmu-miR-3966
1,9312663	up	mmu_circRNA_018725	Scaper	mmu-miR-22-5p	mmu-miR-6946-3p	mmu-miR-3095-5p	mmu-miR-7116-3p	mmu-miR-6344
1,8680823	up	mmu_circRNA_19983	Map4k4	mmu-miR-678	mmu-miR-6950-5p	mmu-miR-107-5p	mmu-miR-7674-5p	mmu-miR-6353
1,5607012	up	mmu_circRNA_015268	Dcbld2	mmu-miR-7086-3p	mmu-miR-378a-5p	mmu-miR-497a-5p	mmu-miR-6419	mmu-miR-6342
1,9702185	up	mmu_circRNA_19003	Actr2	mmu-miR-7661-5p	mmu-miR-7035-5p	mmu-miR-466k	mmu-miR-7048-5p	mmu-miR-669f-5p
1,8101587	up	mmu_circRNA_017669	Lrch3	mmu-miR-7230-5p	mmu-miR-130b-5p	mmu-miR-1896	mmu-miR-7682-3p	mmu-miR-7043-3p
1,8623535	up	mmu_circRNA_22928	Actr2	mmu-miR-6971-3p	mmu-miR-6340	mmu-miR-6348	mmu-miR-1668	mmu-miR-185-5p

1,7023112	up	mmu_circRNA_28551	Oxr1	mmu-miR-7079-3p	mmu-miR-7092-3p	mmu-miR-207	mmu-miR-873a-5p	mmu-miR-8103
2,0404291	up	mmu_circRNA_33862	Gpr155	mmu-miR-6405	mmu-miR-1964-3p	mmu-miR-7079-3p	mmu-miR-7235-3p	mmu-miR-3065-5p
1,5201967	up	mmu_circRNA_19594	Pcmtd1	mmu-miR-130b-5p	mmu-miR-7014-3p	mmu-miR-30a-3p	mmu-miR-30e-3p	mmu-miR-30d-3p
2,2570884	up	mmu_circRNA_22326	Nuak1	mmu-miR-468-5p	mmu-miR-6992-3p	mmu-miR-6977-5p	mmu-miR-6916-3p	mmu-miR-181b-2-3p
1,9081068	up	mmu_circRNA_005522	Mkln1	mmu-miR-296-5p	mmu-miR-8103	mmu-miR-135a-5p	mmu-miR-135b-5p	mmu-miR-30d-3p
1,9978407	up	mmu_circRNA_28808	Ddx17	mmu-miR-6963-3p	mmu-miR-6961-3p	mmu-miR-141-5p	mmu-miR-7021-3p	mmu-miR-380-5p
1,8550845	up	mmu_circRNA_40181	Hipk2	mmu-miR-1933-5p	mmu-miR-599	mmu-miR-6913-3p	mmu-miR-7069-5p	mmu-miR-7117-5p
1,8593251	up	mmu_circRNA_011865	Zfp644	mmu-miR-6929-3p	mmu-miR-6952-3p	mmu-miR-301a-5p	mmu-miR-301b-5p	mmu-miR-6981-5p
1,9410242	up	mmu_circRNA_43390	Cbfb	mmu-miR-136-5p	mmu-miR-6896-3p	mmu-miR-7017-3p	mmu-miR-7048-3p	mmu-miR-880-3p
1,5336898	up	mmu_circRNA_22876	Ykt6	mmu-miR-7115-5p	mmu-miR-7006-3p	mmu-miR-7663-5p	mmu-miR-6919-5p	mmu-miR-9768-3p
1,5517122	up	mmu_circRNA_015506	Crim1	mmu-miR-5134-5p	mmu-miR-1969	mmu-miR-6923-3p	mmu-miR-221-5p	mmu-miR-152-5p
1,8746932	up	mmu_circRNA_002334	Zfp236	mmu-miR-669d-5p	mmu-miR-1187	mmu-miR-466i-5p	mmu-miR-466l-5p	mmu-miR-3064-5p
1,6898976	up	mmu_circRNA_19491	Gab1	mmu-miR-210-5p	mmu-miR-7219-3p	mmu-miR-144-5p	mmu-miR-670-3p	mmu-miR-6902-5p
1,7825505	up	mmu_circRNA_28856	Zc3h7b	mmu-miR-320-5p	mmu-miR-337-3p	mmu-miR-6991-3p	mmu-miR-6948-3p	mmu-miR-7672-3p
1,879372	up	mmu_circRNA_36839	Akap2	mmu-miR-7048-3p	mmu-miR-344i	mmu-miR-344c-5p	mmu-miR-344d-1-5p	mmu-miR-9769-3p
2,1128579	up	mmu_circRNA_016692	Insr	mmu-miR-495-5p	mmu-miR-9768-5p	mmu-miR-543-5p	mmu-miR-5134-5p	mmu-miR-1946b
2,1662856	up	mmu_circRNA_35018	Nfatc2	mmu-miR-346-3p	mmu-miR-7001-5p	mmu-miR-7237-5p	mmu-miR-7682-3p	mmu-miR-7679-5p
1,9431148	up	mmu_circRNA_003585	Pias1	mmu-miR-29b-2-5p	mmu-miR-3093-3p	mmu-miR-6983-5p	mmu-miR-7078-5p	mmu-miR-705
1,7870913	up	mmu_circRNA_24086	Mbtd1	mmu-miR-470-5p	mmu-miR-7026-3p	mmu-miR-147-5p	mmu-miR-6939-5p	mmu-miR-1231-5p
1,9904069	up	mmu_circRNA_30959	Strn	mmu-miR-1903	mmu-miR-6923-3p	mmu-miR-6769b-3p	mmu-miR-3154	mmu-miR-5616-5p
1,9471371	up	mmu_circRNA_45629	Ophn1	mmu-miR-7002-5p	mmu-miR-6338	mmu-miR-6950-3p	mmu-miR-7048-3p	mmu-miR-7093-3p
1,5792776	up	mmu_circRNA_018857	Zfp532	mmu-miR-219a-1-3p	mmu-miR-7079-3p	mmu-miR-450b-5p	mmu-miR-107-5p	mmu-miR-378b
1,7503732	up	mmu_circRNA_012583	Zfp532	mmu-miR-6397	mmu-miR-6539	mmu-miR-219a-1-3p	mmu-miR-7079-3p	mmu-miR-7232-5p
1,6425842	up	mmu_circRNA_38400	Ppp1cb	mmu-miR-5616-5p	mmu-miR-29b-2-5p	mmu-miR-1930-5p	mmu-miR-3059-5p	mmu-miR-6910-3p
2,7458318	up	mmu_circRNA_27737	Dpysl2	mmu-miR-673-5p	mmu-miR-6985-3p	mmu-miR-140-3p	mmu-miR-3073a-3p	mmu-miR-1955-5p
1,9949254	up	mmu_circRNA_35858	Pde4dip	mmu-miR-6972-5p	mmu-miR-7011-3p	mmu-miR-6950-5p	mmu-miR-7662-5p	mmu-miR-26a-2-3p
2,403345	up	mmu_circRNA_36755	Erp44	mmu-miR-7668-5p	mmu-miR-8103	mmu-miR-335-3p	mmu-miR-670-3p	mmu-miR-6938-3p
2,4034392	up	mmu_circRNA_008057	Usp3	mmu-miR-6539	mmu-miR-7092-3p	mmu-miR-684	mmu-miR-128-3p	mmu-miR-6537-5p
1,6714312	up	mmu_circRNA_007090	Qrich1	mmu-miR-370-3p	mmu-miR-683	mmu-miR-7044-5p	mmu-miR-191-3p	mmu-miR-3569-3p
1,5728279	up	mmu_circRNA_29131	Crebbp	mmu-miR-599	mmu-miR-7059-3p	mmu-miR-5121	mmu-miR-5625-3p	mmu-miR-707
3,1325776	up	mmu_circRNA_31359	Cdh2	mmu-miR-2136	mmu-miR-511-5p	mmu-miR-3106-3p	mmu-miR-6985-5p	mmu-miR-7018-5p
1,536642	up	mmu_circRNA_002179	Hipk2	mmu-miR-1892	mmu-miR-6929-3p	mmu-miR-101c	mmu-miR-327	mmu-miR-203-5p
1,6406772	up	mmu_circRNA_39951	Calu	mmu-miR-6964-3p	mmu-miR-6944-3p	mmu-miR-1930-5p	mmu-miR-6398	mmu-miR-6901-5p
2,4107824	up	mmu_circRNA_25571	Vash1	mmu-miR-7665-3p	mmu-miR-9-5p	mmu-miR-693-3p	mmu-miR-3075-3p	mmu-miR-7083-3p
1,8224514	up	mmu_circRNA_32437	Asah2	mmu-miR-3154	mmu-miR-7214-5p	mmu-miR-450a-1-3p	mmu-miR-574-5p	mmu-miR-450b-3p
1,8286232	up	mmu_circRNA_26219	Slc35b3	mmu-miR-6999-5p	mmu-miR-7066-5p	mmu-miR-7054-5p	mmu-miR-207	mmu-miR-7226-5p
1,5278291	up	mmu_circRNA_005749	Tcf25	mmu-miR-7008-3p	mmu-miR-6909-5p	mmu-miR-8103	mmu-miR-7069-5p	mmu-miR-7056-5p
1,7998607	up	mmu_circRNA_38398	Ppp1cb	mmu-miR-5616-5p	mmu-miR-29b-2-5p	mmu-miR-7686-5p	mmu-miR-33-3p	mmu-miR-1930-5p
1,8620897	up	mmu_circRNA_37720	Pum1	mmu-miR-7665-5p	mmu-miR-7118-5p	mmu-miR-6953-5p	mmu-miR-7661-5p	mmu-miR-7064-5p
1,5100022	up	mmu_circRNA_20993	Ivns1abp	mmu-miR-7054-5p	mmu-miR-182-5p	mmu-miR-300-5p	mmu-miR-8094	mmu-miR-450a-1-3p
1,877713	up	mmu_circRNA_19057	Pum2	mmu-miR-7661-5p	mmu-miR-743b-3p	mmu-miR-6339	mmu-miR-7092-5p	mmu-miR-6984-5p
1,5105875	up	mmu_circRNA_21763	Akap7	mmu-miR-1903	mmu-miR-5616-5p	mmu-miR-3059-5p	mmu-miR-5627-3p	mmu-miR-327

5,6514069	up	mmu_circRNA_25584	Adck1	mmu-miR-1966-5p	mmu-miR-1956	mmu-miR-770-3p	mmu-miR-7032-5p	mmu-miR-1199-5p
1,6161125	up	mmu_circRNA_40531	Aak1	mmu-let-7b-3p	mmu-miR-1192	mmu-miR-30c-1-3p	mmu-miR-7689-3p	mmu-let-7g-5p
1,5539453	up	mmu_circRNA_19444	Dusp16	mmu-miR-7651-3p	mmu-miR-6916-5p	mmu-miR-5124b	mmu-miR-7020-5p	mmu-miR-1a-2-5p
1,515236	up	mmu_circRNA_25173	Trappc6b	mmu-miR-450b-5p	mmu-miR-362-5p	mmu-miR-7214-3p	mmu-miR-216c-5p	mmu-miR-6516-5p
2,1695141	up	mmu_circRNA_19450	Calm3	mmu-miR-3113-3p	mmu-miR-490-3p	mmu-miR-7649-3p	mmu-miR-7093-3p	
1,9817539	up	mmu_circRNA_44528	Usp3	mmu-miR-7092-3p	mmu-miR-684	mmu-miR-6537-5p	mmu-miR-7651-3p	mmu-miR-683
1,6838755	up	mmu_circRNA_31199	Zeb1	mmu-miR-6981-5p	mmu-miR-5110	mmu-miR-466c-5p	mmu-miR-466i-3p	mmu-miR-669d-3p
1,5769758	up	mmu_circRNA_013863	Wwc2	mmu-miR-676-3p	mmu-miR-6394	mmu-miR-6971-3p	mmu-miR-207	mmu-miR-1903
2,0113303	up	mmu_circRNA_19525	Usp3	mmu-miR-7665-5p	mmu-miR-7092-3p	mmu-miR-6946-5p	mmu-miR-6976-5p	mmu-miR-7016-5p
1,5301125	up	mmu_circRNA_33964	Ube2e3	mmu-miR-504-3p	mmu-miR-6965-5p	mmu-miR-7047-5p	mmu-miR-7232-5p	mmu-miR-1249-5p
1,5910451	up	mmu_circRNA_18945	Wdfy1	mmu-miR-6946-5p	mmu-miR-7010-5p	mmu-miR-5110	mmu-miR-7665-5p	mmu-miR-1958
1,5789821	up	mmu_circRNA_23700	Ywhae	mmu-miR-215-3p	mmu-miR-3092-3p	mmu-miR-3098-3p	mmu-miR-148b-5p	mmu-miR-7073-5p
1,7356944	down	mmu_circRNA_43584	Gm20388	mmu-miR-7664-3p	mmu-miR-6335	mmu-miR-466q	mmu-miR-672-3p	mmu-miR-152-3p
15,546486	down	mmu_circRNA_33321	Mapkap1	mmu-miR-7092-3p	mmu-miR-5107-5p	mmu-miR-466m-3p	mmu-miR-466c-3p	mmu-miR-466b-3p
5,1021939	down	mmu_circRNA_42962	Cpe	mmu-miR-667-5p	mmu-miR-3101-3p	mmu-miR-6402	mmu-miR-6912-5p	mmu-miR-298-3p
4,5057746	down	mmu_circRNA_29796	Bbx	mmu-miR-7116-3p	mmu-miR-6946-3p	mmu-miR-1903	mmu-miR-7678-3p	mmu-miR-432
4,7287323	down	mmu_circRNA_24792	Cpsf3	mmu-miR-370-5p	mmu-miR-6539	mmu-miR-7019-3p	mmu-miR-128-3p	mmu-miR-1193-3p
3,7318909	down	mmu_circRNA_33765	Ppig	mmu-miR-6344	mmu-miR-7116-3p	mmu-miR-6916-5p	mmu-miR-6942-5p	mmu-miR-7081-5p
1,7687952	down	mmu_circRNA_015474	Eif3a	mmu-miR-93-3p	mmu-miR-6918-5p	mmu-miR-7094-1-5p	mmu-miR-7005-5p	
1,7585547	down	mmu_circRNA_19297	Prpf3	mmu-miR-466a-5p	mmu-miR-466e-5p	mmu-miR-466p-5p	mmu-miR-1187	mmu-miR-297c-5p
3,6083614	down	mmu_circRNA_45284		mmu-miR-6999-5p	mmu-miR-1231-5p	mmu-miR-760-3p	mmu-miR-762	mmu-miR-7023-5p
3,9076718	down	mmu_circRNA_45242	Golga4	mmu-miR-1906	mmu-miR-7038-3p	mmu-miR-3544-3p	mmu-miR-3154	mmu-miR-1898
1,514699	down	mmu_circRNA_21402	Kif26b	mmu-miR-9768-3p	mmu-miR-7043-3p	mmu-miR-1843a-5p	mmu-miR-3110-5p	mmu-miR-6379
1,5432671	down	mmu_circRNA_23053	Rel	mmu-miR-326-5p	mmu-miR-6420	mmu-miR-6999-5p	mmu-miR-7072-3p	mmu-miR-669o-5p
15,824359	down	mmu_circRNA_19996	Pantr1	mmu-miR-7018-5p	mmu-miR-7222-3p	mmu-miR-326-5p	mmu-miR-298-5p	mmu-miR-3154
3,812288	down	mmu_circRNA_41708	Sv2b	mmu-miR-1249-5p	mmu-miR-7054-5p	mmu-miR-6896-3p	mmu-miR-5110	mmu-miR-7047-5p
4,831377	down	mmu_circRNA_39531	Por	mmu-miR-6996-3p	mmu-miR-324-3p	mmu-miR-210-5p	mmu-miR-1933-3p	mmu-miR-3058-5p
2,7997751	down	mmu_circRNA_27526	Ktn1	mmu-miR-6946-3p	mmu-miR-7092-3p	mmu-miR-7116-3p	mmu-miR-1903	mmu-miR-103-1-5p
2,3364565	down	mmu_circRNA_012419	D430042O09Rik	mmu-miR-212-5p	mmu-miR-693-3p	mmu-miR-5114	mmu-miR-5121	mmu-miR-7020-3p
1,5957573	down	mmu_circRNA_20616	Pign	mmu-miR-145a-5p	mmu-miR-145b	mmu-miR-361-3p	mmu-miR-7078-3p	mmu-miR-7093-3p
1,5469947	down	mmu_circRNA_27842	Akap11	mmu-miR-148b-5p	mmu-miR-544-3p	mmu-miR-7064-5p	mmu-miR-450b-5p	mmu-miR-6926-3p
1,5343775	down	mmu_circRNA_32629	Hpse2	mmu-miR-7092-3p	mmu-miR-6946-5p	mmu-miR-7116-3p	mmu-miR-5110	mmu-miR-1903
1,7252412	down	mmu_circRNA_36102	Usp53	mmu-miR-7016-3p	mmu-miR-344h-5p	mmu-miR-344e-5p	mmu-miR-135b-5p	mmu-miR-1904
1,579866	down	mmu_circRNA_19269	Rpn2	mmu-miR-383-3p	mmu-miR-673-5p	mmu-miR-6985-3p	mmu-miR-431-5p	mmu-miR-7222-5p
1,5090269	down	mmu_circRNA_20892	Kdm5b	mmu-miR-3074-1-3p	mmu-miR-1903	mmu-miR-433-3p	mmu-miR-19b-2-5p	mmu-miR-19b-1-5p
4,478475	down	mmu_circRNA_30123	Brwd1	mmu-miR-6902-5p	mmu-miR-7094-1-5p	mmu-miR-7214-5p	mmu-miR-670-3p	mmu-miR-6946-3p
1,9042016	down	mmu_circRNA_25020	Nrcam	mmu-miR-7214-5p	mmu-miR-3103-3p	mmu-miR-7091-5p	mmu-miR-7679-3p	mmu-miR-302c-3p
1,6926273	down	mmu_circRNA_29033	Ano6	mmu-miR-433-3p	mmu-miR-7213-5p	mmu-miR-6981-5p	mmu-miR-3090-5p	mmu-miR-7069-5p
1,8586114	down	mmu_circRNA_32914	Upf2	mmu-miR-3103-3p	mmu-miR-669b-5p	mmu-miR-1903	mmu-miR-6950-3p	mmu-miR-7092-3p
1,5693471	down	mmu_circRNA_33751	Cers6	mmu-miR-6372	mmu-miR-204-3p	mmu-miR-1949	mmu-miR-3102-5p	mmu-miR-6898-5p
1,5163649	down	mmu_circRNA_015487	Tead2	mmu-miR-546	mmu-miR-5619-3p	mmu-miR-1249-5p	mmu-miR-6972-5p	mmu-miR-7685-3p
1,6217441	down	mmu_circRNA_32271	Vps13a	mmu-miR-712-5p	mmu-miR-96-3p	mmu-miR-6984-5p	mmu-miR-7646-5p	mmu-miR-544-5p

3,1475094	down	mmu_circRNA_20485	Gigyf2	mmu-miR-6946-3p	mmu-miR-346-3p	mmu-miR-6922-3p	mmu-miR-5113	mmu-miR-1904
1,586006	down	mmu_circRNA_41512	U80893	mmu-miR-7092-3p	mmu-miR-7116-3p	mmu-miR-466c-5p	mmu-miR-1839-5p	mmu-miR-7661-5p
1,530438	down	mmu_circRNA_23259	Sox30	mmu-miR-218-5p	mmu-miR-7002-3p	mmu-miR-3083-5p	mmu-miR-7008-3p	mmu-miR-686
1,6532361	down	mmu_circRNA_24239	Kansl1	mmu-miR-6946-5p	mmu-miR-7661-5p	mmu-miR-7012-5p	mmu-miR-7092-3p	mmu-miR-1187
1,8872203	down	mmu_circRNA_23236	4930553C11Rik	mmu-miR-382-5p	mmu-miR-19b-2-5p	mmu-miR-1187	mmu-miR-466i-5p	mmu-miR-669f-5p
1,8574511	down	mmu_circRNA_20118	Plcl1	mmu-miR-466k	mmu-miR-466i-3p	mmu-miR-669h-3p	mmu-miR-466q	mmu-miR-466e-3p
1,8539599	down	mmu_circRNA_32067	Sall3	mmu-miR-7117-5p	mmu-miR-3104-5p	mmu-miR-7069-5p	mmu-miR-667-5p	mmu-miR-6337
2,6533236	down	mmu_circRNA_26214	Snrnp48	mmu-miR-7116-3p	mmu-miR-8094	mmu-miR-7037-3p	mmu-miR-7083-3p	mmu-miR-3084-3p
1,8651774	down	mmu_circRNA_37432	Faf1	mmu-miR-7001-5p	mmu-miR-346-3p	mmu-miR-6973a-5p	mmu-miR-34a-3p	mmu-miR-135b-3p
3,2152737	down	mmu_circRNA_42391	Htra1	mmu-miR-693-3p	mmu-miR-7033-5p	mmu-miR-7211-5p	mmu-miR-6981-5p	mmu-miR-3095-5p
3,2588444	down	mmu_circRNA_37041	Cntln	mmu-miR-7092-3p	mmu-miR-6935-3p	mmu-miR-130a-5p	mmu-miR-6946-3p	mmu-miR-7036b-3p
1,8608915	down	mmu_circRNA_34101	Lrrc4c	mmu-miR-5625-3p	mmu-miR-145a-5p	mmu-miR-7025-5p	mmu-miR-29a-5p	mmu-miR-6946-3p
1,510102	down	mmu_circRNA_45756	Frmpd3	mmu-miR-107-5p	mmu-miR-103-1-5p	mmu-miR-103-2-5p	mmu-miR-8113	mmu-miR-873a-5p
1,5075793	down	mmu_circRNA_39029	Lin54	mmu-miR-3064-5p	mmu-miR-683	mmu-miR-3085-3p	mmu-miR-6927-3p	mmu-miR-6940-5p
4,9793406	down	mmu_circRNA_20866	Nucks1	mmu-miR-3966	mmu-miR-107-5p	mmu-miR-3084-3p	mmu-miR-7092-3p	mmu-miR-6896-3p
10,004746	down	mmu_circRNA_20885	Mgat4e	mmu-miR-7116-3p	mmu-miR-7092-3p	mmu-miR-6984-3p	mmu-miR-7058-3p	mmu-miR-6344
1,6290014	down	mmu_circRNA_28285	AK084059	mmu-miR-7661-5p	mmu-miR-1187	mmu-miR-574-5p	mmu-miR-466e-5p	mmu-miR-466a-5p
1,5609884	down	mmu_circRNA_39421	Tmem132b	mmu-miR-3090-5p	mmu-miR-1966-5p	mmu-miR-6919-3p	mmu-miR-3085-3p	mmu-miR-7646-3p
1,7136056	down	mmu_circRNA_30572	Kif6	mmu-miR-7086-5p	mmu-miR-1933-5p	mmu-miR-1955-5p	mmu-miR-686	mmu-miR-107-5p
1,6663695	down	mmu_circRNA_24855	Myt1l	mmu-miR-1954	mmu-miR-6939-5p	mmu-miR-3062-5p	mmu-miR-7675-3p	mmu-miR-7011-5p
2,7802688	down	mmu_circRNA_38536	Bod1l	mmu-miR-1903	mmu-miR-6975-3p	mmu-miR-6984-3p	mmu-miR-6946-3p	mmu-miR-6896-3p
1,6078092	down	mmu_circRNA_22247	Gm5134	mmu-miR-742-3p	mmu-miR-1843a-3p	mmu-miR-7042-5p	mmu-miR-7077-3p	mmu-miR-370-3p
1,5890145	down	mmu_circRNA_30544	Ppp2r5d	mmu-miR-193a-5p	mmu-miR-677-5p	mmu-miR-3473e	mmu-miR-3473b	mmu-miR-7682-3p
8,2459976	down	mmu_circRNA_29984	Ltn1	mmu-miR-6985-5p	mmu-miR-7094-1-5p	mmu-miR-6919-3p	mmu-miR-7086-5p	mmu-miR-22-5p
4,2121234	down	mmu_circRNA_19661	A830018L16Rik	mmu-miR-666-3p	mmu-miR-6400	mmu-miR-7211-5p	mmu-miR-683	mmu-miR-3084-5p
1,5340731	down	mmu_circRNA_18996		mmu-miR-8092	mmu-miR-875-3p	mmu-miR-7679-3p	mmu-miR-532-5p	mmu-miR-6481
1,5297504	down	mmu_circRNA_23135	Eml6	mmu-miR-103-1-5p	mmu-miR-103-2-5p	mmu-miR-107-5p	mmu-miR-19b-1-5p	mmu-miR-19b-2-5p
1,6984096	down	mmu_circRNA_40345	Grid2	mmu-miR-1968-5p	mmu-miR-6237	mmu-miR-3084-3p	mmu-miR-367-5p	mmu-miR-122-5p
1,576504	down	mmu_circRNA_37939	Ube4b	mmu-miR-7019-5p	mmu-miR-7035-5p	mmu-miR-6907-5p	mmu-miR-7050-5p	mmu-miR-6998-3p
1,6885741	down	mmu_circRNA_19347	Ube4b	mmu-miR-1966-5p	mmu-miR-7665-5p	mmu-miR-6912-5p	mmu-miR-7035-5p	mmu-miR-7087-3p
1,501348	down	mmu_circRNA_004781	Ralgps1	mmu-miR-876-5p	mmu-miR-6897-5p	mmu-miR-1936	mmu-miR-7578	mmu-miR-489-3p
1,686973	down	mmu_circRNA_19734	Kcnq5	mmu-miR-7092-3p	mmu-miR-1187	mmu-miR-5110	mmu-miR-6981-5p	mmu-miR-466a-5p
1,7299836	down	mmu_circRNA_009955	Usp15	mmu-miR-6929-3p	mmu-miR-320-5p	mmu-miR-6938-3p	mmu-miR-876-3p	mmu-miR-5623-3p
2,8687699	down	mmu_circRNA_21568	Rcor3	mmu-miR-7015-3p	mmu-miR-6948-5p	mmu-miR-598-3p	mmu-miR-6979-3p	mmu-miR-1981-5p
1,8844593	down	mmu_circRNA_24182	Acly	mmu-miR-3085-5p	mmu-miR-6399	mmu-miR-1943-3p	mmu-miR-7014-5p	mmu-miR-3109-3p
1,6299999	down	mmu_circRNA_28664	Lrrc6	mmu-miR-291b-5p	mmu-miR-291a-5p	mmu-miR-7116-3p	mmu-miR-7092-3p	mmu-miR-6416-3p
1,6385722	down	mmu_circRNA_001703	Kif26b	mmu-miR-6914-5p	mmu-miR-6769b-5p	mmu-miR-450a-2-3p	mmu-miR-3094-5p	mmu-miR-7669-3p
1,6020525	down	mmu_circRNA_36501	Tmem55a	mmu-miR-7005-3p	mmu-miR-6940-5p	mmu-miR-500-5p	mmu-miR-193b-5p	mmu-miR-470-5p
1,7076295	down	mmu_circRNA_32008	8030462N17Rik	mmu-miR-7659-3p	mmu-miR-6999-3p	mmu-miR-302d-5p	mmu-miR-6344	mmu-miR-6908-3p
1,5964821	down	mmu_circRNA_30492	Mrps18b	mmu-miR-6924-5p	mmu-miR-7053-5p	mmu-miR-695	mmu-miR-5616-3p	mmu-miR-700-5p
1,5175882	down	mmu_circRNA_30878	Alk	mmu-miR-328-3p	mmu-miR-3102-5p.2-5p	mmu-miR-6395	mmu-miR-3073a-5p	mmu-miR-6945-5p
1,6286074	down	mmu_circRNA_33013	Plxdc2	mmu-miR-705	mmu-miR-215-3p	mmu-miR-3081-5p	mmu-miR-6989-3p	mmu-miR-323-5p

1,6612297	down	mmu_circRNA_25565	Ift43	mmu-miR-6953-5p	mmu-miR-466q	mmu-miR-669f-3p	mmu-miR-466a-3p	mmu-miR-466e-3p
1,5812695	down	mmu_circRNA_23211	Wwc1	mmu-miR-3083-5p	mmu-miR-107-5p	mmu-miR-3102-5p.2-5p	mmu-miR-6940-5p	mmu-miR-3069-3p
1,5665826	down	mmu_circRNA_35961		mmu-miR-6984-3p	mmu-miR-7092-3p	mmu-miR-7116-3p	mmu-miR-466p-5p	mmu-miR-466a-5p
1,5678496	down	mmu_circRNA_41177	Zscan18	mmu-miR-6400	mmu-miR-370-3p	mmu-miR-8103	mmu-miR-6919-3p	mmu-miR-7092-3p
1,8199169	down	mmu_circRNA_28722	Ptk2	mmu-miR-6906-5p	mmu-miR-7009-5p	mmu-miR-1936	mmu-miR-6369	mmu-miR-6361
1,5342122	down	mmu_circRNA_19226	Fbxw4	mmu-miR-6946-3p	mmu-miR-3064-5p	mmu-miR-466h-5p	mmu-miR-7665-5p	mmu-miR-7092-3p
1,525017	down	mmu_circRNA_19528	Ube2cbp	mmu-miR-466f	mmu-miR-669f-5p	mmu-miR-466i-5p	mmu-miR-1187	mmu-miR-574-5p
1,835245	down	mmu_circRNA_28819	Cacna1i	mmu-miR-8104	mmu-miR-7063-5p	mmu-miR-7007-5p	mmu-miR-7013-5p	mmu-miR-7020-5p
1,5028678	down	mmu_circRNA_43279	Cyld	mmu-miR-6984-3p	mmu-miR-3065-5p	mmu-miR-133a-5p	mmu-miR-145a-3p	mmu-miR-7051-3p
1,6721314	down	mmu_circRNA_45016	Nek11	mmu-miR-6950-3p	mmu-miR-1956	mmu-miR-7661-5p	mmu-miR-214-5p	mmu-miR-466i-5p
1,5317345	down	mmu_circRNA_20407	Rhbdd1	mmu-miR-7067-5p	mmu-miR-7668-3p	mmu-miR-129b-3p	mmu-miR-7080-5p	mmu-miR-7072-5p
1,5223698	down	mmu_circRNA_24004	Gdpd1	mmu-miR-7652-5p	mmu-miR-26a-2-3p	mmu-miR-6981-5p	mmu-miR-6997-5p	mmu-miR-6932-3p
1,6362605	down	mmu_circRNA_25152	Slc25a21	mmu-miR-7116-5p	mmu-miR-7047-5p	mmu-miR-7235-5p	mmu-miR-6953-5p	mmu-miR-877-3p
1,5715414	down	mmu_circRNA_19396		mmu-miR-511-5p	mmu-miR-7005-3p	mmu-miR-146a-3p	mmu-miR-683	mmu-miR-7043-3p
1,582145	down	mmu_circRNA_22366	Ano4	mmu-miR-34a-5p	mmu-miR-34c-5p	mmu-miR-449a-5p	mmu-miR-107-5p	mmu-miR-34b-5p
1,9922498	down	mmu_circRNA_32829	4930506M07Rik	mmu-miR-207	mmu-miR-7092-3p	mmu-miR-6919-3p	mmu-miR-7030-5p	mmu-miR-320-5p
1,5334999	down	mmu_circRNA_41535	XLOC_022800	mmu-miR-432	mmu-miR-29b-2-5p	mmu-miR-3074-2-3p	mmu-miR-5110	mmu-miR-7226-5p
1,6744119	down	mmu_circRNA_23853	5730455P16Rik	mmu-miR-1933-5p	mmu-miR-485-5p	mmu-miR-6985-5p	mmu-miR-7090-3p	mmu-miR-871-3p
1,5532225	down	mmu_circRNA_28386	Nipal2	mmu-miR-6990-5p	mmu-miR-1933-3p	mmu-miR-7008-3p	mmu-miR-7061-5p	mmu-miR-429-3p
1,5012895	down	mmu_circRNA_26957	Pde4d	mmu-miR-7054-5p	mmu-miR-6946-5p	mmu-miR-6899-3p	mmu-miR-6925-5p	mmu-miR-29b-1-5p
1,5540671	down	mmu_circRNA_45034	Poc1a	mmu-miR-7212-5p	mmu-miR-6931-5p	mmu-miR-196b-5p	mmu-miR-6239	mmu-miR-665-5p
1,5671162	down	mmu_circRNA_22201	Ipmk	mmu-miR-141-5p	mmu-miR-665-3p	mmu-miR-7008-5p	mmu-miR-6922-5p	mmu-miR-7220-3p
1,6848761	down	mmu_circRNA_44982	Ephb1	mmu-miR-7665-3p	mmu-miR-6964-5p	mmu-miR-433-3p	mmu-miR-7009-5p	mmu-miR-9769-3p
1,6487459	down	mmu_circRNA_19965	Aff3	mmu-miR-7092-3p	mmu-miR-1897-5p	mmu-miR-431-3p	mmu-miR-7084-5p	mmu-miR-149-5p
1,5558678	down	mmu_circRNA_34107	Commd9	mmu-miR-7118-5p	mmu-miR-7665-5p	mmu-miR-7062-5p	mmu-miR-3547-5p	mmu-miR-7088-5p
1,517699	down	mmu_circRNA_25324	Slc38a6	mmu-miR-7020-5p	mmu-miR-7054-5p	mmu-miR-7082-5p	mmu-miR-3076-5p	mmu-miR-6997-5p
1,5089579	down	mmu_circRNA_32190	Slc29a2	mmu-miR-7081-5p	mmu-miR-210-5p	mmu-miR-5110	mmu-miR-6916-5p	mmu-let-7e-5p
1,6385785	down	mmu_circRNA_19386	Hip1r	mmu-miR-7035-3p	mmu-miR-6357	mmu-miR-6345	mmu-miR-6916-5p	mmu-miR-15b-5p
1,627841	down	mmu_circRNA_19385	Hip1r	mmu-miR-6357	mmu-miR-6345	mmu-miR-6916-5p	mmu-miR-15b-5p	mmu-miR-6942-5p
1,5668364	down	mmu_circRNA_34276	Bub1b	mmu-miR-7090-5p	mmu-miR-6340	mmu-miR-7066-5p	mmu-miR-296-3p	mmu-miR-148b-5p
1,5243575	down	mmu_circRNA_28235	Ttc23l	mmu-miR-500-5p	mmu-miR-6340	mmu-miR-3082-5p	mmu-miR-7214-5p	mmu-miR-7024-3p
1,6497568	down	mmu_circRNA_30803	Ptprm	mmu-miR-1291	mmu-miR-5625-3p	mmu-miR-6403	mmu-miR-9-5p	mmu-miR-1936
1,766927	down	mmu_circRNA_30869	Fam179a	mmu-miR-7226-5p	mmu-miR-505-5p	mmu-miR-3081-5p	mmu-miR-6340	mmu-miR-1903
2,0015365	down	mmu_circRNA_36895	Pappa	mmu-miR-3475-3p	mmu-miR-298-5p	mmu-miR-9769-3p	mmu-miR-6981-5p	mmu-miR-6972-5p
1,8197999	down	mmu_circRNA_24480	Slc38a10	mmu-miR-6942-5p	mmu-miR-5110	mmu-miR-6916-5p	mmu-miR-3104-5p	mmu-miR-214-3p
1,6344086	down	mmu_circRNA_19080	Serpina3h	mmu-miR-7665-5p	mmu-miR-466k	mmu-miR-1187	mmu-miR-466i-5p	mmu-miR-574-5p
1,6341897	down	mmu_circRNA_43410	Edc4	mmu-miR-6337	mmu-miR-6998-3p	mmu-miR-3075-5p	mmu-miR-7656-3p	mmu-miR-7055-3p
1,7110971	down	mmu_circRNA_003912	Cdc42bpa	mmu-miR-1964-5p	mmu-miR-214-3p	mmu-miR-6419	mmu-miR-5133	mmu-miR-7051-5p
2,5637246	down	mmu_circRNA_39631	Daglb	mmu-miR-7053-3p	mmu-miR-6972-5p	mmu-miR-6991-3p	mmu-miR-7228-5p	mmu-miR-486b-5p
1,6041045	down	mmu_circRNA_20039	Tmeff2	mmu-miR-199a-5p	mmu-miR-679-3p	mmu-miR-3109-3p	mmu-miR-6900-5p	mmu-miR-6370
1,5467164	down	mmu_circRNA_39552	Nyap1	mmu-miR-6939-5p	mmu-miR-7669-3p	mmu-miR-6931-5p	mmu-miR-763	mmu-miR-346-3p
1,5605858	down	mmu_circRNA_27685	Wdfy2	mmu-miR-6964-3p	mmu-miR-145b	mmu-miR-145a-5p	mmu-miR-7680-5p	mmu-miR-34c-5p

1,6697625	down	mmu_circRNA_27052	Cadps	mmu-miR-7673-5p	mmu-miR-7682-3p	mmu-miR-6944-3p	mmu-miR-23b-3p	mmu-miR-1968-5p
1,5255781	down	mmu_circRNA_27136	Nkiras1	mmu-miR-378d	mmu-miR-330-5p	mmu-miR-298-5p	mmu-miR-7667-5p	mmu-miR-7686-5p
1,6247496	down	mmu_circRNA_37243	Raver2	mmu-miR-3552	mmu-miR-3110-5p	mmu-miR-3069-5p	mmu-miR-6962-3p	mmu-miR-222-5p
1,7010971	down	mmu_circRNA_42025	Nup98	mmu-miR-370-3p	mmu-miR-5615-5p	mmu-miR-3064-5p	mmu-miR-7094b-2-5p	mmu-miR-2136
1,5672582	down	mmu_circRNA_43326	Crnde	mmu-miR-103-2-5p	mmu-miR-103-1-5p	mmu-miR-107-5p	mmu-miR-3474	mmu-miR-148b-3p
1,5926495	down	mmu_circRNA_39830	Ica1	mmu-miR-6908-3p	mmu-miR-6975-3p	mmu-miR-149-5p	mmu-miR-500-5p	mmu-miR-7009-5p
1,6879972	down	mmu_circRNA_39714	Wdr95	mmu-miR-125a-3p	mmu-miR-6340	mmu-miR-22-5p	mmu-miR-717	mmu-miR-15b-5p
6,0817763	down	mmu_circRNA_42050	AY512917	mmu-miR-686	mmu-miR-7231-3p	mmu-miR-488-3p	mmu-miR-466i-5p	mmu-miR-7119-3p
3,8803916	down	mmu_circRNA_19065	Klhl28	mmu-miR-7027-5p	mmu-miR-7665-5p	mmu-miR-6999-5p	mmu-miR-5110	mmu-miR-6946-5p
2,6152381	down	mmu_circRNA_20495	Gigyf2	mmu-miR-6961-3p	mmu-miR-6946-3p	mmu-miR-3059-5p	mmu-miR-7116-3p	mmu-miR-1904
1,5412153	down	mmu_circRNA_30522		mmu-miR-1903	mmu-miR-877-3p	mmu-miR-6946-3p	mmu-miR-6919-3p	mmu-miR-207
4,7353033	down	mmu_circRNA_29850	Dcbld2	mmu-miR-23a-5p	mmu-miR-1903	mmu-let-7g-3p	mmu-miR-7086-3p	mmu-miR-6996-5p
2,9511695	down	mmu_circRNA_012939	Wdr7	mmu-miR-7050-5p	mmu-miR-8119	mmu-miR-7012-5p	mmu-miR-8113	mmu-miR-3091-3p
2,3052795	down	mmu_circRNA_26052	Arid4b	mmu-miR-7089-3p	mmu-miR-7686-5p	mmu-miR-30e-3p	mmu-miR-30a-3p	mmu-miR-6946-3p
2,4386044	down	mmu_circRNA_016423	Plcl2	mmu-miR-7092-3p	mmu-miR-6904-5p	mmu-miR-489-3p	mmu-miR-1903	mmu-miR-504-5p
1,565523	down	mmu_circRNA_41712		mmu-miR-7092-3p	mmu-miR-7116-3p	mmu-miR-6344	mmu-miR-466a-5p	mmu-miR-466e-5p
1,7541475	down	mmu_circRNA_43021	Ap1m1	mmu-miR-122-3p	mmu-miR-6919-3p	mmu-miR-6975-3p	mmu-miR-6339	mmu-miR-207
1,5119576	down	mmu_circRNA_39062	Mapk10	mmu-miR-3547-5p	mmu-miR-7688-3p	mmu-miR-7118-5p	mmu-miR-7074-5p	mmu-miR-204-3p
2,5025053	down	mmu_circRNA_005365	Ep300	mmu-miR-136-5p	mmu-miR-6961-3p	mmu-miR-152-5p	mmu-miR-130b-5p	mmu-miR-7055-3p
1,7343285	down	mmu_circRNA_29144	Hmox2	mmu-miR-6896-3p	mmu-miR-6917-5p	mmu-miR-677-3p	mmu-miR-3078-3p	mmu-miR-1231-5p
1,5945622	down	mmu_circRNA_19482	Athl1	mmu-miR-7002-5p	mmu-miR-6914-5p	mmu-miR-7005-3p	mmu-miR-6931-5p	mmu-miR-574-5p
1,7035714	down	mmu_circRNA_33174	Nelfb	mmu-miR-873a-5p	mmu-miR-34a-5p	mmu-miR-6900-3p	mmu-miR-7089-3p	mmu-miR-449a-5p
1,5032839	down	mmu_circRNA_29709	Igsf11	mmu-miR-1934-3p	mmu-miR-324-3p	mmu-miR-3087-5p	mmu-miR-6357	mmu-miR-6909-5p
1,6176171	down	mmu_circRNA_22216	Rsph14	mmu-miR-7665-5p	mmu-miR-6971-5p	mmu-miR-7092-3p	mmu-miR-7016-3p	mmu-miR-6931-5p
1,5147386	down	mmu_circRNA_32240	Patl1	mmu-miR-7669-3p	mmu-miR-380-5p	mmu-miR-5106	mmu-miR-871-5p	mmu-miR-7670-5p
1,5999277	down	mmu_circRNA_32153	Lrp5	mmu-miR-344d-1-5p	mmu-miR-344c-5p	mmu-miR-344d-3-5p	mmu-miR-344b-5p	mmu-miR-344-5p
1,8025162	down	mmu_circRNA_20530	Lrrfip1	mmu-miR-130b-5p	mmu-miR-6999-3p	mmu-miR-207	mmu-miR-6964-3p	mmu-miR-7028-3p
1,746014	down	mmu_circRNA_015078	Bc1	mmu-miR-7032-5p	mmu-miR-1902	mmu-miR-6405	mmu-miR-669k-5p	mmu-miR-3547-5p
1,5494687	down	mmu_circRNA_33274	Nup214	mmu-miR-1903	mmu-miR-6918-5p	mmu-miR-125a-3p	mmu-miR-6987-5p	mmu-miR-485-5p
1,5936471	down	mmu_circRNA_28225	Slc1a3	mmu-miR-7094b-2-5p	mmu-miR-3088-3p	mmu-miR-3089-3p	mmu-miR-6953-5p	mmu-miR-3071-5p
1,6307149	down	mmu_circRNA_30406	Mapk14	mmu-miR-7050-3p	mmu-miR-330-5p	mmu-miR-22-5p	mmu-miR-3099-5p	mmu-miR-5112
1,5274433	down	mmu_circRNA_39429	Glt1d1	mmu-miR-712-5p	mmu-miR-6948-3p	mmu-miR-6984-3p	mmu-miR-501-5p	mmu-miR-6945-3p
1,5541063	down	mmu_circRNA_20357	Ttll4	mmu-miR-7015-5p	mmu-miR-3062-5p	mmu-miR-6769b-3p	mmu-miR-29a-3p	mmu-miR-219c-5p
1,9408442	down	mmu_circRNA_26172	E2f3	mmu-miR-7665-5p	mmu-miR-8100	mmu-miR-7027-5p	mmu-miR-6971-5p	mmu-miR-6980-5p
1,5754896	down	mmu_circRNA_45367	Cask	mmu-miR-761	mmu-miR-6356	mmu-miR-7027-5p	mmu-miR-6344	mmu-miR-8104
1,5565904	down	mmu_circRNA_004775	Dennd1a	mmu-miR-1943-5p	mmu-miR-344g-3p	mmu-miR-6901-3p	mmu-miR-760-3p	mmu-miR-7070-3p
1,526873	down	mmu_circRNA_36138	Alpk1	mmu-miR-330-5p	mmu-miR-877-3p	mmu-miR-5101	mmu-miR-1934-5p	mmu-miR-6960-5p
1,7207914	down	mmu_circRNA_40903	Cecr2	mmu-miR-1903	mmu-miR-6946-3p	mmu-miR-6919-3p	mmu-miR-7009-3p	mmu-miR-6769b-3p
2,4919703	down	mmu_circRNA_005834	9930021J03Rik	mmu-miR-7116-3p	mmu-miR-6344	mmu-miR-7092-3p	mmu-miR-7062-3p	mmu-miR-129b-5p
1,5373884	down	mmu_circRNA_42480		mmu-miR-6928-5p	mmu-miR-6368	mmu-miR-5710	mmu-miR-3547-5p	mmu-miR-6924-5p
3,2915798	down	mmu_circRNA_24038	Rad51c	mmu-miR-6903-5p	mmu-miR-1903	mmu-miR-7681-3p	mmu-miR-7019-5p	mmu-miR-6984-5p
1,6388425	down	mmu_circRNA_40432	Ctnna2	mmu-miR-6942-5p	mmu-miR-7075-5p	mmu-miR-5110	mmu-miR-6981-5p	mmu-miR-7118-5p

1,6666828	down	mmu_circRNA_19417		mmu-miR-7022-5p	mmu-miR-466m-3p	mmu-miR-6957-5p	mmu-miR-7652-3p	mmu-miR-7688-3p
1,5326299	down	mmu_circRNA_19281	Nbea	mmu-miR-7661-5p	mmu-miR-8100	mmu-miR-5113	mmu-miR-7092-3p	mmu-miR-6946-5p
1,5284176	down	mmu_circRNA_31571	Reep2	mmu-miR-6982-3p	mmu-miR-136-3p	mmu-miR-3095-3p	mmu-miR-6898-5p	mmu-miR-7665-3p
1,6352194	down	mmu_circRNA_31970	Myo5b	mmu-miR-23a-5p	mmu-miR-7037-5p	mmu-miR-107-5p	mmu-miR-92a-2-5p	mmu-miR-6923-5p
1,5739141	down	mmu_circRNA_20275	Map2	mmu-miR-7117-3p	mmu-miR-320-5p	mmu-miR-693-3p	mmu-miR-7021-3p	mmu-miR-6909-3p
1,545263	down	mmu_circRNA_38627	Tbc1d19	mmu-miR-93-3p	mmu-miR-15b-3p	mmu-miR-6353	mmu-miR-6369	mmu-miR-6361
2,049755	down	mmu_circRNA_30483	BC051142	mmu-miR-7226-5p	mmu-miR-8091	mmu-miR-468-3p	mmu-miR-6384	mmu-miR-361-3p
1,7362404	down	mmu_circRNA_24559	Dtnb	mmu-miR-3066-5p	mmu-miR-103-1-5p	mmu-miR-103-2-5p	mmu-miR-107-5p	mmu-miR-6930-5p
1,7634045	down	mmu_circRNA_42683	Whsc1l1	mmu-miR-7081-5p	mmu-miR-7578	mmu-miR-6946-3p	mmu-miR-7028-3p	mmu-miR-5110
1,5967119	down	mmu_circRNA_001946	Cdr1	mmu-miR-7b-5p	mmu-miR-7a-5p	mmu-miR-7074-5p	mmu-miR-450b-3p	mmu-miR-7685-3p
1,5012584	down	mmu_circRNA_23406	Fam114a2	mmu-miR-1903	mmu-miR-7092-3p	mmu-miR-504-3p	mmu-miR-7018-5p	mmu-miR-6981-5p
1,6434326	down	mmu_circRNA_009782	Anks1b	mmu-miR-141-5p	mmu-miR-7026-5p	mmu-miR-7652-3p	mmu-miR-7077-3p	mmu-miR-7048-3p
4,2042919	down	mmu_circRNA_26264	Atxn1	mmu-miR-7020-5p	mmu-miR-6906-5p	mmu-miR-5110	mmu-miR-669f-3p	mmu-miR-466m-3p
1,5754385	down	mmu_circRNA_27142	Ube2e2	mmu-miR-7092-3p	mmu-miR-5110	mmu-miR-7226-5p	mmu-miR-6981-5p	mmu-miR-7116-3p
1,9456732	down	mmu_circRNA_30129	Brwd1	mmu-miR-216b-5p	mmu-miR-1954	mmu-miR-146a-3p	mmu-miR-1903	mmu-miR-673-5p
1,6236253	down	mmu_circRNA_26308	Cenpp	mmu-miR-5113	mmu-miR-7092-3p	mmu-miR-7054-5p	mmu-miR-1966-5p	mmu-miR-7016-5p
1,5506647	down	mmu_circRNA_45699	Brwd3	mmu-miR-1955-5p	mmu-miR-216c-3p	mmu-miR-6918-5p	mmu-miR-411-5p	mmu-miR-142a-3p
1,5354842	down	mmu_circRNA_22654	Zfc3h1	mmu-miR-382-5p	mmu-miR-7210-5p	mmu-miR-7231-3p	mmu-miR-493-5p	mmu-miR-669c-5p
1,53108	down	mmu_circRNA_26845	Gtf2h2	mmu-miR-130a-5p	mmu-miR-691	mmu-miR-5129-3p	mmu-miR-9769-3p	mmu-miR-455-5p
1,5142397	down	mmu_circRNA_39556	Zkscan1	mmu-miR-216c-3p	mmu-miR-7019-5p	mmu-miR-5616-5p	mmu-miR-7033-5p	mmu-miR-1942
1,5339433	down	mmu_circRNA_24681	1110057K04Rik	mmu-miR-871-5p	mmu-miR-7220-5p	mmu-miR-6939-5p	mmu-let-7d-5p	mmu-miR-5623-5p
1,5486163	down	mmu_circRNA_29893	Epha3	mmu-miR-9769-3p	mmu-miR-7669-3p	mmu-miR-207	mmu-miR-1934-3p	mmu-miR-7037-5p
1,5657522	down	mmu_circRNA_30083	Hlcs	mmu-miR-5133	mmu-miR-6938-5p	mmu-miR-7118-5p	mmu-miR-6911-5p	mmu-miR-712-5p
1,5707729	down	mmu_circRNA_21686	Hivep2	mmu-miR-466i-3p	mmu-miR-669h-3p	mmu-miR-466p-3p	mmu-miR-466c-3p	mmu-miR-466b-3p
2,4293805	down	mmu_circRNA_21625	Sash1	mmu-miR-6940-5p	mmu-miR-7027-3p	mmu-miR-6346	mmu-miR-762	mmu-miR-5624-5p
2,8230745	down	mmu_circRNA_25472	Rbm25	mmu-miR-7026-3p	mmu-miR-3095-5p	mmu-miR-6944-5p	mmu-miR-7031-5p	mmu-miR-5623-3p
1,5981603	down	mmu_circRNA_39601	Mmd2	mmu-miR-764-3p	mmu-miR-7077-5p	mmu-miR-7062-5p	mmu-miR-5123	mmu-miR-7239-5p
1,8801287	down	mmu_circRNA_33490	Gtdc1	mmu-miR-8100	mmu-miR-7027-5p	mmu-miR-7665-5p	mmu-miR-6981-5p	mmu-miR-7054-5p
5,3443133	down	mmu_circRNA_35732	AK141565	mmu-miR-6975-3p	mmu-miR-6971-5p	mmu-miR-361-3p	mmu-miR-346-3p	mmu-miR-6384
1,573252	down	mmu_circRNA_22174	Ank3	mmu-miR-344c-5p	mmu-miR-344d-1-5p	mmu-miR-344b-5p	mmu-miR-344-5p	mmu-miR-344d-3-5p
1,6678233	down	mmu_circRNA_36502	Tmem55a	mmu-miR-6362	mmu-miR-7007-3p	mmu-miR-7005-3p	mmu-miR-6940-5p	mmu-miR-500-5p
3,1677041	down	mmu_circRNA_21161	4930558K02Rik	mmu-miR-7075-5p	mmu-miR-466m-3p	mmu-miR-5110	mmu-miR-466o-3p	mmu-miR-669o-3p
1,6581593	down	mmu_circRNA_32707	Cnnm2	mmu-miR-7050-5p	mmu-miR-8104	mmu-miR-22-5p	mmu-miR-6400	mmu-miR-7037-5p
1,5976778	down	mmu_circRNA_37178	Fggy	mmu-miR-7680-5p	mmu-miR-205-5p	mmu-miR-669h-3p	mmu-miR-3057-3p	mmu-miR-669k-3p
1,5274735	down	mmu_circRNA_40302	Fam188b	mmu-miR-7020-5p	mmu-miR-7092-3p	mmu-miR-691	mmu-miR-133b-5p	mmu-miR-880-3p
1,609836	down	mmu_circRNA_21661	Utrn	mmu-miR-1968-5p	mmu-miR-6958-3p	mmu-miR-6998-3p	mmu-miR-7093-3p	mmu-miR-19b-2-5p
1,548416	down	mmu_circRNA_43341	Ogfod1	mmu-miR-145b	mmu-miR-145a-5p	mmu-miR-677-3p	mmu-miR-7032-5p	mmu-miR-320-3p

XII EHRENWÖRTLICHE ERKLÄRUNG

„Hiermit erkläre ich, dass ich die vorliegende Arbeit selbständig und ohne unzulässige Hilfe oder Benutzung anderer als der angegebenen Hilfsmittel angefertigt habe. Alle Textstellen, die wörtlich oder sinngemäß aus veröffentlichten oder nichtveröffentlichten Schriften entnommen sind, und alle Angaben, die auf mündlichen Auskünften beruhen, sind als solche kenntlich gemacht. Bei den von mir durchgeführten und in der Dissertation erwähnten Untersuchungen habe ich die Grundsätze guter wissenschaftlicher Praxis, wie sie in der „Satzung der Justus-Liebig-Universität Gießen zur Sicherung guter wissenschaftlicher Praxis“ niedergelegt sind, eingehalten. Ich versichere, dass Dritte von mir weder unmittelbar noch mittelbar geldwerte Leistungen für Arbeiten erhalten haben, die im Zusammenhang mit dem Inhalt der vorgelegten Dissertation stehen, und dass die vorgelegte Arbeit weder im Inland noch im Ausland in gleicher oder ähnlicher Form einer anderen Prüfungsbehörde zum Zweck einer Promotion oder eines anderen Prüfungsverfahrens vorgelegt wurde. Alles aus anderen Quellen und von anderen Personen übernommene Material, das in der Arbeit verwendet wurde oder auf das direkt Bezug genommen wird, wurde als solches kenntlich gemacht. Insbesondere wurden alle Personen genannt, die direkt an der Entstehung der vorliegenden Arbeit beteiligt waren.
Mit der Überprüfung meiner Arbeit durch eine Plagiatserkennungssoftware bzw. ein internetbasiertes Softwareprogramm erkläre ich mich einverstanden.“

Datum

Unterschrift

XIII DANKSAGUNG

In erster Linie möchte ich mich bei Prof. Braun für die Unterstützung und die Möglichkeit meine Promotion am Max-Planck-Institut in Bad Nauheim in seiner Abteilung durchführen zu können bedanken. Des Weiteren danke ich Dr. André Schneider, der viel Zeit für die Betreuung meiner Arbeit aufgewandt hat und immer ein offenes Ohr für Fragen oder Sorgen hatte. Mein Dank gilt außerdem der ganzen Arbeitsgruppe Schneider für die Zusammenarbeit, insbesondere Michael Hofmann, der mich im und um das Labor unterstützt hat. Außerdem möchte ich mich bei Prof. Looso und Dr. Preussner für die Hilfe bei der Analyse der RNA-Sequenzierungsdaten bedanken. Zu guter Letzt bedanke ich mich bei meiner Familie, meiner Freundin und bei meinen Freunden, die mich motiviert haben weiter zu arbeiten und die Promotion abzuschließen.